Development of Core-shell Polymeric Nanostructures for Delivery of Diagnostic and Chemotherapeutic Agents

By

Nikorn Pothayee

Dissertation submitted to the Faculty of the Virginia Polytechnic Institute and State University in partial fulfillment of the requirements for the degree of

Doctor of Philosophy

in

Macromolecular Science and Engineering

Approved By
Judy S. Riffle
James E. McGrath
Richey Davis
S. Richard Turner
Nammalwar Sriranganathan

December 8, 2010
Blacksburg, Virginia

key words; intracellular bacteria, aminoglycosides, block ionomers, magnetic nanoparticles, theranostic

Development of Core-shell Polymeric Nanostructures for Delivery of Diagnostic and Chemotherapeutic Agents

Nikorn Pothayee

Abstract

Macromolecular complexes of anionic-nonionic block copolymers and cationic antibiotic aminoglycosides have been formed by electrostatic condensation. Amphiphilicity of the complexes was introduced into the shells by incorporating a hydrophobic poly(propylene oxide) segment into the block copolymer. The resulting particles have an average hydrodynamic diameter of ~ 200 nm and contain up to 30-40 % of the drug payload. *In vitro* efficacies of such nanostructures in reduction of intracellular pathogens like *Salmonella*, *Listeria*, and *Brucella* were demonstrated. Current effort focuses on translation of this nano-drug delivery concept to *in vivo* model of intracellular infectious diseases.

Atom transfer radical polymerization (ATRP) was utilized to prepare well-defined polymeric dispersion stabilizers that readily adsorb onto metal oxide surfaces. Two unimolecular bis(phosphonate) ATRP initiators were designed and prepared in good yield. These special initiators were successfully used to initiate polymerization of poly(N-isopropylacrylamide) (PNIPAM) in a controlled manner yielding PNIPAM with a bis(phosphonate) moiety at one terminus. The polymers readily adsorbed onto magnetite nanoparticle surfaces, thus creating thermosensitive magnetic nanostructures that form nanosized clusters upon heating above the lower critical solution temperature of PNIPAM. It is envisioned that modularity of this approach, relying on the applicability of ATRP to

polymerize a vast array of monomers, could be used to prepare a library of polymeric shells for magnetic iron oxide nanoparticles.

Medical intervention in drug delivery that includes detectability of drug carriers is greatly desirable. A real-time assessment of disease prognosis could be highly beneficial for developing personalized treatment strategies. As an example of this conceptual innovation, block ionomer functionalized magnetite complexes were synthesized and investigated as carriers for delivery of aminoglycosides into phagocytic cells for treatment of intracellular bacterial infections. The ionic block of copolymer contains multiple carboxylates for binding onto the iron oxide surface. The remaining unbound carboxylate anions were used to complex with cationic gentamicin in nanoshells of these complexes. The iron oxide particle core provides an imaging modality and serves as a pseudo-crosslinking site to enhance stabilities of the polyelectrolyte complexes, thus preventing them from disintegrating in the physiological environment. Currently, these hybrid complexes are being investigated in possible pharmaceutical formulations to eradicate intracellular pathogens in animal models.

Acknowledgement

I would like to express my sincere gratitude and appreciation to my advisor Dr. Judy Riffle for her support, guidance, encouragement, and trust throughout my career at Virginia Tech. She has given me the opportunity to grow as a scientist and a person through many years. I am very fortunate to have her as my advisor ever since I came to Virginia Tech 6 years ago. It is also my honor to be advised by a group of prominent and brilliant committee members, Dr. James E. McGrath, Dr. Richey Davis, Dr. Richard Turner, and Dr. Nammalwar Sriranganathan. All of these professors have my utmost respect.

I would like to extend my deepest gratitude to Angie Flynn, without whom I would have not made it through my graduate career. The same thanks go to Mary Jane Smith who has helped me organize all tools and materials required to conduct an experiment. I would especially like to thank Mark Flynn for help with SEC and the Australian folks for contributing their physics expertise and for the magnetic property measurements. I very much appreciate the help from Dr. Yinian Lin in preparation of many small molecule intermediates necessary for my research. This thesis would not be completed without great collaboration from my colleagues, Ashish Ranjan, Neeta Jain, and Eva Restis.

Finally I would like to extend my deepest thanks to all group members and friends that I have met and the others that walked through my life. I owe so much for the friendship and life lessons that we share. And for this, I wish you all the best.

Dedication

To my beloved family and my partner, no word can describe how much all of you mean to me. I am what I am today because of the love and strength that you have given to me. In going forward, I promise that I will try to become better as a person and do anything I can to return every drop of your kindness…

To the Mother Nature and Evolution, thank you so much for giving us a chance to survive and a power of imaginative creation…

Happiness is nothing unless it can be shared with the others…

Table of Contents

Abbreviations

ATRP	atom transfer radical polymerization
MBICs	magnetic block ionomer complexes
LCST	lower critical solution temperature
MIVM	multi inlet vortex mixer
PNIPAM	poly(N-isopropylacrylamide)
PEO	poly(ethylene oxide)
PPO	poly(propylene oxide)
PAA	poly(acrylic acid)
SEC	size exclusion chromatography
DLS	dynamic light scattering
TGA	thermal gravimetric analysis
TEM	transition electron microscopy
ICP-AES	inductively coupled plasma atomic emission spectroscopy
NMR	nuclear magnetic resonance spectroscopy
SQuID	superconducting quantum interference device
Me_6TREN	tris[2-(dimethylamino)ethylamine]
PMDETA	N-N'-N'-N"-N"-pentamethyldiethylenetriamine
TMSBr	trimethylsilyl bromide
$Fe(acac)_3$	iron (III) acetylacetonate
THF	tetrahydrofuran
DMF	dimethylformamide
DMSO	dimethylsulfoxide
PBS	phosphate buffered saline
CFU	colony forming unit
M_n	number average molecular weight
PDI	polydispersity index

List of Figures

List of Tables

Chapter 1

Introduction and research motivation

Nanotechnology has received great attention due to its high promise that can potentially revolutionize every industrial field in which it is being exploited. In the healthcare sector, nanotechnology is already beginning to make an impact. Development of a wide spectrum nanoscale technology for applications in disease diagnosis, treatment, and prevention has explosively expanded within the past decades. These technological innovations and their applications, termed as "nanomedicines" by the National Institutes of Health, have considerable potential as a next generation platform for medicine that can greatly improve upon patient lives with widespread advantages by providing early detection, targeted treatment, and new methodologies for monitoring progress.

Several classes of "nano" carriers have been investigated, such as liposomes, polymeric micelles, nanoparticles, dendrimers, and nanocrystals. Polymeric core-shell nanoparticles, whose 3-dimentional structures are defined and designed to possess "core" and "shell" domains have been extensively studied.[1-3] Flexibility to engineer the core and shell structure and components gives rise to vast opportunities for incorporating various molecules and functionalities. Capitalizing on the unique and versatile nature of these nanostructures, our research group has reported the development of delivery systems for delivery of chemotherapeutic and imaging agents.[4-7]

In this dissertation, a particular system for delivery of charged antibiotics into immune cell-localized pathogens is described. Block copolymers consisting of nonionic and anionic segments were synthesized and utilized as polymeric carriers to allow

cooperative electrostatic complexation with cationic aminoglycosides to spontaneously form core-shell nanostructures (Figure 1.1). The effectiveness of these delivery vehicles to eradicate intracellular bacterial infections will be discussed.

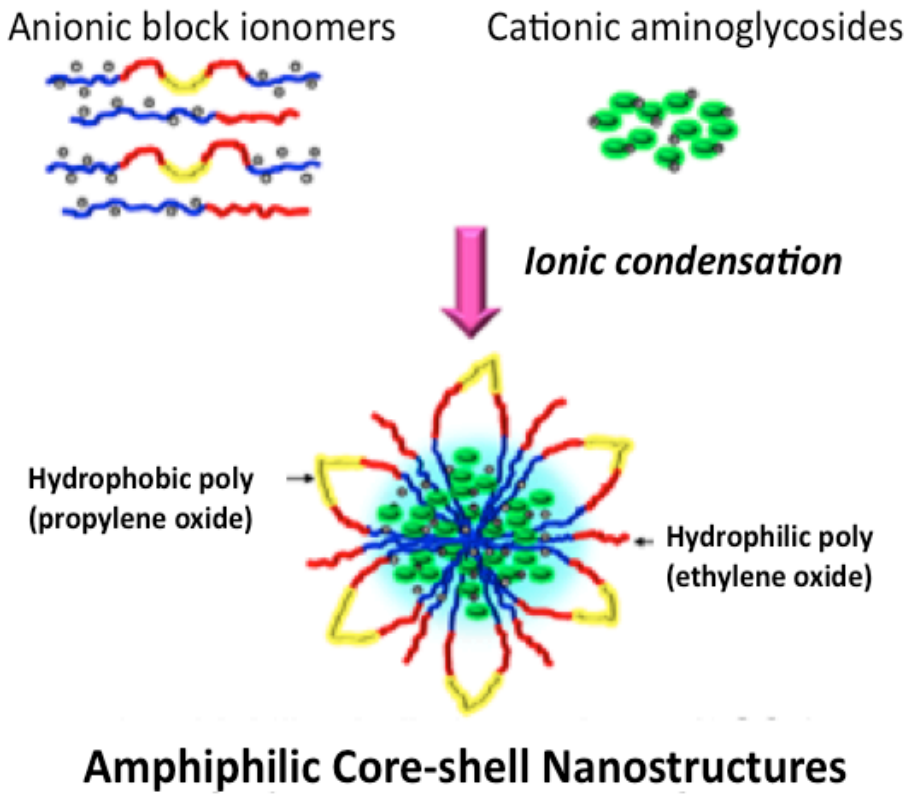

Figure 1.1 Schematic formation of core-shell block copolymer-antibiotic nanostructures via electrostatic complexation

Attention on another area of nanomedicine will be paid through the design, synthesis and characterization of well-defined, magnetic nanoparticles for use as MRI contrast agents. Our research group has previously reported numerous work on polyether functionalized magnetic nanoparticles. Macromolecules like poly(ethylene oxide) (PEO) and its copolymers with polypropylene (oxide) (PPO) were bound to magnetite surfaces

via specially designed carboxylate, ammonium, and phosphonate anchor groups.[6, 8] In this thesis, a new method to append polymeric nanoshells will be described. Atom transfer radical polymerization (ATRP) was used as a polymerization tool to synthesize polyacrylate and polyacrylamide nanoshells by utilizing an "anchor" initiator. The resultant functional polymer could be readily attached to magnetic nanoparticles by ligand adsorption (Figure 1.2)

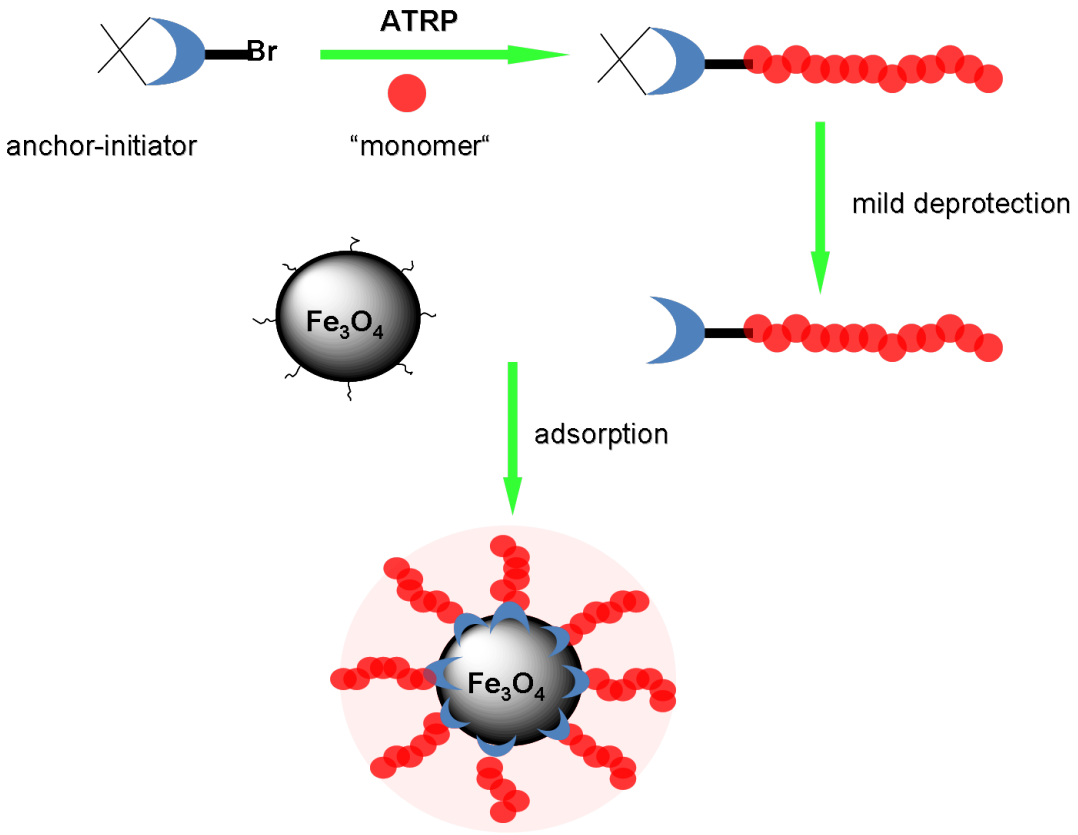

Figure 1.2 Synthesis of heterobifunctional polymers with ammonium bis(phosphonate) initiators via ATRP and adsorption onto iron oxide nanoparticle surfaces

The recent progress in nanotechnology has also focused on combining different nanostructured materials that could enable the development of multifunctional

nanomedical platforms for real-time imaging or simultaneous diagnosis and therapy.[9, 10] Our particular interest is on nanostructures in which the core contains iron oxide and the shell comprises a double layer corona that is suitable for drug encapsulation. In this approach, simple block ionomer assembly on the iron oxide surface was employed to form a core-shell nanocarrier (Figure 1.3). Efficacy of such nanovehicles to enhance intracellular accumulation of MRI imaging agents and therapeutic drugs will be determined.

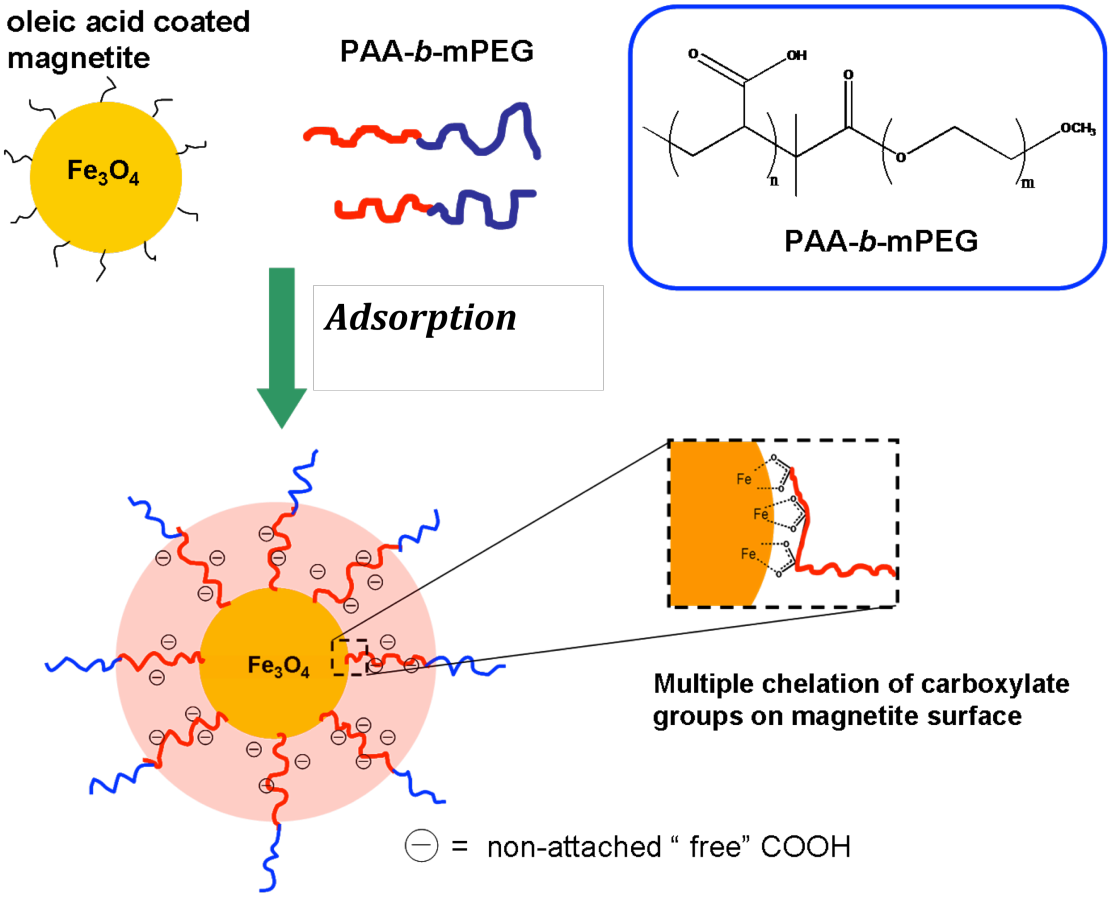

Figure 1.3 Schematic illustration of nanomagnetite with doubly ionic-nonionic shells by adsorption of block copolymers on magnetite templates from organic media. The ionic segment of the corona was then used to bind various oppositely charged drug molecules.

Chapter 2

Literature Review

2.1 Overview

This literature review will discuss areas directly related to the research topic and is divided into five sections. The first section presents an overview of the utilization of core-shell polymeric nanostructures, with emphasis on block ionomer complexes (BICs), as drug delivery vehicles. Intracellular infections and their treatment complications will be discussed in section two followed by a review of aminoglycoside antibiotics and drug delivery systems in section three. An overview of magnetic nanoparticles in section four will include synthesis and modification of these particles for their uses in biomedical applications. Section five will emphasize atom transfer radical polymerization (ATRP), which was employed as a polymerization tool to afford polymeric components that constitute this dissertation.

2.2 Nanotechnology and drug delivery systems

In the field of drug delivery systems, nanotechnological applications build upon conventional drug delivery systems that happen to be in the nanometer size range. The importance of nanotechnology in drug delivery is in the concept and ability to manipulate molecules and supramolecular structures for producing devices with programmed functions. In contrast to classical systems, manipulation in the nanoscale range of materials can provide a number of advantages. In particular, they can enhance therapeutic activity by prolonging drug half-life, improving solubility of hydrophobic drugs, reducing potential immunogenicity, and/or releasing drugs in a sustained or stimuli-triggered fashion. Thus, the toxic side effects of drugs can be reduced, as well as the administration

frequency. In addition, nanoscale particles can passively accumulate in specific tissues (e.g., tumors) through the enhanced permeability and retention (EPR) effect. This phenomenon is generally explained by the fast growing of cancernous cells often relies on an increase need of food supply. Therefore, the production of blood vessels must be stimulated to bring enough nutrition and oxygen. The newly form vessels are usually premature and commonly coined by "leaky" nature and more permeable to certain sizes of particles and macromolecule compared to normal tissues.[11]

It was in early 1960 that liposomes, the first kind of nanocarrier, were introduced. Since then, nanotechnology has made significant impact on development of drug delivery systems. A variety of inorganic and organic nanomaterials have been utilized to create effective therapeutic modalities. The timeline of significant breakthroughs in development of nano-delivery systems during the past five decades is shown in Figure 2.1.

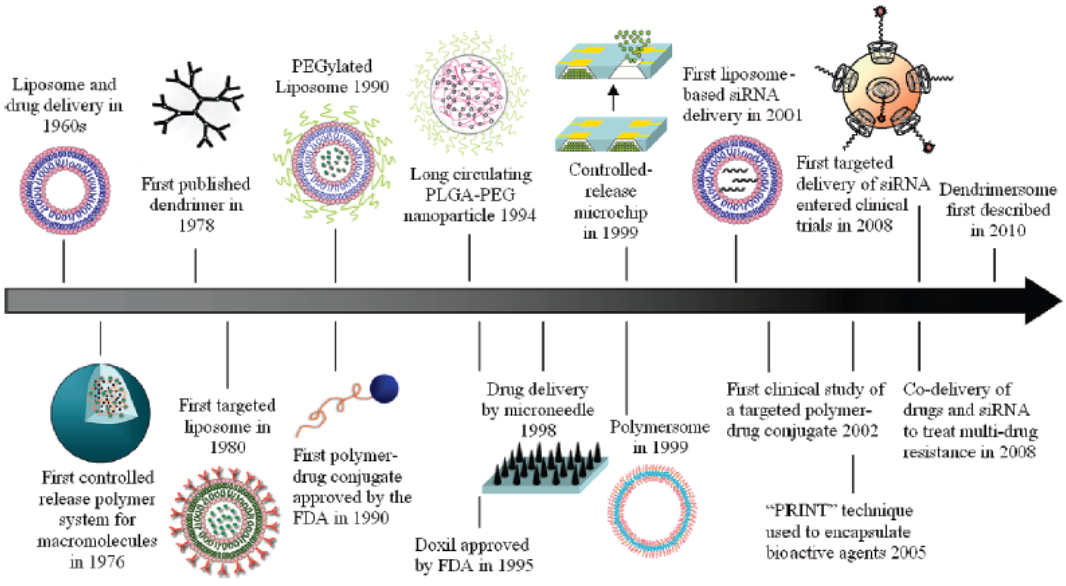

Figure 2.1 Evolution of nanotechnology-based drug delivery systems.[12]

2.3 Core-shell polymeric nanostructures in drug delivery systems

Core-shell nanostructures are classes of materials that consist of two distinct components, the core and the shell, and these are made of different materials and structures (Figure 2.2). The shell of the nanostructures functions as a protecting layer for encapsulated cargo and improves solubility and stability of particles in physiological milieu. It can also be decorated with various functionalities allowing conjugation with biomolecules and specific active compounds onto the nanostructure surfaces. On the other hand, the cores of the nanostructures comprise spaces where drug molecules are stored and protected. It can be designed such that release of guest molecules can be controlled and tailored to suit specific needs.

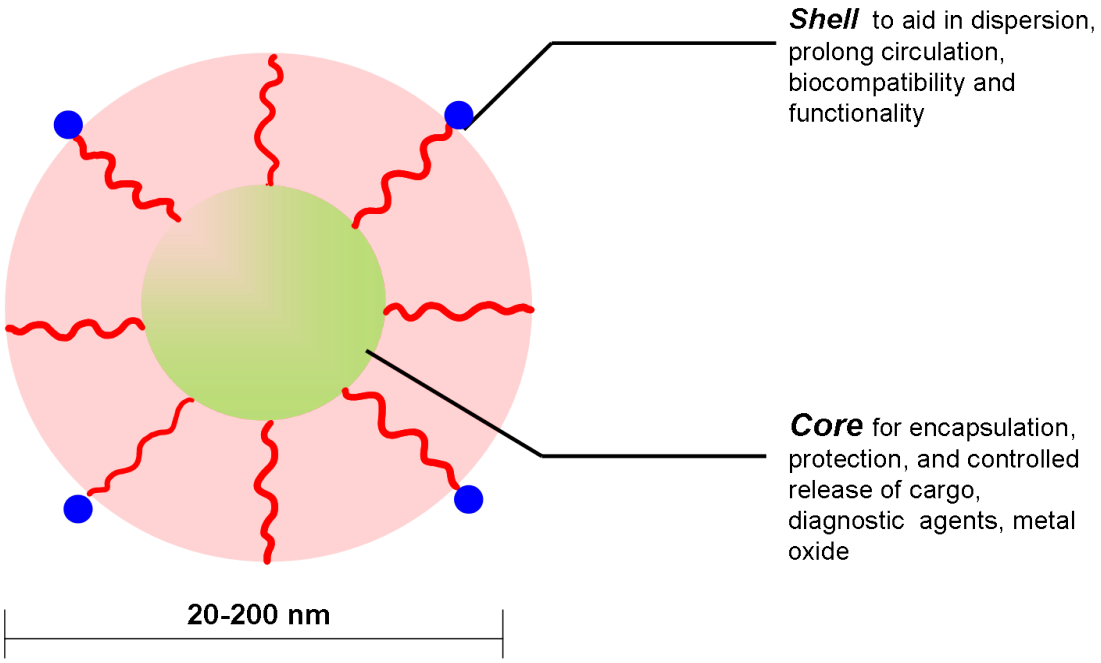

Figure 2.2 Depiction of core-shell nanostructures

Several classes of core-shell nanostructures have been constructed from organic, inorganic, and hybrid organic/inorganic materials. Of particular significance, polymeric micelles whose core and shell are both made of polymers have been widely investigated.[13-15]Polymeric micelles are usually formed by self-assembly of amphiphilic copolymers in a non-solvent system for the hydrophobic domain of the particular polymer. Upon introduction of a non solvent, the polymer chains organize into three dimensional structures where hydrophobic segments aggregate and form a core domain while hydrophilic chains protrude into the aqueous environment forming the corona shell (Figure 2.3). However, the cores of such nanostructures are suitable for loading only hydrophobic molecules.[16, 17]

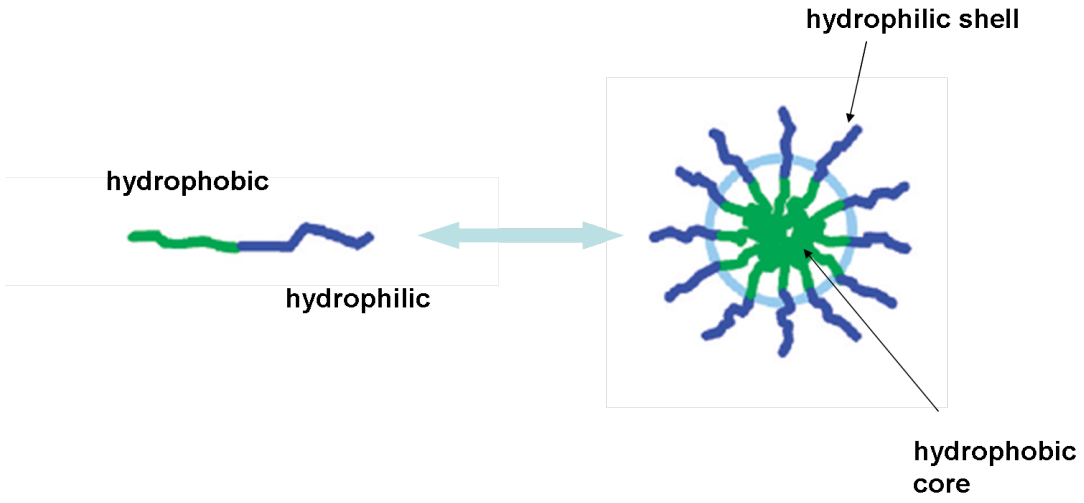

Figure 2.3 Self-assembly of polymeric amphiphiles to form a micelle

There is another class of polymeric core-shell nanostructures whose entire constituents are composed of ionic and nonionic parts. These types of nanocarriers are often called “block ionomer complexes (BICs)” or “polyion complexes (PICs)”. Similar systems of these types were independently pioneered in the mid-1990's by Kabanov

(BICs)[18-21] and Kataoka (PICs).[22, 23] Their investigation focused on block copolymers comprised of a polyelectrolyte block and a nonionic soluble block and showed that such materials could bind electrostatically with molecules of opposite charge to form complexes. They recognized early on that these non-covalently bound complexes formed core-shell structures that were seemingly ideal for encapsulating and releasing charged drugs and therapeutic macromolecules such as proteins or polynucleotides.[19, 22-25] Further research demonstrated that judicious manipulation of their structures expanded their utility to complex with polyions, surfactants, metal ions and oxides as well as proteins and nucleic acids.

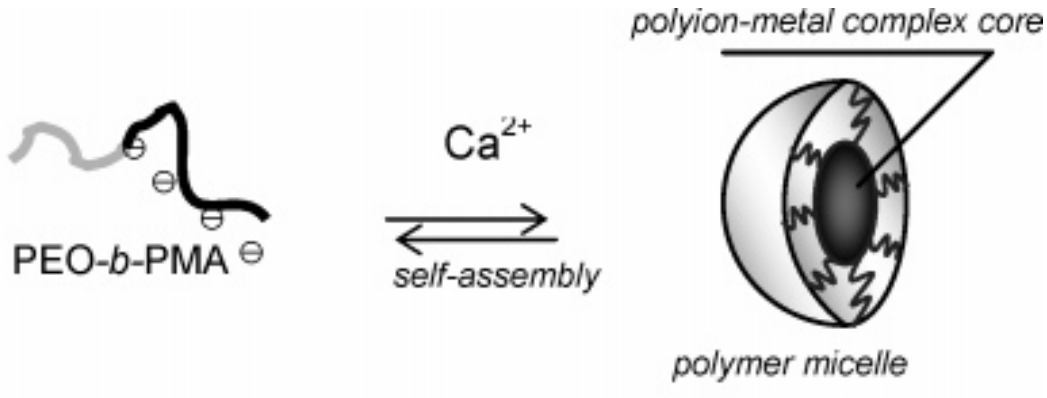

Figure 2.4 Example of block ionomer complexes (BICs) pioneered by Bronich and Kabanov et al.

Hybrid nanostructures consisting of organic/inorganic materials have also been extensively investigated. The particles in this class commonly have metal and metal oxide cores encased within polymer or low molecular weight organic shells (Figure 2.5). Combining the unique properties of inorganic cores with tunable polymeric shells can create multifunctional nanosystems that enable simultaneous advanced diagnostics and delivery. For example, Lee et al. have reported a methodology to form an "all-in-one"

nanoparticle probe that provides both therapeutic delivery and multimodal imaging. In their work, manganese ferrite ($MnFe_2O_4$) nanoparticle probes were conjugated with cancer-cell-specific targeting moieties and fluorescent dyes for delivery of siRNAs. Such development has been shown to be effective in targeting cancer cells *in vitro* as evidenced by enhanced magnetic resonance (MR) and fluorescence imaging as well as increased gene silencing activity (Figure 2.6).[26]

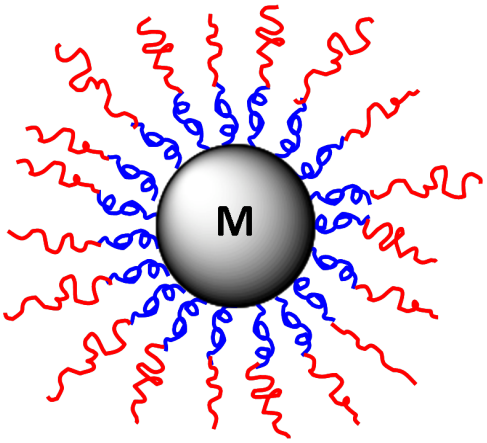

Figure 2.5 Core-shell nanostructures with core containing metal/metal oxide.

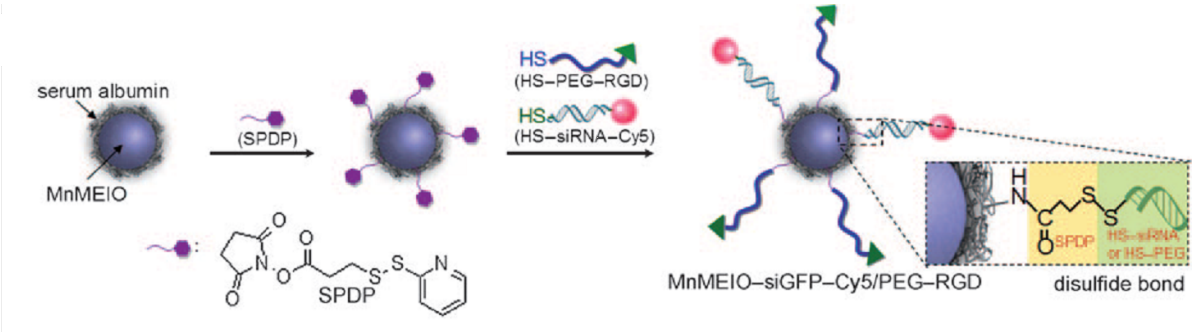

Figure 2.6 Multi-functional core-shell nanostructures with "all-in-one" cell specific targeting, multimodal imaging, and therapeutic delivery

2.4 Intracellular bacterial infections and their complications

Intracellular bacterial infections are especially difficult to eradicate because the bacteria have developed strategies for their survival. The "smart" mechanisms utilized by these bacteria include inhibition of phagosome–lysosome fusion, resistance to attack by the host macrophages, escape from the phagosome into the cytoplasm. Therefore, facultative intracellular bacterial pathogens such as *Salmonella* spp., *Listeria monocytogenes*, *Mycobacterium tuberculosis*, *Brucella abortus* and obligate intracellular pathogens such as *Legionella pneumophila* pose a major threat. Intracellular bacteria are found most often in phagocytic cells, mostly macrophages. However, they also find their venue into other cells such as epithelial cells, hepatocytes and fibroblasts. The facultative intracellular pathogens pose a greater predicament by using macrophages as a reservoir for pathogens leading to the recurrence of systemic infections.

Many intracellular bacteria are inert or dormant, and they These bacteria are can endure for long times without replication.[27] Thus, their susceptibility to antibacterial agents is reduced.[28] Moreover, microorganisms in infected tissues are sheltered by various biological barriers providing increased protection and hence increased resistance to antibacterial agents.[27, 29] The intracellular activity of antibiotics depends on many factors including entry, retention, and intracellular distribution (Figure 2.7). The ratio of the intracellular concentration to the extracellular concentration (C_i/C_e) is the parameter used to classify cellular accumulation of antibiotics. Poor penetration into the cells and decreased activity at the cellular level are major drawbacks and lead to the limited activity of most antibiotics in intracellular infections.

The simple rule in treating the infection is that the antibiotics must reach therapeutic levels at the intracellular site of infection to effectively show bactericidal activity against pathogens. Thus, intracellular infections that are caused by these bacteria are difficult to treat due to their ability to evade the mammalian host phagocytic killing mechanism and establish specialized intracellular niches sequestered from the host immune system.[30, 31, 32] The consequence of both low penetration and poor distribution inside the cells is a major reason for therapeutic failure of aminoglycosides against intracellular bacteria. Intracellular microorganisms reside in different specific locations in host cells (Figure 2.8), and in some cases the complications arise when bacteria relocate during the state of infection.

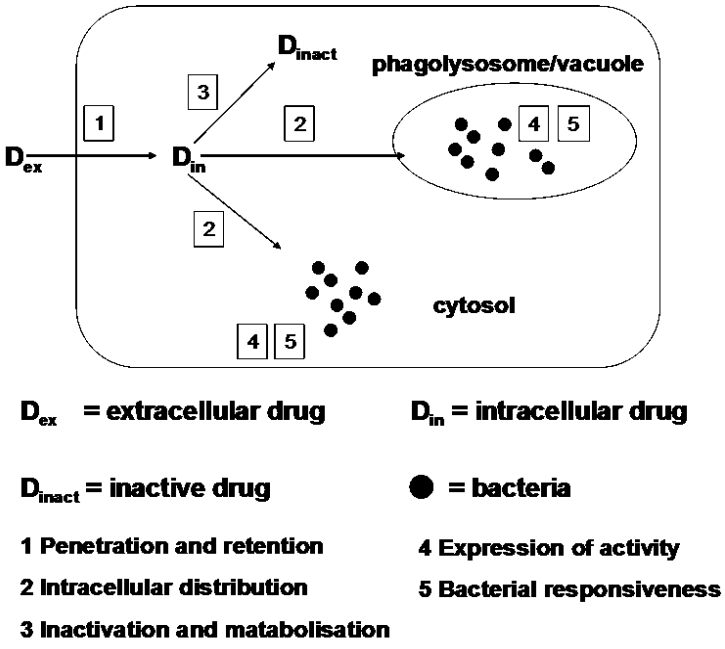

Figure 2.7 Important parameters involved in intracellular activity of antibiotics[33]

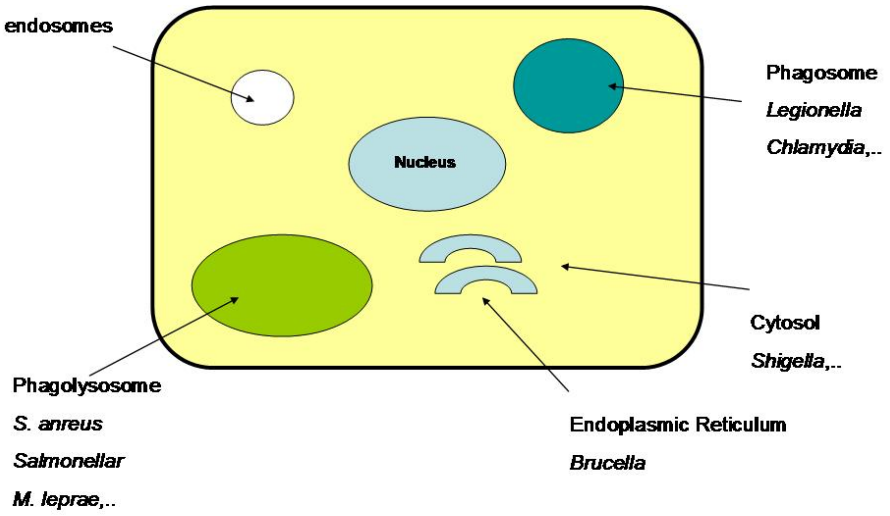

Figure 2.8 Common intracellular compartments that are favorable for survival of bacteria[34]

2.5 Aminoglycoside antibiotics

Aminoglycosides are some of the most commonly used antibiotics in therapies for many bacterial infections. This class of antibiotics is known to have a broad activity against both Gram-negative and Gram-positive bacteria.[35] The history of aminoglycosides began in 1944 with the discovery of streptomycin[36] which promptly accelerated the introduction of a series of several compounds and establishment of this class of antibiotics. Several members of the aminoglycoside antibiotics such as gentamicin, tobramycin, amikacin, kanamycin, streptomycin, neomycin (Figure 2.9) are currently used clinically.

2.5.1 Chemical structure and mechanism of activity

The basic structure of aminoglycosides is an aminocyclitol (1,3-diaminoinositol) linked to other amino sugars via glycosidic linkages. There are four major aminocyclitol

structures that constitute the pharmacophores of aminoglycoside antibiotics. These structures include streptidine, neamine, 2-deoxystreptamine and spectinamine. Among all, 2-deoxystreptamine with subsititutions at the 4, 5 or 4, 6 positions represent the most clinically used compounds. Comprised of amino sugar units, aminoglycosides are strong polar basic molecules. There are positively charged in physiological pH media with formation of ammonium groups.

Most aminoglycosides are bactericidal. Their bactericidal activities are strongly related to the aminocyclitol units. The drugs become inactive without this important structure. Once they internalize into cells to reach the pathogens, they inhibit bacterial protein synthesis by binding to bacterial 30S ribosome subunits with a high affinity for the aminoacyl site of the ribosome ("A-site"), thus interrupting protein translation. As a result, translation is deregulated and this causes incorporation of the wrong amino acids which produce abnormal proteins. The aberrant protein is later utilized by the microorganism to produce a cell membrane, and this leads to permeability alterations that enhance passive transport of drugs and small molecules, and leads to death of the microorganism.[37]

2.5.2 Challenges of aminoglycosides in clinical use

Aminoglycosides are mainly administered parenterally in order to achieve therapeutically adequate serum concentrations. They are highly soluble in water, and after administration, aminoglycosides are primarily distributed within the extracellular fluid and rapidly cleared by the renal system (resulting in short plasma half-lives).[35] The high polar and cationically-charged structure of aminoglycosides is responsible for their

low adsorption by oral routes and poor molecular transport into the central nervous system, bones and conjunctive tissue.[38]

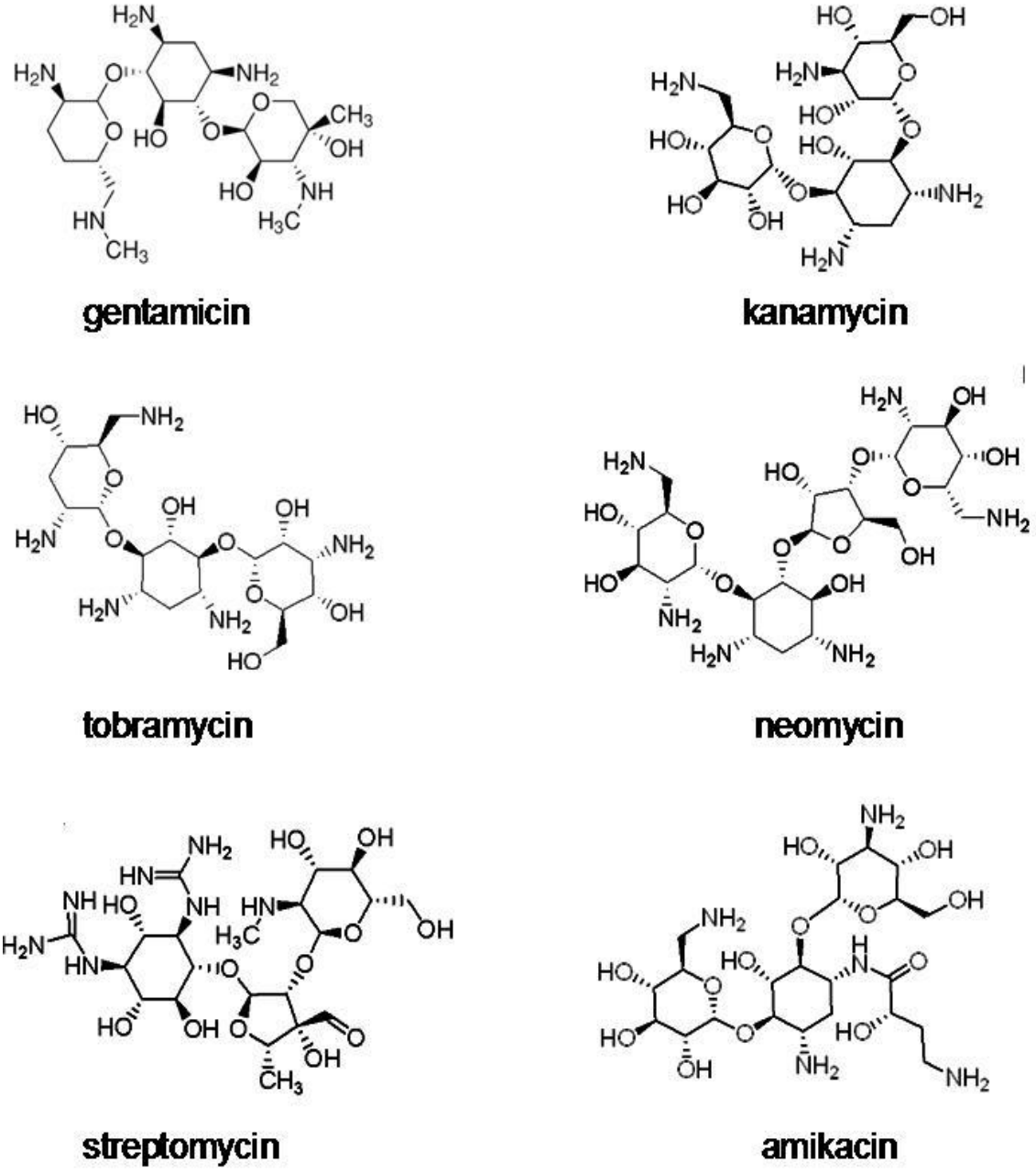

Figure 2.9 Structures of common aminoglycosides

Furthermore, these polar cationic molecules cannot traverse the mammalian host cell membranes efficiently and so they are taken up primarily by endocytosis.[39] This results in high accumulation in endosomes and lysosomes. Hence, the desired intracellular antimicrobial levels for complete clearance of bacteria residing in these specialized niches are not achieved. This results in antimicrobial treatment failure, high incidence of relapse and associated organ toxicity with prolonged treatment.[40] Therefore, it is safe to state that aminoglycosides are very potent but their intracellular activities are severely limited.

Aminoglycosides have potential adverse side effects. The most pronounced potential problems are nepherotoxicity and ototoxicity which are dose-dependent effects. In most cases, nepherotoxicity can be developed after only one week of treatment. The mechanism of renal damage is described by the accumulation of aminoglycosides which rapidly deposit in proximal tubules after systemic administration. The accumulated aminoglycosides thereafter reduce glomerular filtration by several mechanisms including increase in intracellular ions, proteins and enzymes, and this leads to toxic effects including renal failure.

Unlike nepherotoxicity, ototoxicity (damage to hearing organs) is irreversible. The aminoglycosides induce deleterious effects on either auditory or vestibular function by generating free radicals as they form complexes with iron and increasing nitric oxide (NO) levels in vestibular epithelial cells.[41, 42]

Despite the active study of new aminoglycosides, and design for safer molecules, drug delivery and enhancement of dosage should be placed at the heart of the problem.

Safety and enhanced delivery to specific targeted sites will undoubtedly promote the use of aminoglycosides while minimizing problematic effects.

2.5.3 Aminoglycosides and drug delivery systems

With concerns regarding both toxicity and the low therapeutic concentration of aminoglycosides, the use of drug delivery systems has already been employed. The concept of the approach can be simplified by loading therapeutic agents into colloidal carriers, which can carry the drug cargo into the cells and enhance therapeutic activity (Figure 2.10). Another major advantage of antibiotic delivery that one can expect from using carriers is reduced toxicity by avoiding rapid accumulation in the renal system and hearing organs.

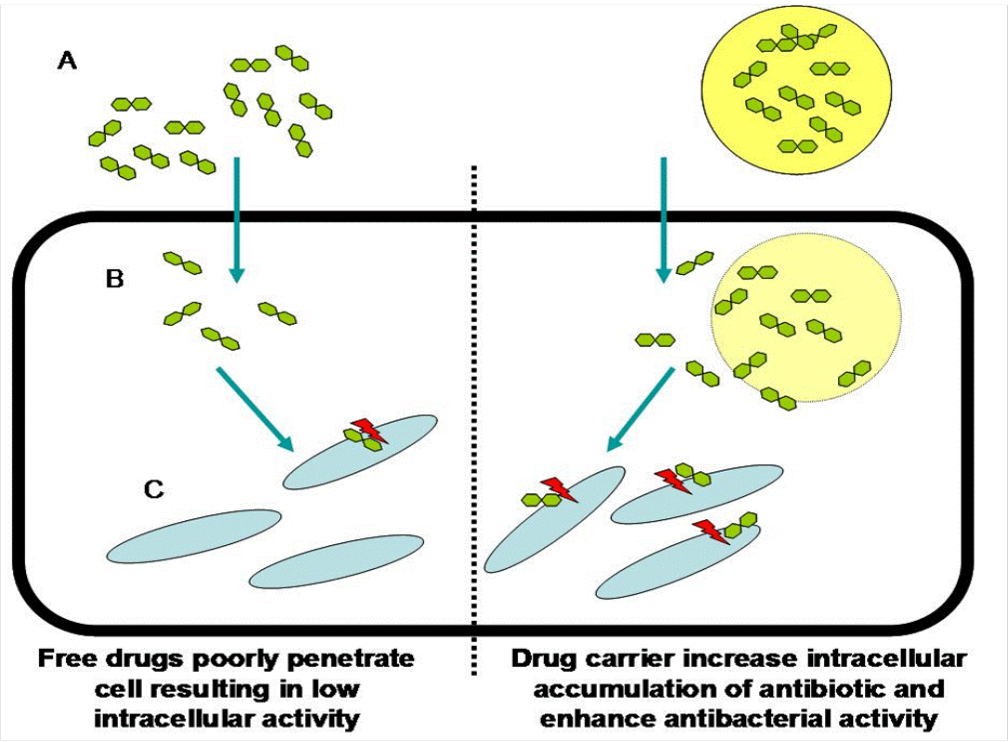

Figure 2.10 Enhanced delivery of aminoglycosides by colloidal carriers

Liposomes

Liposomes are vesicles with a membrane-like structure comprised of one or several lipid bilayers. They generally contain naturally-derived phospholipids with mixed lipid chains or pure surfactant components like dioleoylphosphatidylethanolamine (DOPE). Liposomes usually contain a core of aqueous solution which can be used to encapsulate many water soluble substances including antibiotics. There are at least three major classes of liposomes, with their classifications based on their size and number of bilayers: 1) small unilamellar vesicles (SUV), 2) large unilamellar vesicles (LUV) and 3) large multilamellar vesicles (MLV) or multivesicular vesicles (MVV) (Figure 2.11).

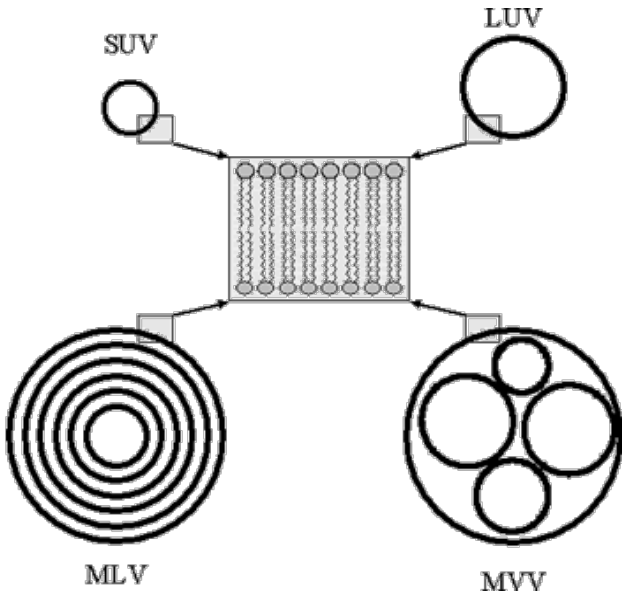

Figure 2.11 General structures of liposomes[43]

SUVs have diameters of 20 to approximately 100 nm. LUVs, MLVs, and MVVs range in size from a few hundred nanometers to several microns. Their lipid bilayer structure is believed to promote good cell interactions due to cell membrane-like structure. Liposome-encapsulated aminoglycosides have been extensively studied for both local

and intravenous administrations. The increased activity of the free aminoglycosides in mouse monocytes, macrophages or bovine mononuclear cells infected with *Brucella*. spp., *M. avium* and *S. aureus* have been demonstrated.[44, 45, 46]

The concentration of incorporated aminoglycosides is generally low and this makes it difficult to encapsulate sufficient drug for therapeutic efficacy.[47, 48, 49] Liposomal approaches, moreover, suffer from their stability issues, both during storage and after injection. Therefore, the process to optimize liposome characteristics remains an issue and needs further improvement to enable practical applications for intracellular delivery of aminogycosides.

Biodegradable microspheres and nanospheres

In past decades, biodegradable microspheres and nanospheres have been widely adopted for a wide variety of therapeutic agents.[50-53] Aliphatic polyesters are well known candidates for use as carriers. Among them, poly(lactide) (PLA), poly(lactide-co-glycolide) (PLGA), and poly(caprolactone) (PCL) (Figure 2.12) have been extensively investigated.

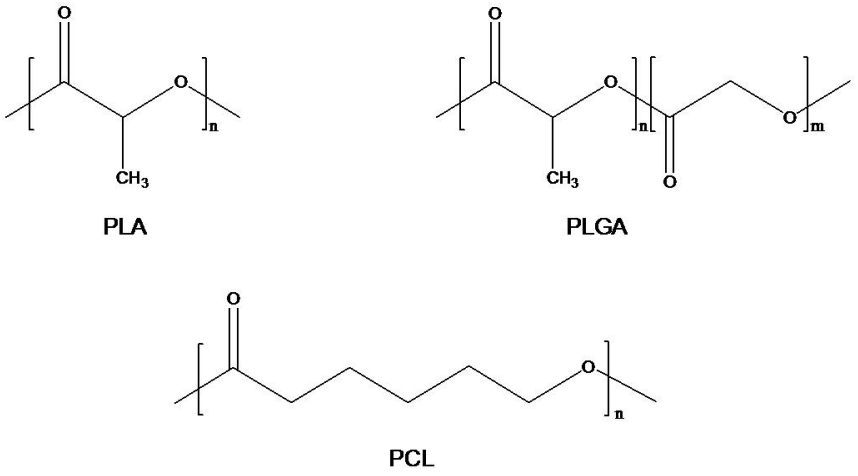

Figure 2.12 Structures of common biodegradable aliphatic polyesters

The main advantage of these biodegradable particles is that they release encapsulated drugs in a sustained manner, depending on the physicochemical properties of the polymer and drug. The polymeric nature of these micropheres/nanospheres also impart more stability compared to liposomes.

Despite the advantages of biodegradable microspheres containing aminoglycosides, only low loading capacities are normally achieved. Encapsulation of aminoglycosides into polyester carriers is carried out by the entrapment of drug molecules during polymer micro/nano precipitation. Several techniques have been employed including emulsion solvent evaporation and spray drying. As mention above, the level of aminoglycosides that can be loaded into polymer carriers is very limited.[40, 54] This obstacle can be explained by the lack of interaction between the hydrophobic polyester and the highly hydrophilic aminoglycosides (causing immiscibility). Therefore, increase hydrophilicity of polyesters favors higher entrapment as it promotes stronger interaction of aminoglycosides and a carrier.[55] Several formulation efforts to improve encapsulation efficiency have been carried out, but the levels of incorporation remain very low and are generally less than 1 wt% of particles. The marked low loading content considerably limits use of these systems. High polymer consumption is needed to achieve the required dose of aminoglycosides for treatment of infections in humans.[56] Apart from low encapsulation capacity, it is worth noting that the lack of therapeutic activity of the aminoglycosides loaded into microspheres has been reported and result in death of animal.[57] The problem has been attributed to inappropriate microsphere size and aggregation, which leads to capillary and pulmonary accumulation rather than distribution throughout infected organs. From this point of view, microspheres with large

sizes are considered to be less suitable in treatment regimes compared to nanoparticles. With sizes less than one micrometer, nanoparticles are more prone to avoid capillary network entrapment.[58]

Mesoporous particles

Several mesoporous materials such as calcium phosphate,[59] bioactive glasses,[60] calcium carbonate nanoparticles,[61] and mesoporous silica nanoparticles[62,63] have been developed and employed for localized (particularly for bone treatment) and controlled drug delivery applications. The drug incorporation in these materials is generally carried out by soaking of matrix in a concentrated drug solution and subsequent drying. Hence, adsorptive properties of mesoporous materials are key to determining the sizes of molecules that can be incorporated in the pores. It has been demonstrated that amiglycosides, particularly gentamicin, can be loaded into porous silica particles with drug loads from 20 to 45 wt%.[64, 65] These impressive drug loading capacities result from the highly porous structure of materials, enabling large volumes of drugs to be encapsulated.

However, in view of intracellular delivery, as far as size of carrier is concerned, mesoporous particles containing aminoglycosides have recently been reported in the range of ten micrometers,[64, 65, 66] and this may notably inhibit cellular internalization.[67, 68] There is another major problem for most of the mesoporous drug delivery systems. Since drug molecules were trapped by physical adsorption, and they are released from the scaffold with a fast initial rate, resulting in high burst release. Since aminoglycosides are highly soluble in water, release of the antibiotics from the ceramic carriers is completely

diffusion dependent. This causes high and premature release. This is a great disadvantage for intracellular delivery which requires drugs to be released mainly inside the cells. Stimuli-responsive mesoporous materials have been of great interest in recent years. The trigger mechanisms including pH, temperature, and light have been actively investigated and the approaches have been constituted as hybrid systems.[69, 70]

Macromolecular polyelectrolyte microcapsules

Electrostatic complexation of oppositely-charged species is well-known and exemplifies an attractive approach for self-directing macromolecular assembly. Significant systems have been developed such as layer-by-layer (LbL) deposition, membranes with unique separation properties for micro/nanoencapsulation, and DNA condensation.[71-77]

Aminoglycosides have been incorporated into polyanion-based implant materials.[78, 79] However, attempts to form electrostatically-derived polyplexes of antibiotics and polyanions with micro/nano-scale particles have not been successful. Simple mixing of oppositely charged aminoglycosides and polyelectrolyte solutions leads to difficulties in controlling the size and colloidal stability and results in eventual aggregation.[80, 81] Nonetheless, the strategy of charge complexation has been demonstrated to yield high drug loading. Gentamicin, in particular, was encapsulated into polyplex carriers at up to 44 % of total complex weight.[80]

Recently, the LbL technique with polyelectrolytes has been integrated with the use of sacrificial colloidal templates.[82-87]. In this process, ultrathin microcapusules with different pairs of polyelectrolyte building blocks can be prepared after core removal (Figure 2.13).

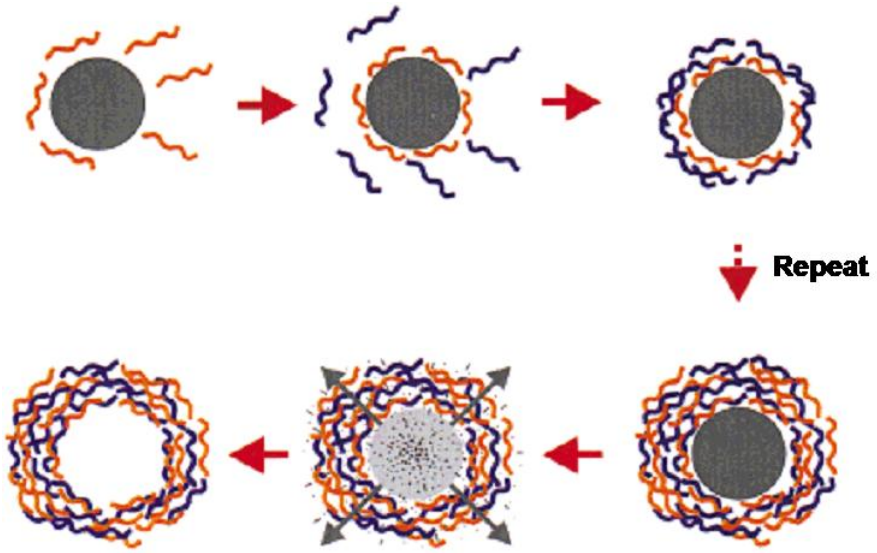

Figure 2.13 Schematic illustration of microcapusule formation via polyelectrolyte deposition and subsequent core removal

Selecting suitable core templates and the number of layers to be deposited can precisely control particle sizes and thicknesses of capsules. LbL assembly onto colloidal particles is not limited to other applications. Incorporating various charged organic/inorganic dyes has already been established.[88]

Since aminoglycosides are polycationic in nature, they can be implemented into polyelectrolyte microcapsules with remarkable loading as high as 60 wt% wt.[89] The fascinating features of the techniques not only include precisely controlled particle sizes but also tunable release of the antibiotics.[79, 89] The latter can be achieved by regulating the number of deposited layers and type of polyelectrolytes. This is a great advantage as controlled release is of prime importance in treatment of infectious diseases.

Despite all that this unique technique offers, there is one possible barrier that may limit the use of microcapsules parenterally, and this is the non-biodegradability of most

polyelectrolytes. Thus, development of more biodegradable polyions will unquestionably open more channels for utilizing microcapsule platforms.

2.6 Magnetic iron oxide nanoparticles in biotechnological applications

Magnetic nanoparticles, especially magnetite (Fe_3O_4), when coated with biocompatible macromolecules, are of great interest in a wide range of potential biomedical applications including targeted drug delivery, retinal detachment therapy, cell separations and contrast-enhanced magnetic resonance imaging (MRI).[90-95] Hydrophilic macromolecules such as poly(ethylene oxide) (PEO) and dextran have been widely used to stabilize magnetic nanoparticles since they afford water solubility, optimum size and biocompatibility for *in vivo* applications.

2.6.1 Synthesis of magnetitc nanoparticles

Different methods have been developed to synthesize magnetic nanoparticles for biomedical applications. The main challenge consists of defining experimental conditions that produce narrow particle size distributions with suitable size. The second critical parameter is to select a reproducible process that can be implemented on an industrial scale without any complex purification process. The most common procedure is the chemical co-precipitation of aqueous iron salts in the presence of strong bases such as ammonium hydroxide or sodium hydroxide.[96, 97] The chemical reaction of magnetite formation can be written as shown in equation 1.

$$Fe^{2+} + 2Fe^{3+} + 8OH^- \rightarrow Fe_3O_4 + 4H_2O \qquad (1)$$

According to the thermodynamics of this reaction, complete prepcipitation of magnetite should be expected at pH's of 8 to 14, with a stoichiometric ratio of 2:1 Fe^{3+}/Fe^{2+} in the

absence of oxygen or other oxidizing agents.[98] Magnetite is prone to oxidation and transformed into maghemite (γ-Fe_2O_3) in the presence of oxygen.

The main advantage of the co-precipitation (of iron salts) technique is that a large amount of nanoparticles can be prepared easily and economically. However, control of particle size distribution is limited and aggregates and clusters are commonly obtained (Figure 2.14).

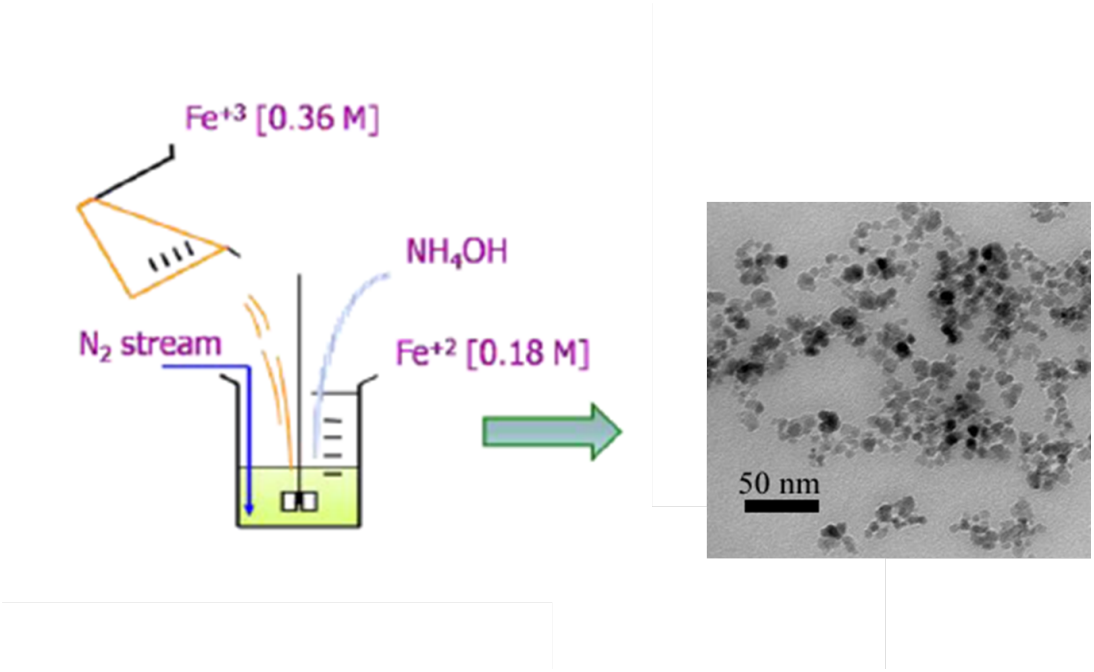

Figure 2.14 Illustration of the formation of small clusters of magnetic nanoparticles after synthesis by the co-precipitation method

Given that the co-precipitation method generates particles with a broad size distribution and aggregation, other approaches have been developed to produce particles with more uniform dimensions. Calero et al. have reported the synthesis of magnetic nanoparticles using reverse micelle templates to improve upon control over size and prevent aggregation.[99] In this methodology sodium bis(2-ethylhexyl)sulfosuccinate (AOT) was

used as a surfactant to form reverse micelles, allowing separation of the aqueous phase from the bulk organic media. Formation of cobalt ferrite nanoparticles was achieved at room temperature after mixing a solution of reverse micelles containing a mixture of metal salts (Fe^{+3} : $2Co^{+2}$) with a solution of reverse micelles containing the precipitating agent (NH_4OH). The nanoparticles had a narrow size distribution, but were highly hydrophobic due to condensation of the AOT surfactant onto the nanoparticle surface.

To effectively produce monodisperse magnetic nanoparticles, the nucleation and growth step must be separated. Sun et al. was first to pioneer a high-temperature reduction of iron(III) acetylacetonate with 1,2-hexadecanediol in the presence of oleic acid and oleylamine in a high boiling point solvent like benzyl ether (b.p. 300 ^{o}C) to obtain monodisperse magnetite nanoparticles.[100] In this method, oleic acid and oleylamine were used as surfactants while alkane-diol species was utilized as the reducing agent.

Other high boiling point solvents have been explored, especially when the solvent itself can act as the reducing agent to control growth of the particles. Pinna et al. reported synthesis of magnetite nanoparticles with high crystallinity and magnetization by decomposing iron(III) acetylacetonate in benzyl alcohol at the relux temperature of 205 ^{o}C.[101] The particles were fairly narrowly dispersed and could be made soluble in organic solvents or water by coating with appropriate ligands.

2.6.2 Modifications to afford water soluble magnetic nanoparticles

One of the main challenges for utilizing magnetic nanoparticles in biomedical applications is to prepare water dispersible particles which exhibit good colloidal stability in physiological media. Several approaches have been developed to coat iron oxide

nanoparticles, including in situ coating and post-synthesis coating. In the first approach, particles were coated during the synthesis. For example Josephson et al. reported a co-precipitation process in the presence of dextran. The post-synthesis coating method consists of grafting the polymer onto the particles after they were synthesized. In both cases, polymers commonly contain functional groups like carboxylate, amine, sulfonate, or phosphate which can bind to the surface of iron oxide via electrostatic attraction and chelation. Various polymeric materials or surfactants have been used to produce water dispersible polymer-iron oxide nanoparticle complexes. In the literature reported so far, the most common materials are dextran, carboxymethyl dextran, starch, sulfonated styrene-divinyl benzene, polyethylene glycol (PEG), polyvinyl alcohol (PVA), poloxamers, and polyoxamines.[102-104]

2.6.2.1 Polysaccharides

Dextran is a polysaccharide polymer comprised exclusively of α-D-glucopyranosyl units with varying degrees of chain length and branching. Molday and Mackenzie were the first to report formation of magnetite in the presence of dextran.[105] Ferumoxtran-10 and ferumoxides are prepared by the Molday co-precipitation method with *in situ* coating by dextran. The same process is used for Ferucarbotran® and ferumoxytol with *in situ* coating by carboxymethyl dextran, respectively. Ferumoxtran-10™, which has a small hydrodynamic diameter (15-30 nm), and Ferumoxytol™ (hydrodynamic diameter of 30 nm) show prolonged blood residence times, which allows these USPIOs to access macrophages located in deep and pathologic tissues (such as lymph nodes, kidney, brain, osteoarticular tissues, etc. However, the dextran molecules can be desorbed from the iron oxide surface by heating or dilution.[106, 107] Efforts to avoid

desorption of dextran include reacting it with a crosslinking agent such as epichlorhydrin.[108]

Another polysaccharide of interest for coating onto magnetite is an alginate, an electrolytic polysaccharide with many carboxyl groups. Researchers have speculated that the COO- of the polyalginate and iron ion would interact and that the electrostatic repulsion may make the superparamagnetic iron oxide nanoparticles (SPIONs-alginate) stable. Recently, several investigations dealing with the preparation of iron oxide nanoparticles with alginate have been carried out.[109, 110] The chemical synthesis consists of three steps: (a) gelation of alginate with ferrous ions, (b) *in situ* precipitation of ferrous hydroxide through alkaline treatment of alginate, and (c) oxidation of ferrous hydroxide with an oxidizing agent such as O_2 or H_2O_2. This method is, however, complex. Ma et al. have developed a new modified two-step co-precipitation method.[111] Their results revealed that typical iron oxide nanoparticles were Fe_3O_4 with a core diameter of 5-10 nm and that SPIONs-alginate had hydrodynamic diameters of 193.8 - 483.2 nm indicating agglomerations of particles.

In addition to anionic polysaccharides, chitosan is one of the most abundant biopolymers to be used as coating agents for iron oxide nanoparticles. Chitosan is an alkaline, nontoxic, hydrophilic, biocompatible, and biodegradable polymer. Therefore, preparations of magnetic nanoparticles encapsulated in chitosan are of great interest.[112] Kim et al. have synthesized SPIO by a sonochemical method.[113] They synthesized ferrofluids for use as MRI contrast agents by coating them with oleic acid as a surfactant and then dispersing them in the chitosan, which is a suitable carrier for bioapplications. These spherical particles of about 15 nm in diameter showed superparamagnetic

behavior. Microspheres comprised of superparamagnetic iron oxide nanoparticles and chitosan were developed as a novel MRIdetectable embolic material. Lee et al. have prepared spherical SPIO nanoparticles about 15 nm in radius by sonochemistry and embedded them in chitosan to synthesize a ferrofluid. The SPIO-chitosan microspheres showed a strong enhancement of MR image contrast *in vitro.*[114]

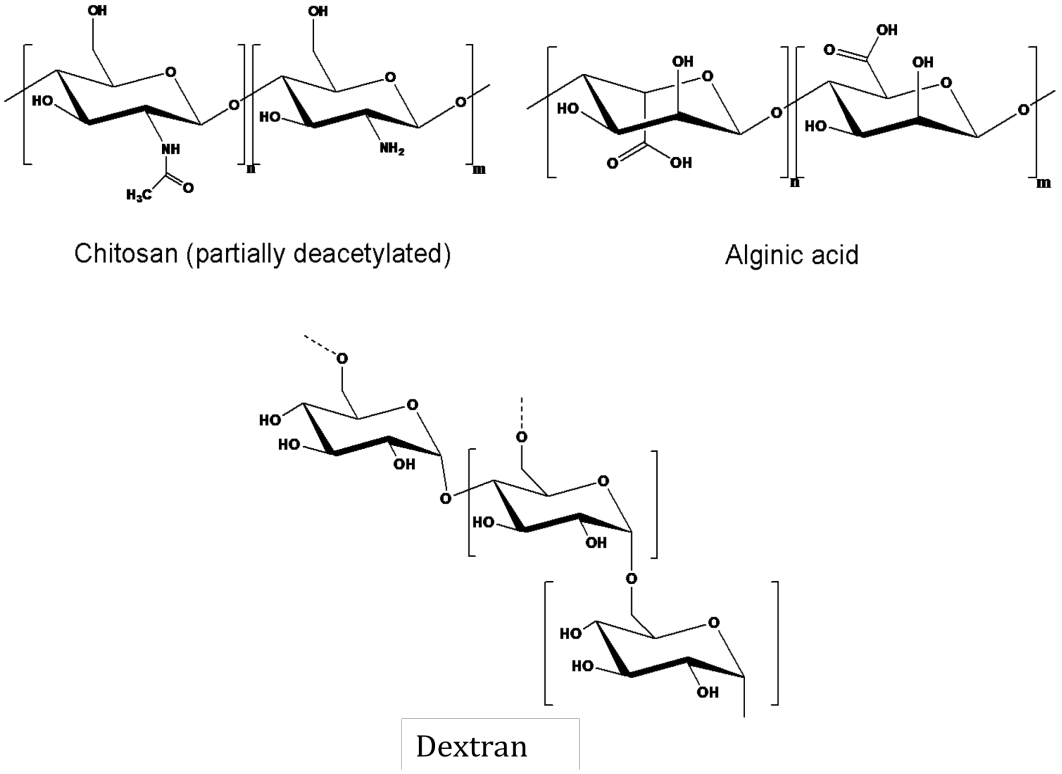

Figure 2.15 Chemical structures of polysaccharides that have been used to coat magnetic iron oxide nanoparticles

2.6.2.2 Polyethylene oxide (PEO)

PEO is a hydrophilic, water-soluble, biocompatible polymer. Several investigations have reported the use of PEO to increase the biocompatibility of the iron oxide dispersions and blood circulation times.[115, 116] PEO has been investigated as an agent to resist protein adsorption, to promote non-antigenicity, and as biocompatible

components of many devices or delivery systems. Some studies have shown that this polyether reduces nonspecific protein adsorption in addition to macrophage clearance, thus allowing nanoparticles to traverse cell membranes.

Harris et al. developed a series of triblock copolymers containing PEO tail blocks with carboxylic acid functional polyurethane central anchor blocks.[117] The research focused on developing magnetite complexes coated with hydrophilic stablizers for dispersion in aqueous media. They investigated various tail and central block molecular weights to obtain the maximum concentration of magnetite in the overall polymer-magnetite complex.

Recently, it has been shown that phosphonate-functionalized PEO has more superior adsorption on magnetite surface relative to PEO with carboxylate and ammonium functionalities. This novel phosphonate end group has been shown to improve colloidal stability of polymer-magnetite complexes in physiological media.[6]

2.6.2.3 Thermosensitive polymers

Polymers that exhibit an environmental response to changes in pH or temperature are attractive for biomedical applications.[118, 119] Thermo-responsive hydrogels, such as those based on poly(N-isopropylacrylamide) (pNIPAM) are of interest in biotechnology. pNIPAM exhibits a phase transition at 32 ^{o}C, changing from a hydrophilic state to a hydrophobic state at this so-called lower critical solution temperature (LCST).[120] At this temperature the enthalpic contribution of water hydrogen-bonded to the polymer chain decreases, which results in loss of bound water to the bulk solution as illustrated in Figure 2.16.

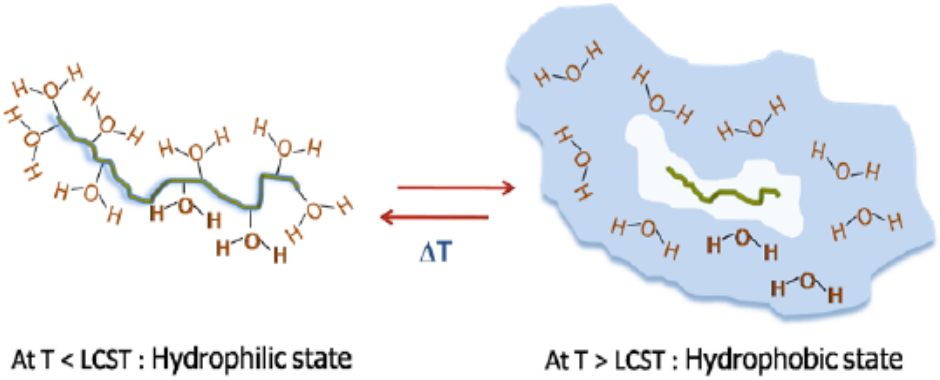

Figure 2.16 Transition of a thermosensitive polymer chain

The phase transition point of pNIPAM can be shifted above 32 °C through incorporation of hydrophilic co-monomers of N-alkylacrylamide based materials, and this may enable the use of this thermo-responsive polymer in biomedical applications such as drug delivery. In this application, the hydrogel is first swollen in an aqueous solution containing a drug at a temperature below the LCST. Drug release is reportedly achieved when the hydrogel is exposed to a temperature increase above the LCST, which causes a contraction in the hydrogel structure.[118, 120] The combination of pNIPAM hydrogels with magnetic nanoparticles leads to formation of functional materials may be able to merge magnetic properties with the thermo-responsive effect.[121] In such systems, temperature increase may be attainable through application of an oscillating magnetic field.

2.7 Atom transfer radical polymerization (ATRP)

ATRP methods for controlled free radical polymerization have primarily been developed by Matyjaszewski et al..[122, 123] ATRP can be mediated by numerous redox-active transition metal complexes (Cu has been the most often used transition metal but other studied metals include Ru, Fe, Mo, Os)**.**

2.7.1 Mechanism

ATRP relies on fast initiation, fast deactivation, and a low stationary concentration of radicals to expand the lifetime of the polymer chain, resulting in increased control over the final polymers.[124, 125] Activated alkyl halides (RX) function as the initiators, and homolytic cleavage of the carbon–halogen bond, with rate constants k_a^0 and k_a, is promoted by a low oxidation state transition metal complex (Mt^nLY), forming a higher oxidation state metal and an active radical species ($XMt^{n+1}LY$). The active radical adds monomer (k_i and k_p) until it is deactivated (k_d^0 and k_d), forming the dormant species and regenerating the lower oxidation state metal complex (Figure 2.17). If the concentration of radicals is low enough, the contribution of termination (k_t^0 and k_t) can be neglected.[126]

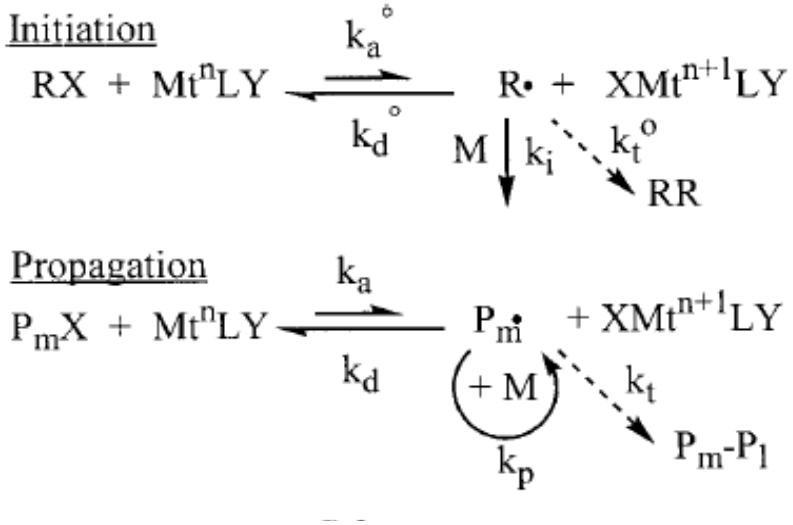

Figure 2.17 Schematic mechanism of ATRP

Various monomers have been polymerized using ATRP: styrenes, (meth)acrylates, (meth)acrylamides, dienes, acrylonitrile, and other monomers which contain substituents that can stabilize the propagating radicals. The product of k_p and the equilibrium constant (k_a/k_d) essentially determines the polymerization rate. ATRP will occur very slowly if the equilibrium constant is too small.[127, 128] Therefore, polymerization of less reactive monomers such as olefins, halogenated alkenes, and vinyl acetate has been less successful. Because each monomer has a specific equilibrium constant, optimal conditions for polymerization that include concentration and type of the metal species, temperature, ligands, and solvent may be quite different.

The metal reaction promoters in ATRP are important. It is a key to ATRP since it determines the position of the atom transfer equilibrium and the dynamics of exchange between the dormant and active species.[129]

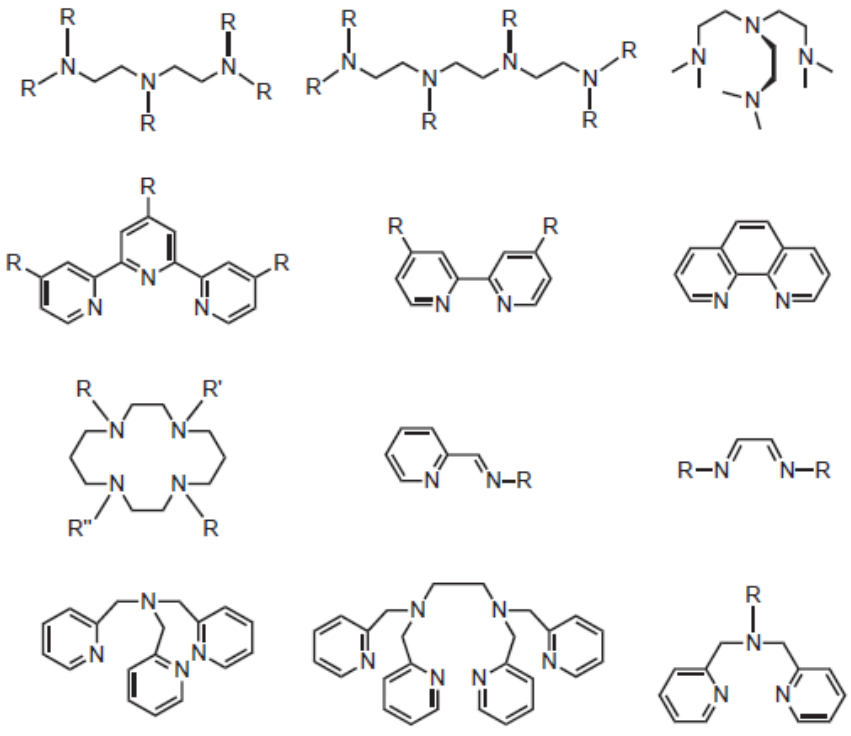

Figure 2.18 Common ligands for copper-mediated ATRP

There are several prerequisites for an efficient transition metal species. First, the metal center must have at least two readily accessible oxidation states separated by one electron. Second, the metal center should have reasonable affinity toward a halogen. Third, the coordination sphere around the metal should be expandable upon oxidation to selectively accommodate a (pseudo)-halogen. Fourth, the ligand should complex the metal relatively strongly. Eventually, the position and dynamics of the ATRP equilibrium should be appropriate for the particular system. The most studied ligands to date are shown in Figure 2.18.

2.7.2 Control of functionality

Functional groups can be incorporated into ATRP polymers in three different ways: (a) Use of functional ATRP initiators to introduce functionality at the chain end and the chain centre, (b) Direct polymerization of functional monomers provides functional groups along the backbone, and (c) Chemical transformation of the alkyl halide endgroup using nucleophilic substitution, or radical or electrophilic addition. These modifcations can be followed up further by coupling techniques. Lutz et al. have demonstrated the versatility of polymers with azido endgroups and utilized [3+2] cyclo-addition or "click" chemistry to incorporate various functional groups and biomolecules into polymers prepared by ATRP.[130] Efficient end-group modification can also be done by other chemical routes as summarized in Figure 2.19.

2.7.3 Control of molecular architecture

ATRP allows the synthesis of polymers with targeted composition, controlled molecular architecture, predetermined molecular weight with narrow distribution.[131, 132] The chain topologies include statistical, gradient and segmented (block or graft)

copolymers (Figure 2.20). Pukala et al. have reported synthesis of well-controlled gradient copolymers by ATRP which are not accessible by other polymerization techniques.[133] Furthermore, by choosing multi-functional initiator and monomers, the chain architecture can be varied in a controlled manner to include combs, brushes, multi-arm stars and dendritic macromolecules with controlled degrees of branching (Figure 2.21)

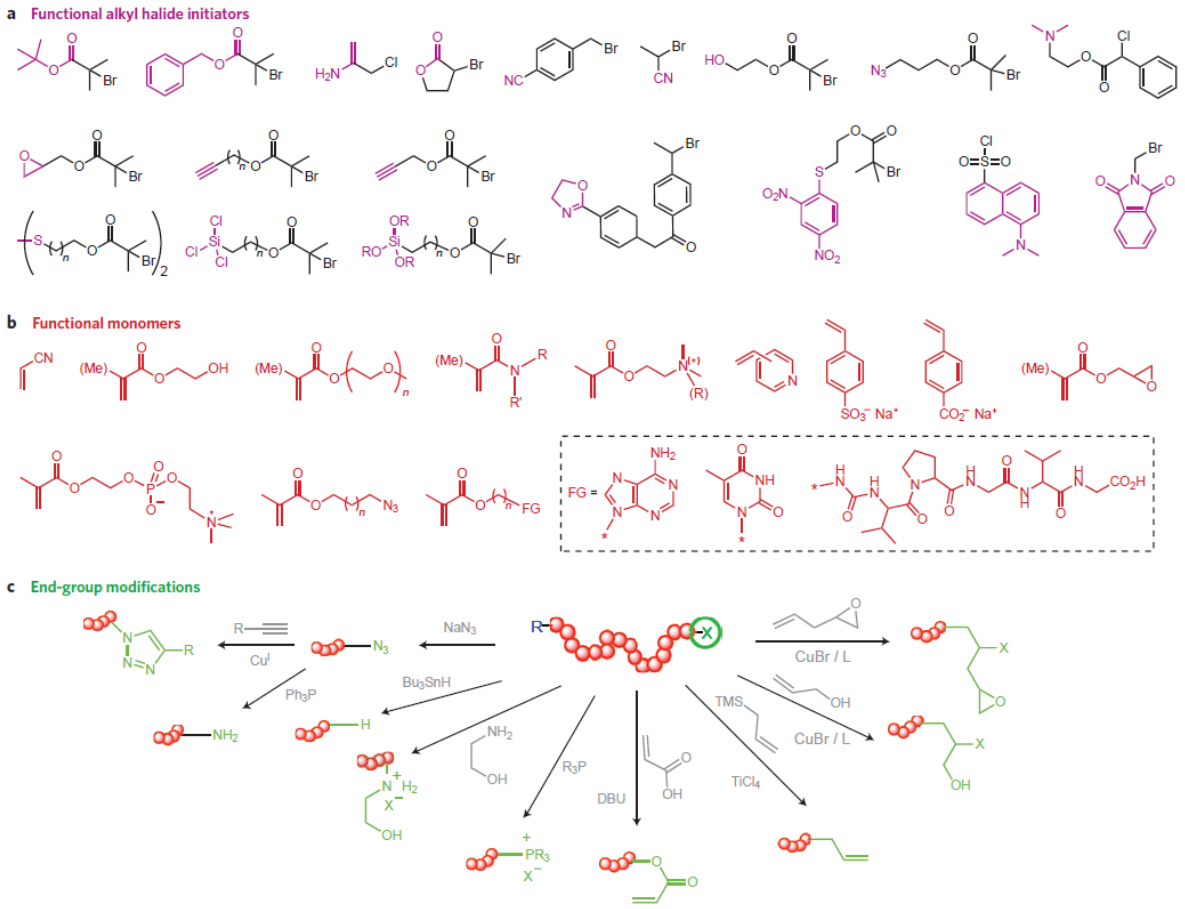

Figure 2.19 Introduction of functional groups of polymers prepared by ATRP

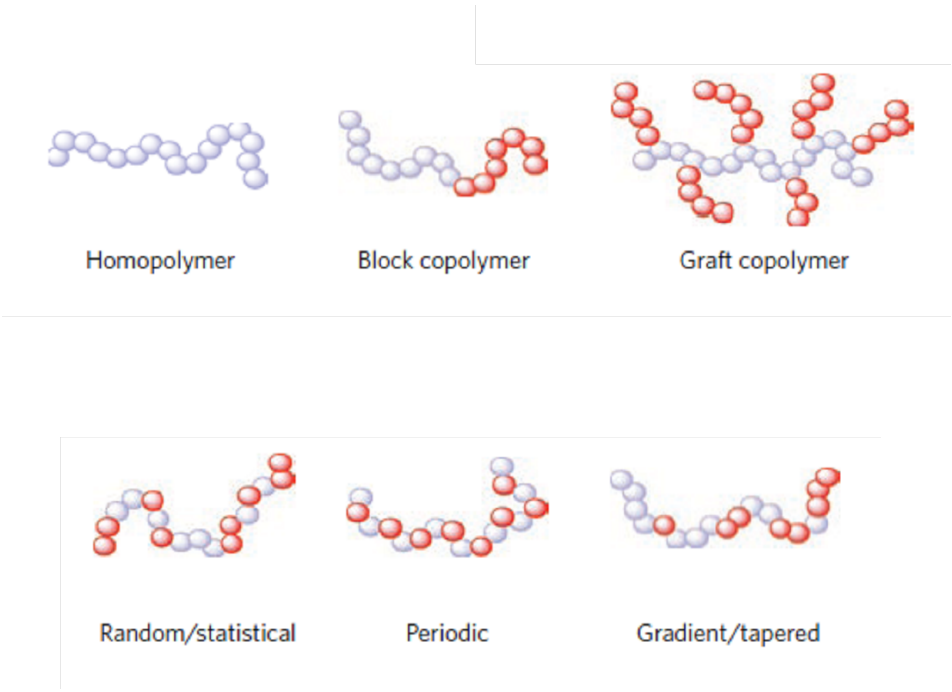

Figure 2.20 Controlled microstructure and composition of polymers prepared by ATRP

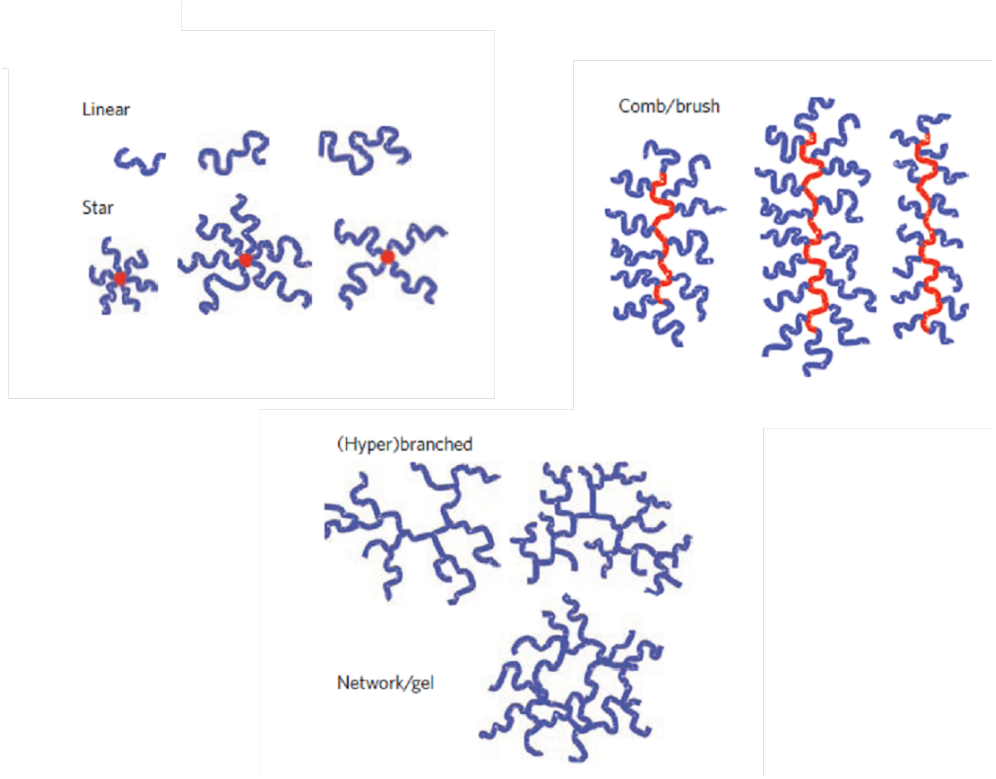

Figure 2.21 Control of polymer topology

Chapter 3

Development of amphiphilic core-shell nanostructures encapsulating gentamicin and their efficacy against *in-vitro Salmonella* and *Listeria* intracellular infection models

3.1 Synopsis

In this chapter, we describe the synthesis of block ionomers and their use in fabricating core-shell nanostructures containing gentamicin. Copolymers of polyacrylate-polyether (PAA-*b*-PEO-b-PPO-*b*-PEO-*b*-PAA and PAA-*b*-PEO) were synthesized and used as polymeric carriers. A methodology for encapsulating aminoglycoside antibiotics, particularly gentamicin, into colloidal drug carriers with core-shell nanostructures has been developed for treating salmonellosis and listeriosis. The assemblies comprised a polyacrylate-aminoglycoside core surrounded by hydrophilic poly(ethylene oxide) (PEO) or amphiphilic poly(ethylene oxide-*b*-propylene oxide-*b*-ethylene oxide) (PEO-*b*-PPO-*b*-PEO) shells. High concentrations of the drugs (~25 wt%) were incorporated into the cores of these complexes through cooperative electrostatic attractions among carboxylates on the polyacrylate and ammonium ions on the drugs. Enhanced *in vitro* efficacies of these amphiphilic nanostructures in reducing intracellular *Salmonella* were demonstrated.

3.2 Experimental

3.2.1 Materials

The chemicals were purchased from Sigma-Aldrich unless otherwise noted. *Tert*-butyl acrylate (98%) was fractionally distilled from calcium hydride under reduced

pressure and sealed under nitrogen prior to use. Copper (I) bromide (98%), N-N'-N'-N"-N"-pentamethyldiethylenetriamine (PMDETA, 97%), triethylamine (99%), 2-bromoisobutyryl bromide (98%), monobasic potassium phosphate, dibasic sodium phosphate, potassium chloride, sodium chloride, boric acid, sodium hydroxide, *o*-phthalaldehyde solution in water (1 mg/mL), and mercaptoethanol (98%) were used as received. Trifluoroacetic acid (Alfa-Aesar, 98%) was used as received. Poly(ethylene oxide) (M_n ~2,000 g mol^{-1} from ^1H NMR) and Pluronic P85™ (BASF, M_n ~4,600 g mol^{-1} from SEC) was dried at 70 °C under reduced pressure for 24 h prior to use. Toluene (Fisher, HPLC Grade) was sparged with nitrogen for 1 h prior to use. Tetrahydrofuran (Fisher, HPLC Grade) was dried and distilled from sodium and benzophenone under a nitrogen atmosphere prior to use. Hexane, dichloromethane, chloroform, diethyl ether and isopropanol (Fisher, all HPLC grade) were used as received. Gentamicin sulfate (Bioworld, neat salt, 590 μg gentamicin per mg) was used as received. Fluorescence N-hydroxy succinamide (NHS) was purchased from Thermo Scientific (IL, USA)

3.2.2 Synthesis of block copolymer carriers

Block copolymers were synthesized via controlled Atom Transfer Radical Polymerization (ATRP) through a method adapted from the literature.[134, 135]

Synthesis of PAA_{26}-PEO_{26}-PPO_{41}-PEO_{26}-PAA_{26}. Dry Pluronic P85™ triblock copolymer (*HO-PEO-b-PPO-b-PEO-OH,* 10.16 g, 2.20 x 10^{-3} mol), was dissolved in 100 mL of dry THF in a 250-mL flame-dried, round-bottom flask equipped with a stir bar. Triethylamine (0.920 mL, 6.60 x 10^{-3} mol) was added to the reaction flask and the solution was stirred and cooled to 0 °C using an ice water bath. 2-Bromoisobutyryl bromide (0.820 mL, 6.61 x 10^{-3} mol) was charged to the flask and the solution was stirred

for 20 min. The ice bath was removed and the reaction was stirred at ambient temperature for 24 h. The triethylammonium bromide salts were removed via gravity filtration and the THF was removed via rotary evaporation. Br-PEO-*b*-PPO-*b*-PEO-Br was re-dissolved in 100 mL of dichloromethane and washed twice with DI water. The organic layer was collected and the polymer in dichloromethane was concentrated via rotary evaporation and then precipitated into a 50:50 v:v hexane:diethyl ether mixture. The white precipitate was collected and dried under reduced pressure at 40 °C for 24 h.

In a 100-mL flame-dried Schlenk flask equipped with a stir bar, the brominated Pluronic P85™ (Br-PEO_{26}-PPO_{41}-PEO_{26}-Br, 2.0 g, 4.08 x 10^{-4} mol) was dissolved in 4 mL of nitrogen-sparged toluene. *Tert*-butyl acrylate (3.65 g, 2.85 x 10^{-2} mol) was charged to the flask followed by addition of PMDETA (0.071 g, 4.08 x 10^{-4} mol) and then the mixture was freeze-thawed twice. The Schlenk flask was opened under a nitrogen purge, and Cu(I)Br (0.058 g, 4.08 x 10^{-4} mol) was charged to the flask. The solution was resealed with a septum and was freeze-thawed twice. The reaction was allowed to proceed for 12 h at 80 °C. The resultant PtBA-PEO_{26}-PPO_{41}-PEO_{26}-PtBA was dissolved in 100 mL of dichloromethane and the solution was passed through a neutral alumina column twice to remove the copper/ligand complex. The dichloromethane was removed via rotary evaporation, then the PtBA-PEO_{26}-PPO_{41}-PEO_{26}-PtBA was dried at 40 °C overnight under reduced pressure.

In a 250-mL round-bottom flask, $PtBA_{26}$-PEO_{26}-PPO_{41}-PEO_{26}-$PtBA_{26}$ (2.0 g, 1.57 x 10^{-4} mol based on ^{1}H NMR, 9.45 x 10^{-3} mol *t*-butyl groups) was dissolved in 70 mL of dichloromethane. Trifluoroacetic acid (10.77 g, 9.45 x 10^{-2} mol) was charged to the flask with a 10:1 mole ratio of acid to *t*-butyl groups. The solution was stirred at room

temperature for 24 h. The deprotected pentablock copolymer, PAA_{27}-PEO_{26}-PPO_{41}-PEO_{26}-PAA_{27} in dichloromethane was precipitated into hexane and dried in vacuum. The copolymer was re-dissolved in 10 mL THF and placed in a 3,500 g mol^{-1} MWCO cellulose acetate dialysis bag to remove excess monomer and acid. The solution was dialyzed against 4 L of deionized water for 48 h, changing the DI water each day. The copolymer was freeze-dried to remove the DI water.

Synthesis of CH_3O-PEO_{45}-PAA_{110}. In a 250-mL flame-dried round-bottom flask equipped with a stir bar, CH_3O-PEO_{45}-OH (10.0 g, 5.0 x 10^{-3} mol) was dissolved in 100 mL of dry THF. Triethylamine (1.40 mL, 1.0 x 10^{-2} mol) was charged to the flask and the solution was stirred and cooled to 0 °C using an ice water bath, after which 2-bromoisobutyryl bromide (1.24 mL, 1.0 x 10^{-2} mol) was charged to the reaction flask and the solution was stirred for 20 min. The ice water bath was removed and the reaction was allowed to proceed for 24 h at ambient temperature. The work-up followed the same procedure as described for the pentablock copolymer.

Synthesis of the polyether-poly(*tert*-butyl acrylate) diblock copolymer also followed a similar synthetic scheme as described for the pentablock. A 2,150 g mol^{-1} CH_3O-PEO_{45}-Br (2.0 g, 9.30 x 10^{-4} mol) oligomer was dissolved in 4 mL of sparged toluene in a 100-mL flame-dried Schlenk flask equipped with a stir bar. *Tert*-butyl acrylate (17.86 g, 0.139 mol) was charged to the flask, followed by addition of PMDETA (0.161, 9.30 x 10^{-4} mol) and the solution was freeze-thawed twice. Finally, Cu(I)Br (0.133 g, 9.30 x 10^{-4} mol) was charged to the flask and the solution was freeze-thawed two more times. The reaction was allowed to proceed for 12 h at 80 °C. The CH_3O-PEO_{45}-PtBA copolymer was isolated by diluting the reaction mixture with 100 mL

of dichloromethane and the solution was passed through a neutral alumina column twice to remove the copper/ligand complex. The solvents were removed via rotary evaporation and CH_3O-PEO_{45}-$PtBA_{110}$ was dried at 40 °C overnight under reduced pressure.

The CH_3O-PEO_{45}-$PtBA_{110}$ copolymer was deprotected following a similar procedure as previously described for the pentablock. In a 250-mL round-bottom flask equipped with a stir bar, CH_3O-PEO_{45}-$PtBA_{110}$ (2.0 g, 1.67 x 10^{-4} mol, 1.36 x 10^{-2} mol *t*-butyl groups) was dissolved in 80 mL of dichloromethane, and trifluoroacetic acid (15.56 g, 1.36 x 10^{-1} mol) was charged to the flask. The solution was stirred at room temperature for 24 h. The dichloromethane and trifluoroacetic acid were removed via rotary evaporation. The copolymer was re-dissolved in 10 mL of THF and placed in a 3,500 g mol^{-1} MWCO cellulose acetate dialysis bag to remove residual monomer and excess acid. The solution was dialyzed against 4 L of DI water for 48 h, changing the DI water each day, then the diblock copolymer was freeze-dried for 48 h to remove the water.

3.2.3 Preparation of gentamicin-block copolymer complexes

Mixtures of copolymers were condensed with gentamicin to form complexes as shown figure 1.1. To prepare the nanostructures, the PAA-*b*-PEO-*b*-PPO-*b*-PEO-*b*-PAA copolymer described above (25 mg, 1.68 x 10^{-4} eq of anions) and 25 mg of PEO-*b*-PAA (1.63 x10^{-4} eq of anions) were charged to a 100-mL round-bottom flask and dissolved in 25 mL PBS. The solution was placed in a sonication bath and 5 mL of gentamicin sulfate solution (5.2 mg mL^{-1} gentamicin sulfate equal to 31 mg gentamicin, 3.31 x 10^{-4} eq of cations) was added via syringe to form a slightly turbid dispersion. The resulting complexes were collected by ultra-centrifugation of the solution at 20,000 rpm for 15 min (Optima™ L-XP Ultracentrifuge, Beckman Coulter Inc.). The supernatant was carefully

removed and the centrifugate was redispered in DI water. Finally, the complex was recovered by freeze-drying.

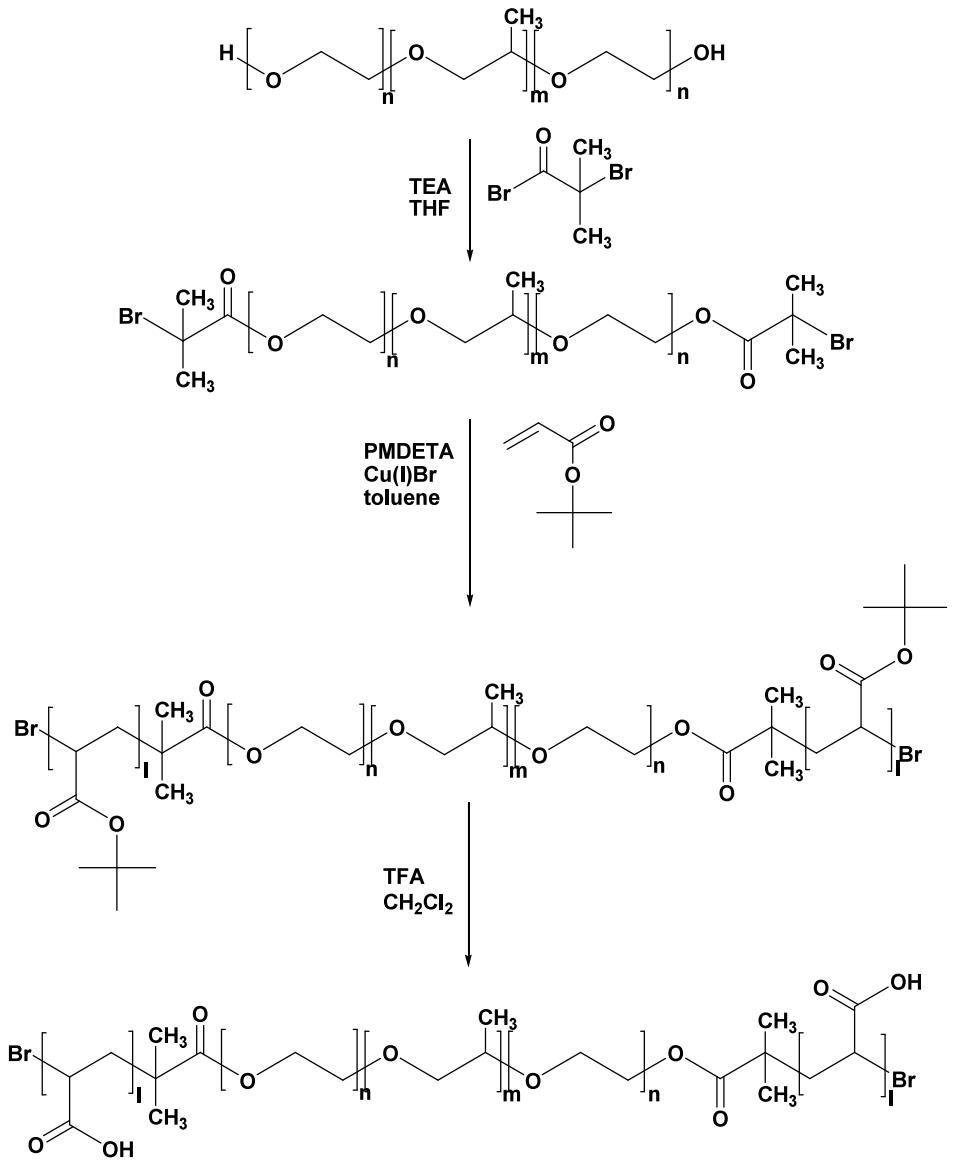

Figure 3.1 Synthesis PtBA-*b*-PEO-*b*-PPO-*b*-PEO-*b*-PtBA and subsequent deprotection of the tert-butyl groups to form PAA-*b*-PEO-*b*-PPO-*b*-PEO-*b*-PAA. For Pluronic P85, n = 26 and m = 41.

3.2.4 Preparation of fluorescent complexes

Fluorescein-NHS (10 mg, 2.10 x 10^{-5} mol) dissolved in 0.5 mL DMF was slowly added to a gentamicin solution (37 mg gentamicin sulfate, 22 mg gentamicin, 5.15 x 10^{-5} mol, 1.55 x 10^{-4} mol primary amines) in 2 mL phosphate buffer, pH 7.4. The mixture was allowed to react in the dark at room temperature for 24 h and used without further purification. Fluorescent particles were prepared by adding the solution of fluorescein-gentamicin (1 mL, 8.8 mg gentamicin) to 4 mL of the gentamicin sulfate solution (37 mg gentamicin sulfate, 22 mg gentamicin) in DI water. This mixture was subsequently added drop wise to the polymer solution (with sonication) to prepare the nanostructures. Nanostructures was recovered as described above by ultracentrifugation followed by freeze-drying.

3.2.5 Intracellular trafficking of gentamicin-block copolymer complexes

J774A.1 macrophages were grown in tissue culture flasks using Dulbecco's Modified Eagle Medium (DMEM) supplemented with 10% fetal bovine serum (FBS) and 1% penicillin–streptomycin at 37 ^{o}C with 5% CO_2 in an incubator. Macrophages were harvested by gently scraping in 5 mL of culture media at 70–90% confluency, then re-suspended in 45 mL of culture media and seeded with 2 mL of cell suspension (1.25 x 10^5 cells/mL) in 24-well cell culture plates. Prior to the experiment, the culture medium was discarded from 24 wells and cells in the wells were incubated with fresh serum-free DMEM medium. To study the effect of various inhibitors on uptake of the nanostructures, the cells were pre-incubated with the clathrin (chlorpromazine), caveolar (filipin) and fluid phase endocytosis (sucrose) inhibitors at the following concentrations: (i) 10 µg/mL of chlorpromazine for 30 min, (ii) 5 µg/mL of filipin for 30 min, (iii) 450

mM of sucrose for 30 min as described previously.[136] Following this, the cells were incubated with 15 μg mL^{-1} for 2 h, then the culture media was discarded, and the cells were recovered by gentle scraping in 2 mL of cold Hanks Balanced Salt solution (HBBS) in 15-mL falcon tubes. The cell suspension was centrifuged at 1500 rpm for 5 min to obtain a cell pellet, rinsed with HBBS buffer, spun down, resuspended in 100 μL of HBBS, and subsequently the fluorescence intensity of each sample was analyzed by FACS flow cytometry (BD FACS Aria, USA) with an excitation wavelength of 488 nm and analyzed with a 530/30 nm emission filter by counting 5,000 single cell events. Only the viable cells were gated for fluorescence analysis. The geometric mean fluorescence intensity of the cells was computed from the histogram plot calculated from triplicate data.

3.2.6 Cellular uptake and confocal microscopy

For microscopic examinations, 1 x 10^5 J774A.1 cells suspended in 250 μL of DMEM with 10% FBS were seeded into the 10-mm diameter microwells of 35-mm petridishes (MatTek Corporation) and incubated for 1 h at 37 °C in a humidified 5% CO_2 atmosphere to allow the cells to attach onto the glass surface. After incubation, the remainder of the dish was gently filled with 2 mL of DMEM containing 10% FBS and the dishes were incubated for 48 h at 37 °C in a humidified 5% CO_2 atmosphere. Prior to the experiment, the cells in each microwell were washed with 2 mL of PBS. 10 μg/well of either fluorescent nanostructures or Alexa fluor 488 (positive control for endosomal pathway) was added in each well, followed by with 2 mL of DMEM supplemented with 10% FBS. The contents were incubated for 2 h at 37 °C in a humidified 5% CO_2 atmosphere. In addition, an Image-iT live lysosomal and nuclear labeling kit (Invitrogen)

was used to stain the lysosome/endosome and nuclear compartments of the cells. After incubation with the nanostructures for 2 h, the cells were washed twice with PBS. Hoechst 33342 (excitation/emission maxima ~350/461 nm) was added to the microwells to reach concentration of 2.0 μg mL^{-1} and the contents were incubated for 5 min at 37 °C in a 5% CO_2 atmosphere to stain the nuclei. Later, the cells were washed three times with 1 mL each of HBSS and incubated with LysoTracker Red DND-99 (excitation/emission maxima ~577/590 nm) for 1 min at room temperature. The LysoTracker Red DND-99 dye was used at a concentration of 100 nM per well for staining acidic cell organelles such as endosomes and lysosomes. Following incubation, the cells were washed twice with 1 mL each of HBSS and mounted on the microscope slide. The wells were examined using a 63x oil-immersion objective on a Zeiss LSM 510 META confocal microscope (Thornwood, USA).

3.2.7 *In-vitro* toxicity assessment

An *in-vitro* homogeneous, colorimetric method for determining the number of viable J774A.1 cells using the CellTiter 96® AQ_{ueous} Non-Radioactive Cell Proliferation Assay (Promega, USA) was used to determine any cytotoxic effects of P85™ Pluronic and the core-shell nanostructures. Briefly, ~2 x 10^4 J774A.1 cells suspended in 200 μL of DMEM supplemented with 10% fetal calf serum (FCS), L-glutamine, $NaHCO_3$, pyridoxine-HCl, and 45,000 mg L^{-1} glucose and preserved with 1% penicillin-streptomycin solution were seeded in 96-well plates and incubated for 24 hours at 37 °C in a 5% CO_2 atmosphere. Later, the J774A.1 cells were incubated with a dose range of 5-50 μg/well of free gentamicin, Pluronic P85™ (PEO-*b*-PPO-*b*-PEO), the block copolymers (PAA-*b*-PEO-*b*-PPO-*b*-PEO-*b*-PAA), or the core-shell nanostructures along

with an untreated control for 24 hours. Following this, the culture media was discarded and the cells in each well were washed with PBS and re-suspended with 100 µL of cell culture media. Then 20 µL of CellTiter 96® AQ_{ueous} reagent solution was pipetted into each well, and the plates were incubated for 4 hours at 37 °C in a humidified 5% CO_2 atmosphere. The absorbance at 490 nm was recorded using a 96-well plate reader.

3.2.8 *In-vitro* cell culture experiment

The ability of the nanostructures to kill intracellular bacteria was evaluated in an intracellular *Salmonella typhimurium* strain $LT2^{137}$ and *Listeria monocytogenes (wild type)* infection model. Initially, J774A.1 cells were seeded at 2×10^5 cells/well in 24-well plates and grown at 37 °C in 5% CO_2 in DMEM plus 10% FCS for 48 h. Then, stock cultures of *S. typhimurium* and *L. monocytogenes* adjusted to a multiplicity of infection (MOI) of 10 bacteria per macrophage in DMEM supplemented with 10% FCS were added to the macrophages and incubated at 37 °C in 5% CO_2 for 30 min. After incubation, the culture medium was discarded, each well was incubated with 2 mL of fresh DMEM supplemented with 10% FCS containing 25 µg/mL gentamicin for 30 min to kill extracellular bacteria, then washed twice with PBS containing Ca^{++} and Mg^{++} and further incubated with 2 mL of fresh DMEM supplemented with 10% FCS. At this stage, infected cells were treated with 25 µg/mL of gentamicin in solution or the nanostructures, then uptake and treatment were allowed to proceed for 6 h at 37 °C in 5% CO_2. A control group of cells without drug or nanostructures was compared. Finally, the wells were washed with PBS containing Ca^{++} and Mg^{++}, the number of colony forming units (CFU)/well was determined after lysing the macrophages with cold 1% Triton X-100 for 15-20 min at 37 °C and plating the serial dilutions of the lysates onto Tryptic soy agar

(TSA) plates at 37 °C for 24 h. For each treatment and control, triplicate assays were performed for statistical analysis. For statistics, groups were compared for differences in mean CFU using ANOVA followed by Tukey's procedure for multiple comparisons.

3.3 Results and discussion

3.3.1 Block copolymer synthesis

PtBA-*b*-PEO-*b*-PPO-*b*-PEO-*b*-PtBA and PEO-*b*-PtBA were synthesized via controlled radical polymerization (Atom Transfer Radical Polymerization, ATRP) through a method adapted from the literature.[134, 135] Hydroxyl functional CH_3O-PEO-OH and HO-PEO-*b*-PPO-*b*-PEO-OH were capped with bromoisobutyryl bromide to yield *tert*-bromoalkane endgroups, then utilized to initiate the tert-butylacrylate for preparing the diblock and pentablock copolymers. Proton NMR spectra provided the compositions of the copolymers, and as expected these agreed well with the targeted compositions corrected for the monomer conversions that were attained in the free radical polymerizations. If one utilizes the block lengths of the macroinitiators and the relative compositions of the final polymers, and assumes that no premature termination occurs, one would predict that the diblock would be a PEO (2000 M_n)-*b*-PtBA(14,100 M_n) and the pentablock would be a PtBA (3330 M_n)-*b*-PEO (1100 M_n)-*b*-PPO (2400 M_n)-*b*-PEO (1100 M_n)-*b*-PtBA (3330 M_n). The actual molecular weights derived from SEC, however, were somewhat higher than these predicted sizes, and this is attributed to some coupling during the controlled free radical polymerizations (Table 3.1). For example, a nominal PEO (2000 M_n)-*b*-PtBA (14,100 M_n) diblock had a M_n by SEC of 19,700 with a molecular weight distribution of 1.18, and the pentablock with a nominal composition of

PtBA (3460 M_n)-*b*-PEO (1100 M_n)-*b*-PPO (2400 M_n)-*b*-PEO (1100 M_n)-*b*-PtBA (3460 M_n) had a M_n by SEC of 22,000 with a molecular weight distribution of 1.15. Interestingly, while coupling in a free radical polymerization is normally considered to be a termination reaction, coupling in the "pentablock" case leaves behind propagating radicals on either end. Thus, while the concentration of reactive species is reduced, the polymer can continue propagating to form a multiblock material. This resulted in significant higher molecular weight determined with SEC relatively to NMR.

Polymer	**M_n NMR g mole^{-1}**	**M_n SEC[a] g mole^{-1}**	**PDI**
PEO	2,100	2,000	1.08
PEO-*b*-PtBA	16,200	19,700	1.14
PEO-*b*-PPO-*b*-PEO	4,900[b]	4,200	1.17
PtBA-*b*-PEO-*b*-PPO-*b*-PEO-*b*-PtBA	11,800	22,000	1.22

Table 3.1 Polymer molecular weight

[a]in chloroform as a solvent. [b]the molecular weight was calculated after derivatization with isobutyryl bromide from proton NMR spectra utilizing the isobutyl groups as an internal standard

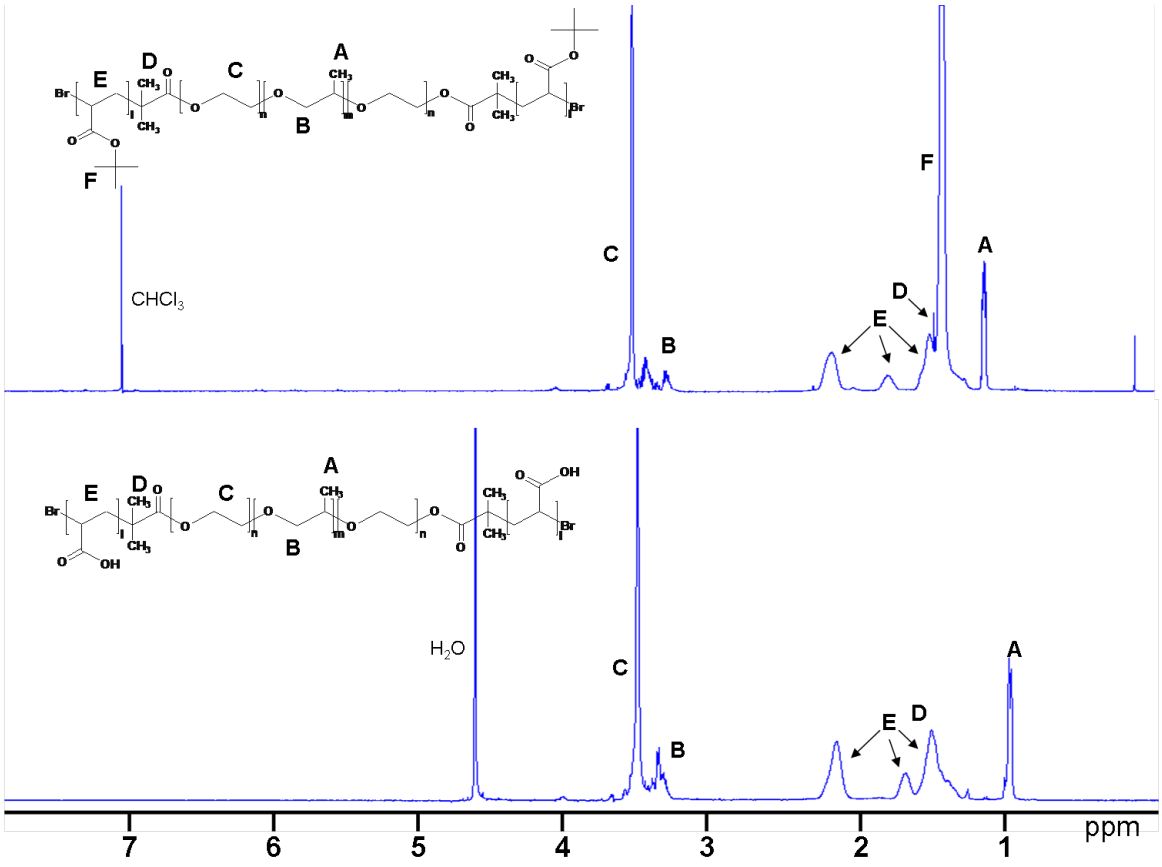

Figure 3.2 ^{1}H NMR spectra of PtBA-*b*-PEO-*b*-PPO-*b*-PEO-*b*-PtBA in $CDCl_3$ (top) and PAA-*b*-PEO-*b*-PPO-*b*-PEO-*b*-PAA in D_2O (bottom), showing the complete disappearance of the *tert*-butyl resonance at ~1.3 ppm after deprotection

3.3.2 Formation of complexes

To fabricate the nanostructured complexes, PEO-*b*-$PAA^{-+}Na$ and $PAA^{-+}Na$-*b*-PEO-*b*-PPO-*b*-PEO-*b*-$PAA^{-+}Na$ were co-dissolved in PBS then gentamicin sulfate solution was added to the polymer solution to form a final one-to-one ratio of anions to cations. The upper pK_a of gentamicin is ~8.6.[138] The ionic exchange that occurs upon nanostructure formation can be expressed as

$$5\ COO^-\ Na^+ \ +\ Gen^{5+}\ 5/2\ SO_4^{2-} \ \rightarrow\ COO^-\ Gen^+ \ +\ 5/2\ (Na_2^{2+}\ SO_4^{2-})$$

It is well known that the stability of polyelectrolyte complexes is greatly sensitive to the ionic strength of media because of the shielding effect of ionic species on the electrostatic interactions. Consequently, the feasibility of controlling the activity and enhancing the stability of charges molecules through the core-shell complexes seems to be limited. As shown in this work, the complexation between hydrophilic PEO-*b*-PAA and gentamicin did not form due to presence of ionic strength from sodium chloride ions. This suggests that electrostatic interaction alone was not enough to maintian integrity of the complexes. While the pentablock PAA-*b*-PEO-*b*-PPO-*b*-PEO-*b*-PAA can form complexes with gentamicin, it should be noted that the complexes rapidly aggregated and form macroscale agglomeration followed by eventual precipitation from the solution. The 1:1 by weight of diblock and pentablock copolymers was founded to be an optimum composition to successfully form stable complexes. The diblock PEO-*b*-PAA was added to the system to provide steric stabilization where the PEO can prevent inter-particle complexation. The hydrophobicity from PPO segment seemed to enhance stability of the complexes in presence of physiological ionic strength.

Upon adding the aminoglycoside, the solutions became slightly turbid. The ratio of copolymer to homopolymer was varied and the hydrodynamic sizes of these complexes were measured by DLS (Table 3.2). At 1:1 diblock to pentablock ratio, the intensity average hydrodynamic diameters changed from ~6-7 nm up to ~200 nm as the polyelectrolyte unimeric polymers formed complexes with the drug molecules. Thus, the complexes that constructed form the blend system was chosen to perform further characterization and in vivo and in vitro efficacy experiments.

Complex	%wt P85PAA	%wt PEOPAA	Average hydrodynamic size (nm)	Zeta potential (mV)	PDI
100P85PAA	100	0	agglomeration	nd	nd
50P85PAA	50	50	200 +/- 9	-7 +/- 3	0.147
100PEOPAA	0	100	7[a]	nd	nd

Table 3.2 Characteristics of gentamicin-block copolymer complexes. All complexes were prepared in 0.01 M phosphate buffer pH 7.4, 0.1 M NaCl and the feed ratio of cation to anion was 1:1. [a] The complex formation as measured by light scattering are not formed due to high ionic strength.

3.3.3 Gentamicin encapsulation efficiency

To quantify the amount of encapsulated gentamicin, the complexes were dissolved in borate buffer at pH 9.7 to disintegrate the particles and release the drug in the free amine form. The primary amine on gentamicin was then reacted with an excess of phthalaldehyde in the presence of mercaptoethanol to produce a derivative that was quantified via UV-visible spectroscopy (Figure 3.3).[139] Gentamicin solution, phthalaldehyde reagent containing mercaptoethanol, and isopropanol (to avoid precipitation of the products) were reacted for 30 minutes at room temperature, and the absorbances of the products were measured at 335 nm.

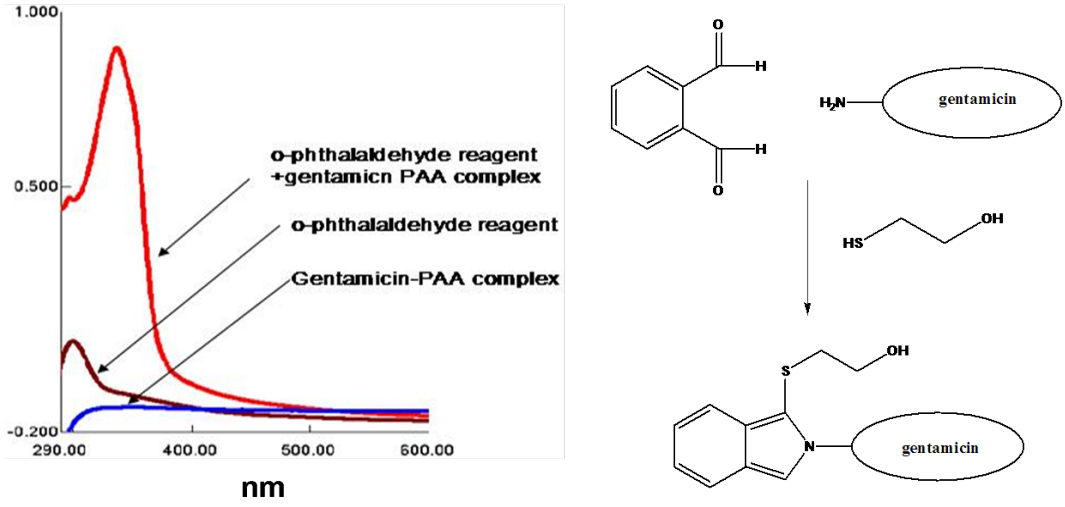

Figure 3.3 Derivatization of gentamicin with phthalaldehyde-mercaptoethanol and its quantification by UV-visible spectroscopy

The remarkable loading of 20-25 wt% of gentamicin in the complexes is attributed to strong interactions between the cationic gentamicin and the anionic polymers. This high loading is 20 to 50-fold higher than the values reported by Prior and co-workers[55] where gentamicin was loaded into hydrophobic microspheres or nanospheres. This is of great potential benefit in parenteral administration of drugs where dosage is a limiting factor in efficacy.[56]

3.3.4 Uptake of polymer-antibiotic nanostructures into macrophages and intracellular trafficking

The nanostructures were labeled with fluorescent tags to monitor their uptake into macrophage cells. The primary amine group of gentamicin was reacted with the N-succinimidyl ester of fluorescein (fluorescein-NHS). This labeled gentamicin was then mixed with unlabeled drug and subsequently incorporated into complexes with both the

hydrophilic and amphiphilic shells. Confocal images of the resultant fluorescent nanostructures confirmed that the labeling method was successful.

Confocal microscopy was utilized to qualitatively visualize uptake of the nanostructures into the macrophages. As shown in figure 3.2, Co-localization studies showed the complexes in the endosomes/lysosome indicated by distinct yellow-to-orange spots formed by co-localization of green particles and red lysotracker inside the cells (Fig 3.2b). In addition, nanostructures were also observed in cell cytoplasm suggesting the uptake by a different mechanism. In contrast, majority of Alexa fluor-488, positive control for endosomal pathway, appeared to reside in endosomes (Figure 3.4)

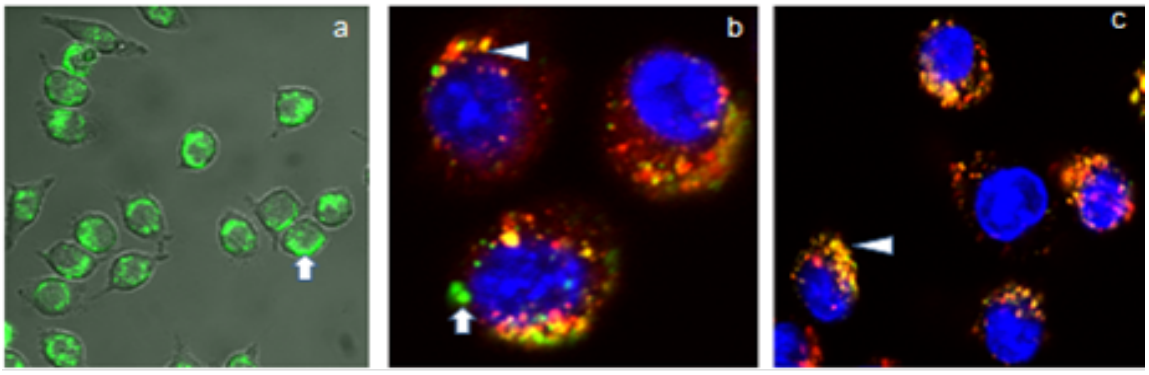

Figure 3.4 Confocal images of. (a) Uptake of FITC-labeled nanostructures into J774A.1 cells. Colocalization of (b) nanostructures and (c) Alexa fluor with endosome/lysosome (red) after incubation for 2 h. Subcellular colocalization of nanostructures and Alexafluor 488 (arrow head) (c) nanostructures are shown by yellow-to-orange (arrowhead) spots formed by green nanoparticles and red endosomes/lysosomes, showing that a majority of the Alexa-fluor appear to reside in endosomes whereas nanostructructures is distributed all over the cell.

Pathway inhibition studies using median fluorescence intensity from flow cytometry suggests that the uptake of nanostructures is significantly reduced in the

presence of chlorpromazine (~ 46%) and sucrose (~40%) compared to complexes alone. In contrast, filipin is not significant in inhibiting particle uptake (Figure. 3.5). These results suggest that the particle follows both clathrin mediated and an alternative pathway mediated mainly by fluid phase endocytosis

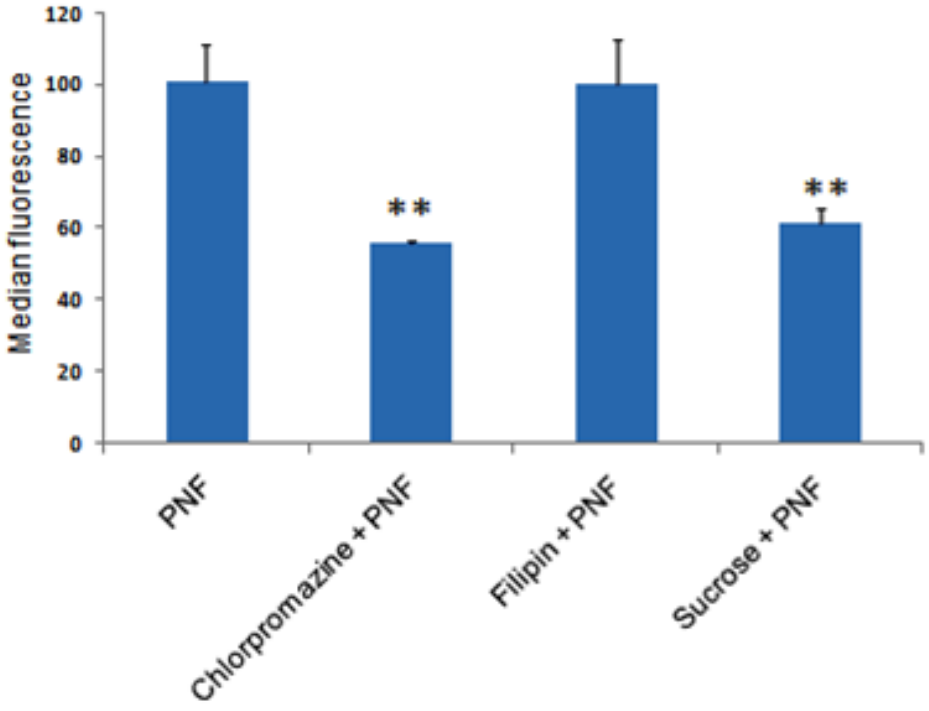

Figure 3.5 Median intracellular fluorescence intensity calculated from flow cytometry considering fluorescence nanostructures as a control (PNF) as 100 %. Each treatment represents mean of three measurements

Though the inhibitor of fluid phase endocytosis (sucrose) can also inhibit clathrin-dependent receptor internalization by blocking clathrin-coated pit formation [140], previous research studies have shown that the inhibition is largely non-specific and affects multiple pathways [136]. Interestingly, inhibition of caveolar mediated pathway (filipin) did not result in any decrease in uptake compared to control. Thus, it is plausible that the

improved intracellular delivery could be an interplay of straight delivery of nanostructures by fluid phase endocytosis into the cytosol or an escape of complexes from the endosome upon uptake by clathrin mediated pathway. Live-cell and real-time microsopy tracking the movement of nanostructures inside cells may shed more light on this phenomenon.

3.3.5 *In vitro* intracellular efficacy of complexes

Gentamicin inspite of being highly efficacious *in vitro* is poorly permeable across the cell membrane.[40] Due to its high solubility and polarity, gentamicin upon parenteral administration at the maximum tolerated doses remains largely in the extracellular location and is filtered rapidly by the kidney.[141, 142]In this study, the efficacy of complexes to augment intracellular bacterial reduction based on sub-cellular location was determined in infected J774A.1 cells. Free gentamicin, copolymer alone or infected control did not show significant difference in their ability to clear intracellular *Salmonella* or *Listeria*. In contrast, the complexes resulted in a significant reduction of intracellular *Salmonella* and Listeria as shown in Table 3.3 and 3.4.

The cytotoxicity of complexes was determined using MTS assay. Co-incubation of J774A.1 cells with the complexes did not result in significant difference in mean absorbance compared to free gentamicin, pluronic P85, copolymer carriers, and untreated control in the dose range of 25-250 μg mL^{-1} ($p<0.05$). For all dose ranges, the absorbance was comparable or higher than untreated control indicating lack of apparent toxicity (Figure 3.6). The concentration of complexes that was use to evaluate *in vitro* efficacy was ~ 100 μg mL^{-1}. Therefore, the reduction of intracellular bacteria was not caused by a lost of macrophage cells due to toxicity.

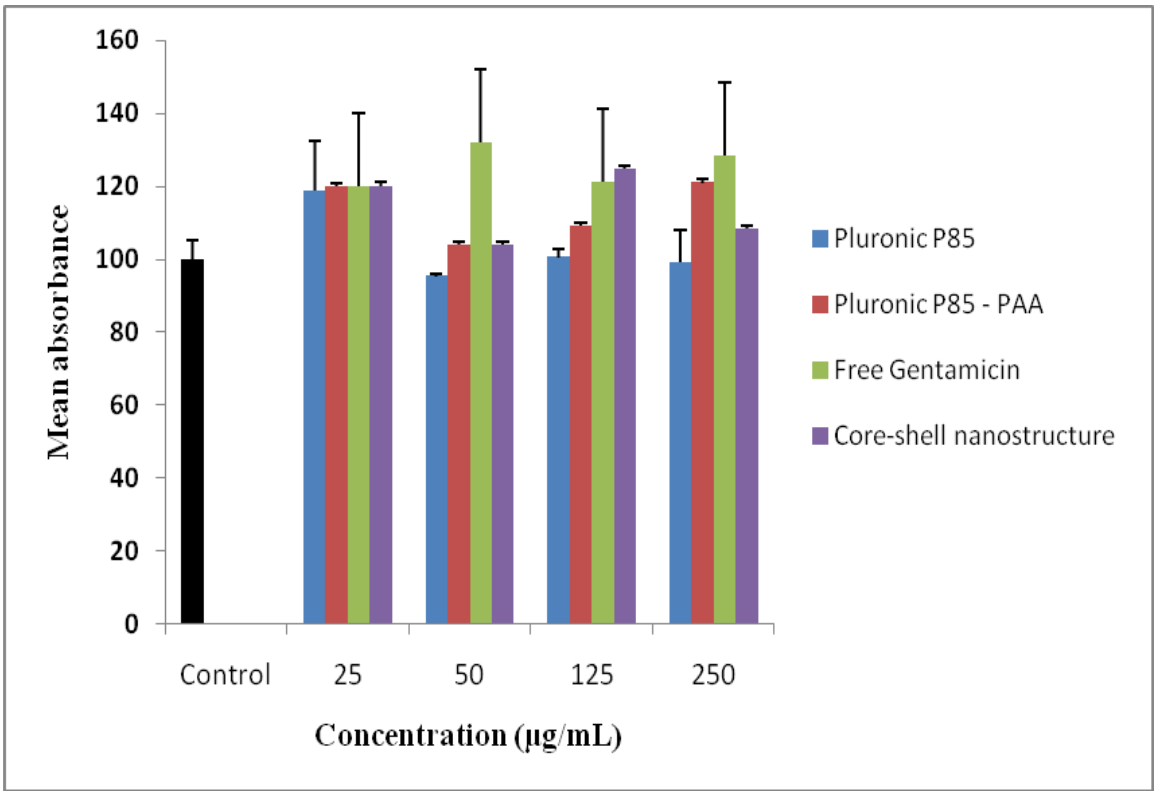

Figure 3.6 MTS assay showing the mean absorbance at wavelength of 490 nm after incubating J774A.1 cells with 50-250 µg mL^{-1} of core-shell nanostructures along with appropriate controls. Results are expressed as means ± SD of six measurements

In addition we also observed that the percentage log reduction compared to control is dependent on the intracellular localization of bacteria Upon treatment with gentamicin, the log reduction achieved for *Salmonella* and *Listeria* was 0.53 log_{10} and 3.11 log_{10} respectively. This is plausible since the vacuolar resident Salmonella are not exposed to a high dose of antimicrobial due to membrane barriers. In contrast, cytoplasm resident *Listeria* can directly interact with the drug molecules like gentamicin favoring efficient clearance. Intracellular escape of *Salmonella* from the cell is partially dependent

on duration of infection. Thus, the observed reduction in *Salmonella* could be due to the escape of flaggelated bacilli from the salmonella contanicn vacuoles (SCV) and direct exposure to the free drug in the cell cytoplasm [143]. In other words, the nanostructures may not be directly targeting the SCV but interacting with the flagellated *Salmonella* which are in cell cytoplasm. Development of delivery system with an ability to release drug in a time dependent manner in the cell cytosol may be highly valuable for such treatment scenarios. Thus, it suggests that efficacy of this system is directly correlated/dependent on the location of the bacterium inside the cells.

Group	**Log CFU (±SD)**	**Log CFU reduction**
Control	4.06 (± 0.16)	0.00
Free gentamicin	3.98 (± 0.05)	0.08
Polymer alone	3.91 (± 0.08)	0.15
Nanostructure	3.53 (± 0.20)	0.53

Table 3.3 Killing of intracellular wild-type *S. typhimurium* LT2 in J774A.1 cells incubated with free gentamicin or nanostructure at a dose of 25 µg gentamicin/mL for 6 h. Each result represents the mean of triplicate assays ± SD performed together. Asterisks represent values found to be significantly different (confidence level, $t = 0.05$) from that for free gentamicin by statistical analysis (ANOVA followed by Tukey's procedure for multiple comparisons)

Group	Log CFU (±SD)	Log CFU reduction
Control	5.63 (± 0.35)	0.00
Free gentamicin	5.67 (± 0.14)	+ 0.04
Polymer alone	5.50 (± 0.10)	0.13
Nanostructure	2.46 (± 0.11)	3.17

Table 3.4 Killing of intracellular wild-type *Listeria monocytogenes* in J774A.1 cells incubated with free gentamicin or nanostructure at a dose of 25 μg/mL for 6 h. Each result represents the mean of triplicate assays ± SD performed together. Asterisks represent values found to be significantly different (confidence level, $t = 0.05$) from that for free gentamicin by statistical analysis (ANOVA followed by Tukey's procedure for multiple comparisons).

3.4 Conclusion

In summary, Core-shell complexes comprised of a polyacrylate block copolymer, homopolymer and aminoglycosides were synthesized with very high drug loading capacities. Successful encapsulation of a core comprised of anionic polyacrylate and aminoglycosides using electrostatic neutralization assembly was demonstrated. Antibiotic susceptibility studies showed that the drugs released from the complexes were active. Fluorescently-labeled nanostructures were prepared to assess influences of the copolymer shells on macrophage uptake and intracellular antimicrobial activity. Results from confocal microscopy and flow cytometry showed that the nanostructured complexes were taken up by the macrophages and localized in both endosome and cytoplasm.

In vitro treatment of infected macrophages also revealed the influence of polymer shells on their intracellular efficacies against *Salmonella* and *Listeria.* The efficacy of this sytem is dependent on the subcellular localization of bacteria. Higher clearance is achieved with the cytoplasm resident bacteria compared to the vacuolar resident bacteria. Future studies aiming to target the different intracellular niche of the bacterium

Chapter 4

Core-shell polymer-antibiotic nanostructures fabricated by multi-inlet vortex jet mixer and their efficacies to eradicate intracellular brucellosis

4.1 Synopsis

This chapter describes the fabrication of polyether-polyacrylate copolymer-gentamicin nanoplexes with very high antibiotic payloads and reports their compositions and drug release profiles. The new fabrication technique was implemented to create technological platform that are constituted through a combination of of polymer science, engineering process, and biology aspects. The complexes were fabricated with an improved process using a multi-inlet-vortex mixer (MIVM) that involves the rapid mixing of solutions of the cationic drug and anionic block copolymers in a small mixing chamber where the flow is turbulent and the mixing time rapid (<50 ms) to promote reproducible and uniform complex formation (Figure 4.1).

The MIVM process has been used to make a variety of nanoparticles based on the rapid mixing of species dissolved in a solvent with an antisolvent stream, typically water, to produce rapid nucleation and growth of particles whose ultimate size was controlled by the adsorption of a steric stabilizer, typically a block copolymer or a homopolymer.[144-148] In this paper, complex formation is driven by electrostatic interactions, not solubility differences, to form complexes between drugs and polymers. Particle size was controlled by the pH of the solution and the net charges of the complex. The nanoplexes are isolated and stored as dry nanostructured solids that can be easily re-dispersed for testing

and use. In vitro results upon incubating the nanoplexes with *Brucella*-infected nurine-like macrophages are discussed.

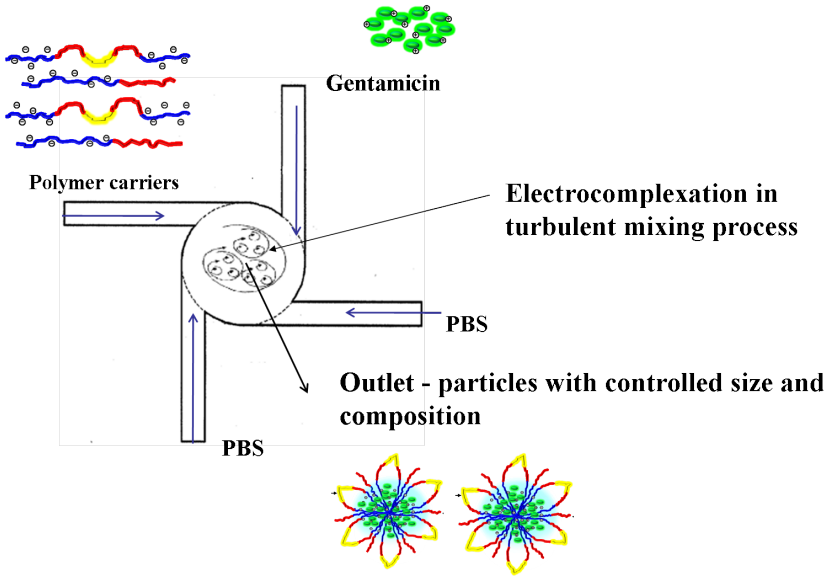

Figure 4.1 Nanofabrication of antibiotic-block ionomer complexes via MIVM process

4.2 Experimental

4.2.1 Materials

The chemicals were purchased from Sigma-Aldrich unless otherwise noted. *Tert*-butyl acrylate (98%) was fractionally distilled from calcium hydride under reduced pressure and sealed under nitrogen prior to use. Copper (I) bromide (98%), *N-N'-N'-N''-N'''* pentamethyldiethylenetriamine (PMDETA, 97%), triethylamine (99%), 2-bromoisobutyryl bromide (98%), monobasic potassium phosphate, dibasic sodium phosphate, potassium chloride, sodium chloride, boric acid, sodium hydroxide, *o*-phthalaldehyde solution in water (1 mg mL^{-1}), and mercaptoethanol (98%) were used as received. Trifluoroacetic acid (Alfa-Aesar, 98%) was used as received. Poly(ethylene oxide) (M_n ~2,000 g mol^{-1} from ^1H NMR) was dried at 40 °C under reduced pressure for

24 h prior to use. Pluronic P85™ (BASF, M_n ~4,600 g mol^{-1} from SEC) was dried at 50 °C under reduced pressure for 24 h prior to use. Toluene (Fisher, HPLC Grade) was sparged with nitrogen for 1 h prior to use. Tetrahydrofuran (Fisher, HPLC Grade) was dried and distilled from sodium and benzophenone under a nitrogen atmosphere prior to use. Hexane, dichloromethane, chloroform, diethyl ether and isopropanol (Fisher, all HPLC grade) were used as received. Gentamicin sulfate (Bioworld, neat salt, 590 μg gentamicin per mg) was used as received. All copolymers were synthesized via ATRP and characterized in similar procedure that was reported in chapter 3. The molecular weights and compositions of polymeric carriers are summarized in Table 4.1. PEO-b-PAA and PAA-b-PEO-b-PPO-b-PEO-b-PAA were obtained after deprotection of tert-butyl ester groups from their correspondent block copolymer precursors.

Polymer	**M_n NMR g $mole^{-1}$**	**M_n SEC g $mole^{-1}$**	**PDI**
PEO_{45}	2,100	2,000	1.08
PEO_{45}-*b*-$PtBA_{117}$	17,000	23,000	1.18
PEO_{26}-*b*-PPO_{41}-*b*-PEO_{26}	4,900	4,200	1.17
$PtBA_{27}$-*b*-PEO_{45}-*b*-PPO_{41}-*b*-PEO_{26}-*b*-$PtBA_{27}$	12,100	24,000	1.15

Table 4.1 Molecular weights of block copolymer precursors for fabrication of complexes via MIVM process. The number in subscription indicates repeat unit of monomer.

4.2.2 Fabrication of block copolymer-gentamicin nanoplexes via MIVM process

Gentamicin sulfate (0.134 g, 0.082 g gentamicin, 1.688 x 10^{-4} mol gentamicin) was dissolved in 25 mL of PBS in a 50-mL Erlenmeyer flask and the pH was adjusted to 5.0 or 7.4 with 1M NaOH to make a solution concentration of 3.28 mg mL^{-1}. CH_3O-PEO_{45}-PAA_{117} (0.050 g, 5.074 x 10^{-4} mol) and PAA_{27}-PEO_{26}-PPO_{41}-PEO_{26}-PAA_{27} (0.050 g, 5.78 x 10^{-4} mol) were dissolved in 25 mL of PBS in another 50-mL Erlenmeyer flask and the pH of the solution was adjusted to pH 5.0 or 7.4 with 1M NaOH, yielding a 4 mg mL^{-1} solution of polymer. Nanoplex fabrication was conducted in a custom-built, small continuous mixer outfitted with four inlets with syringe pumps for introducing solutions at specified rates. Two inlets were filled with 15 mL of PBS to be introduced at a flow rate of 5.00 mL min^{-1}, while the other two inlets were filled with the drug solution and polymer solution, each to be introduced at a flow rate of 12.0 mL min^{-1}. The Reynold's number was 7,900 which corresponded to a mixing time < 50 ms.[148] The final concentrations in the mixer were 1.42 mg mL^{-1} of polymer, 1.16 mg mL^{-1} gentamicin, and 2.58 mg mL^{-1} of nanoplex. The resultant dispersion of nanoplexes was collected and immediately centrifuged with a Thermo-Scientific Sorvall centrifuge at 3750 rpm for ~45 min until all of the eluate had passed through a Millipore centrifugal filter equipped with a 3000 g mol^{-1} MWCO cellulose acetate membrane. The solid nanoplexes were collected on the membrane filter. The nanoplexes were redispersed in a minimal volume of DI water (~10 mL), then freeze-dried.

4.2.3 Characterization of the nanoplexes

The nanoplex sizes were measured by dynamic light scattering at 37 °C in PBS at a concentration of 1.0 mg mL^{-1} immediately after fabrication and filtered through 1 um

Teflon filter. Intensity average diameters are reported as an average of three measurements.To prepare a borate buffer at pH 9.7, boric acid (12.43 g) was dissolved in 400 mL of DI water in a 500-mL Erlenmeyer flask equipped with a magnetic stir bar. The pH was adjusted to 9.7 with 5M NaOH. The solution was diluted to 500 mL with DI water.

An *o*-phthalaldehyde-mercaptoethanol (OPA) assay solution was prepared by charging 1 mL of phthalaldehyde solution (1 mg phthalaldehyde, 7.46 x 10^{-6} mol) and 5 μL of mercaptoethanol (7.1 x 10^{-5} mol) into a scintillation vial for each aliquot needed for a given series of measurements. The solutions were stirred for 1 h at ambient temperature and then stored at 4 °C. The assay solutions were used within one day.

To construct UV calibration curve for assaying gentamicin, gentamicin sulfate (16.6 mg, 10 mg gentamicin, 1.57 x 10^{-5} eq of primary amino groups) was dissolved in the borate buffer (10 mL) in a 20-mL scintillation vial equipped with a magnetic stir bar to make a stock solution of gentamicin with a concentration of 1 mg/mL. From this, a series of dilutions was performed to yield gentamicin concentrations of 31.3, 20.8, 15.7, 10.4, 7.8, 5.6 and 3.7 μg/mL to construct a calibration curve. Aliquots of each solution (0.5 mL) were placed in separate scintillation vials, then 0.5 mL of the *o*-phthalaldehyde-mercaptoethanol assay solution was added followed by 0.2 mL of isopropanol. The vials were wrapped in aluminum foil to minimize UV exposure. The final volumes were brought to 3.0 mL by adding 1.8 mL of borate buffer, then they were reacted for 1 h at ambient temperature. Absorption was measured at 340 nm and a calibration curve was constructed by plotting the absorbance versus gentamicin concentration.

4.2.4 Characterization of gentamicin content

The nanoplex (5 mg) was dissolved in borate buffer (10 mL) and the solution was diluted with borate buffer by a factor of 10. The diluted solution (0.5 mL) was added to a scintillation vial. *o*-Phthalaldehyde-mercaptoethanol solution (0.5 mL) was added, followed by 0.2 mL isopropanol and 1.8 mL borate buffer and the mixtures were reacted at ambient temperature for 1 h. Absorbance was measured at 340 nm and the concentrations of gentamicin in the nanoplexes were determined from the calibration curve.

4.2.5 Release of gentamicin from the nanoplexes.

To determine the release of gentamicin from the nanoplexes in PBS, 5 mg of the nanoplex was dissolved in 3 mL of PBS and placed in a 3,500 MWCO dialysis cassette. The cassette was placed in a 50-mL beaker and 47 mL of PBS as dialysate was added to the beaker. The beaker was covered with parafilm and maintained at 37 °C in a temperature-controlled shaker agitated at 80 RPM. Aliquots of 0.5 mL were taken from the dialysate and placed in separate scintillation vials after each time point. Each time, 0.5 mL of fresh PBS was added to the beaker to retain constant volume. The gentamicin in each aliquot was derivatized and measured using the *o*-phthalaldehyde assay procedure described above.

4.2.6 In vitro cell culture experiment

The efficacy of nanoplexes compared to free drug to kill intracellular *Brucella* was tested in murine macrophage-like cells, J774A.1 (American Type Culture Collection). These cells are routinely grown in Dulbecco's Modified Eagle's Medium (DMEM, Sigma-Aldrich) with 10% heat-inactivated fetal bovine serum (FBS) in a

humidified 5% CO_2 atmosphere at 37 ºC. Macrophages were seeded at a density of $5x10^6$ cells/well in a well cell culture plate (Corning Inc.) 24-36 h prior to infection. At 90% confluency in the wells, the cells were infected with *B. melitensis* for 1 h at a 1:100 multiplicity of infection After phagocytosis, the media was removed and fresh media containing 50 μg/mL gentamicin was added and the cells were incubated for 45 min to kill extracellular bacteria. Again the media was removed and finally the infected cells were incubated with DMEM+10% FBS for 24 h to set up the infection model. At 24 h post-infection, the cells were washed twice with DMEM and either free drug or nanoplexes (25 μg/mL gentamicin) resuspended in DMEM+10% FBS was added to the infected cells and incubated further for 24 h. The media was removed and the cells were washed twice with PBS. To determine the intracellular bacterial load, the cells were lysed using 250 μL of 0.1% Triton X-100™ and 10-fold serial dilutions of lysates were prepared and spread on TSA plates. Colony forming units (CFUs) were determined after incubating the plates for 48 h at 37 ºC under 5% CO_2.

4.3 Results and Discussion

Our overall objective is to develop a platform of polymer-drug nanoplexes for delivering cationic aminoglycosides into immune cells to treat a variety of intracellular pathogens. The delivery vehicles have ionic cores and nonionic shells, and the cationic antibiotics bind to the anionic block of the polymer to form the nanoplex cores. The chemical structures of the amphiphilic polyethers that make up the shells were designed to disperse the nanoplexes in physiological media and to transport them into phagocytic cells where the intracellular bacteria reside. One motivation for designing the shells to be

nonionic was to minimize sensitivity of the colloidal properties of the nanoplexes to ionic components in physiological media.

We have studied three nanoplex systems with similar cores but with different hydrophobicity in the shells.[149-153] The first utilized hydrophilic poly(ethylene oxide) (PEO) shells and these were obtained by incorporating block copolymers of poly(ethylene oxide-*b*-sodium acrylate) (PEO-*b*-$PAA^{-+}Na$) blended with a $PAA^{-+}Na$ homopolymer, then complexed with gentamicin[153] or streptomycin.[149] The second type had a shell comprised of a poly(ethylene oxide-*b*-propylene oxide-*b*-ethylene oxide) (PEO-*b*-PPO-*b*-PEO) triblock containing 19 wt % of the relatively-hydrophobic PPO, and this was flanked by $PAA^{-+}Na$ blocks to form a pentablock copolymer, then complexed with gentamicin.[150, 151] The third, and the most hydrophobic set of nanoplexes, contained 33 wt % PPO in the shells. These systems were prepared with a blend of a $PAA^{-+}Na$-*b*-PEO-*b*-PPO-*b*-PEO-*b*-$PAA^{-+}Na$ pentablock copolymer with a PEO-*b*-$PAA^{-+}Na$ diblock copolymer, then the blend was condensed with gentamicin.[152] Since all of these nanoplexes are formed through non-covalent interactions only, all of them break up significantly within the first few hours after dispersion in aqueous media. Thus, it is important to utilize copolymers that contribute to nanoplex stability so that they will remain intact long enough to interact with infected immune cells during an incubation period. The most hydrophobic nanoplexes had better stability in PBS compared to the first two types of materials, and thus this paper focuses on these more hydrophobic nanoplexes. We reasoned that the enhanced hydrophobicity of the pentablock shells contributed an additional hydrophobic interaction that was important for enhancing stability.

4.3.1 Fabrication of nanoplexes.

The diblock having a PEO hydrophilic shell was blended in a 1:1 wt:wt ratio with the pentablock copolymer with the amphiphilic shell. The composition of the pentablock copolymer was high in the hydrophobic PPO component relative to the hydrophilic PEO. The strategy was to take advantage of the relatively hydrophobic shell of the pentablock copolymer to enhance nanoplex stability. The hydrophilic diblock copolymer was incorporated to ensure that the nanostructures remained well dispersed in aqueous media. In an effort to form complexes with desirable compositions and drug release profiles, we adapted a method pioneered by Prud'homme et al.[148] that utilizes a multi-inlet vortex mixer to enable rapid, turbulent mixing of the polymer and drug solutions. This results in nucleation of the nanoplexes from a homogeneous solution and also provides a means for maintaining the ratio of polymer to drug constant throughout the process so that the composition distribution is narrow.

Fabrication Conditions	Intensity Ave. Diameter (nm), 37 °C (From DLS)	Wt % Gentamicin Charged	Wt % Gentamicin in Complex	% Gentamicin Retained
pH 5.0	170	45.05	42	93.2
pH 7.4	336	45.05	36	79.9

Table 4.2 Nanoplexes prepared in the vortex mixer incorporate high drug payloads

The nanoplexes were centrifuged immediately after formation through a fine membrane to isolate them in solid form to avoid any premature disassembly and release of the drug. The vortex mixing is so rapid that large payloads of drugs become kinetically-trapped in the cores of these complexes (Table 4.2). It is noteworthy that the nanoplex sizes in PBS are larger when they are processed at pH 7.4 as opposed to pH 5 (table 1). This is attributed to strong hydrogen bonding at the lower pH among the

partially-protonated acrylate block in the copolymers with each other and with the ether oxygens of the PEO. R

4.3.2 Determination of gentamicin concentration in the nanoplexes.

Gentamicin was released from the isolated nanoplexes with base and the released gentamicin, which contains three primary amines, was derivatized with phthalaldehyde in the presence of mercaptoethanol. This derivatization method has been utilized extensively by others to sensitively quantify primary amines.[154-158] A calibration curve was prepared relating the absorbance at 340 nm to the concentration of gentamicin-phthalaldehyde-mercaptoethanol derivatives in solution. The derivative is soluble and stable in aqueous solutions and absorbs strongly in the UV, and it has been shown that all three primary amines on gentamicin react quantitatively.[154-158] The calibration curve had a linear regression correlation of 99.7%.

4.3.3 Drug release profiles

Gentamicin release profiles were measured by placing the nanoplexes in a cellulose acetate dialysis bag with a MWCO of 3500 g $mole^{-1}$ in PBS and sampling the receptive media over time. Upon disassembly of the nanoplexes and release of the drug, the gentamicin permeates through the bag and into the receptive media whereas the polymers are too large to pass through the membrane. The gentamicin in the receptive medium was derivatized with phthalaldehyde-mercaptoethanol and absorbance of the derivative was measured at 340 nm and compared to the calibration curve. About half of the drug is released within the first 10 hours and this is followed by slower release up to about 40-60 hours. Interestingly, the complexes that were made at pH 5 shows relatively higher initial burst release compared to the complexes made at pH 7.4. The profile also

suggests that, after initial release, there was faster release of gentamicin from the complexes fabricated at pH 7.4 relatively to ones that were at pH 5. These results indicate that the conditions that polymer chain collapsing during electrostatic condensation with gentamicin may greatly depend on pH of the medium. The mechanism of release of gentamicin and influence of fabrication condition will be studied in the future.

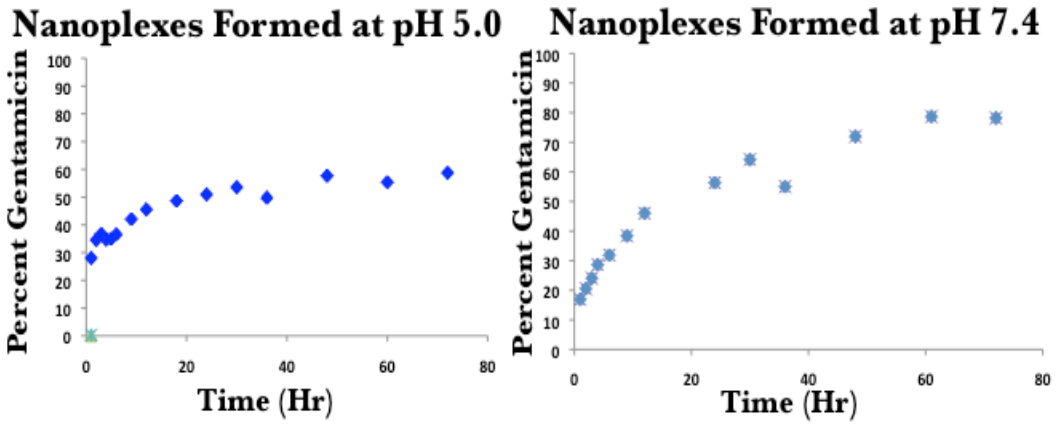

Figure 4.2 In vitro release of gentamicn from complexes

4.3.4 *In vitro* efficacy of the nanoplexes against intracellular Brucella.

Efficacy of the nanoplexes to reduce intracellular *Brucella* was studied in J774A.1 murine macrophage-like cells and compared to free drug. The cells were infected with *Brucella*, extracellular *Brucella* were killed with free gentamicin and discarded, and then the macrophages infected with only the intracellular *Brucella* were incubated with the nanoplexes for 24 hours (Figure 4.3). A significant reduction of 2.78 and 2.85 logs was obtained with nanoplexes synthesized at pH 5 and pH 7.4 respectively (figure 4.4). This reduction was significantly higher than the reduction by free drug (0.75 logs). The results

suggest that the complexes fabricated via MIVM process were efficiently taken up into macrophages *in vitro* and release gentamicin in an active form.

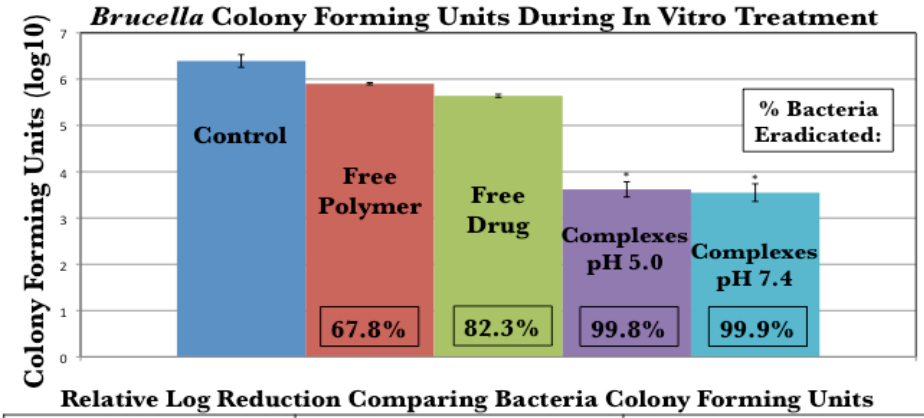

Relative Log Reduction Comparing Bacteria Colony Forming Units

	Log CFU	Log CFU Reduction
Control	6.394 ± 0.237	0.000
Drug	5.641 ± 0.058	0.752
pH 5.0 Complexes	3.620 ± 0.285	2.774
pH 7.4 Complexes	3.549 ± 0.331	2.845

Figure 4.3 In vitro efficacies of complexes in killing intracellular brucella

4.4 Conclusions

The polymer-antibiotic nanoplexes were formed in a continuous process through ionic condensation of the anionic polymer blocks with the cationic drug, and utilizing hydrophobic interactions and hydrogen bonds to enhance nanoplex stability. Our prior work together with the results reported in this study show clearly that in vitro efficacies against intracellular *Brucella, Listeria and Salmonella* are significantly improved with all of the nanoplexes over administration of the free drug. In vitro efficacies reported in this paper of nanoplexes fabricated in the new process against intracellular *Brucella* are remarkable in that 99.8-99.9% of the intracellular *Brucella* are eradicated. This demonstrates that the nanoplexes are very effective transporters for the drug into the

cells. The drug release profiles are characterized by a significant release over the first few hours, and this is followed by slow release of a smaller amount of the drug over 40-60 hours. In vivo investigations are underway to assess how effective such a release profile is for animal models.

Chapter 5

Design and Synthesis of Core-shell Polymeric Nanostructures Containing Iron Oxide Nanoparticles for Biomedical Applications

5.1 Synopsis

Functional anchor groups on polymers aid in their adsorption onto the surface of magnetite. Polymeric dispersion stabilizers containing carboxylate and alkylammonium anchor groups to complex with magnetite nanoparticles have been previously reported by our group and others.[159-161] Over the past decade, significant effort in our laboratories has been devoted to the development of strong anchor moieties for magnetite/polymer complexes. Recently, catechols such as dopamine have been reported as anchor groups for linking PEO to the magnetite surface.[162, 163] However, Shultz *et al*. have reported that the reactive nature of dopamine and iron ions on magnetite surfaces leads to the formation of dopamine quinones that are cytotoxic and facilitate degradation of the nanoparticles, so this may be a concern if the materials are to be used for *in vivo* biomedical applications.[164] We have previously reported that ammonium phosphonate zwitterions provide a robust anchor for binding PEO onto magnetite and that remarkably high surface densities can be achieved.[6] The capacity for phosphonates to form bidentate and tridentate ligands for adsorbing with high affinity onto metal and metal oxides has been described.[165-166]

It has also been shown that certain cellular interactions with nanomaterials are specific and unique with regard to the structure and composition of the materials. For example, Kabanov *et al*. reported that the pathways of intracellular uptake of amphiphilic

block copolyethers (selected Pluronics™) are sensitive and governed by the hydrophilic-hydrophobic balance of the polymers.[167, 168] Our work regarding the rate of cellular uptake of polyelectrolyte complexes also suggests that particles are internalized faster into phagocytic cells when they are amphiphilic rather than hydrophilic.[5] Moreover, polymeric coatings can be used to control the release of therapeutic agents from nanocarriers. Yavuz *et al*. demonstrated "smart" polymer nanoreservoirs with precisely controlled release from a combination of photothermal effects from gold nanocages and thermoresponsive polymeric coatings.[169] Therefore, besides the size and shape of the nanoparticle cores, the chemical compositions and solution morphologies of the polymer coatings can also offer advantages for biotechnological applications of the nanoparticles.

Herein we describe ammonium phosphonate moieties for coating other macromolecules beyond polyethers onto magnetite. The aim of our work is to develop a modular approach for engineering magnetic nanoparticles with tunable polymeric shells and flexibility of chemical functionalization. We have employed atom transfer radical polymerization (ATRP) as a tool due to its flexibility to allow a large pool of monomers to be polymerized in a controlled fashion.[131, 170] This technique also offers halide end-groups that can enable further chain extension to form block copolymers or to functionalize the polymer endgroups with bioactive molecules.[130, 171, 172] Zwitterionic bis(phosphonate)-functional initiators were designed to initiate macromolecules bearing ammonium bis(phosphonate) endgroups via ATRP, and these readily adsorb onto magnetite.

Poly(N-isopropylacrylamide) (PNIPAM) was chosen as the polymeric shell due to its attractive thermoresponsive properties. Aqueous solutions of PNIPAM exhibit a

lower critical solution temperature (LCST) around 33 ^{o}C.[173] As the temperature is raised through this region, PNIPAM undergoes a sharp coil-to-globule transition and becomes insoluble in water.[174] The polymer chains experience volume loss due to expulsion of water molecules resulting from hydrogen bond disruption. When cooled below the LCST, the hydrogen bonds reform and the polymer re-expands in solution. Thus, a thermally-induced hydrophilic-hydrophobic "switch" can be reversibly introduced into the structure.

In this work, PNIPAM was synthesized via ATRP using unimolecular anchor-initiator that contains protected amionobisphonate functional group. After mild deprotection, the polymer with bisphophonic acid end group was then bound to magnetite to afford well-defined polymer-metal oxide nanoparticles (Figures 5.1 and 5.2). Physicochemical and dispersion properties in solution as well as thermo-sensitivity of these particles were examined.

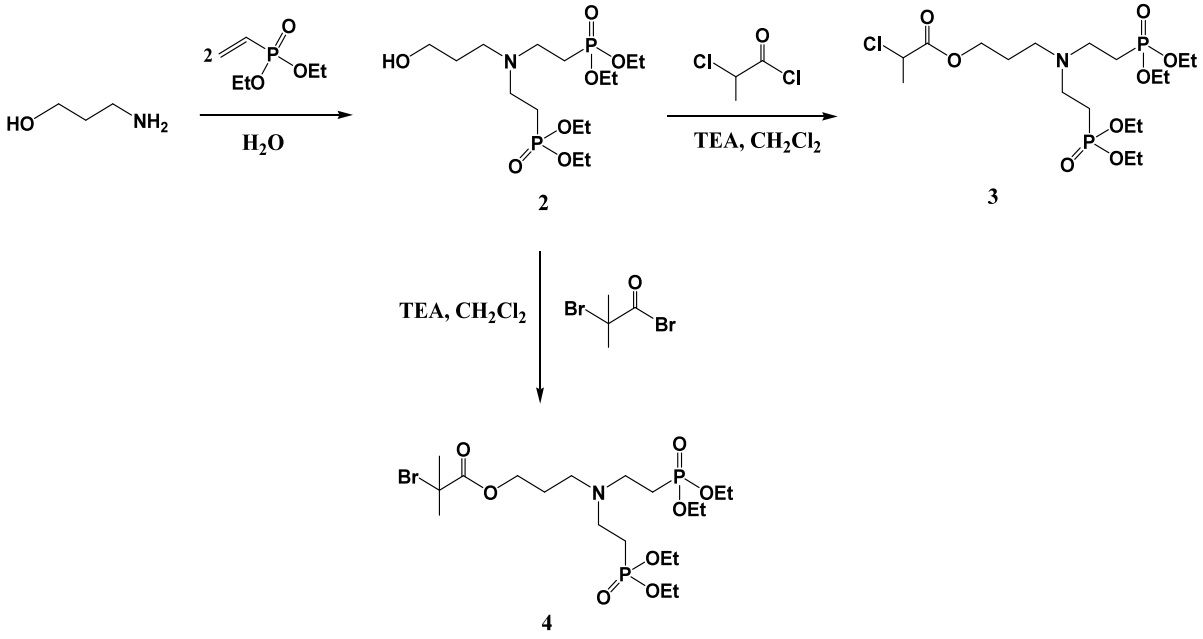

Figure 5.1 Synthesis of ammonium bis(phosphonate)-functional ATRP initiators

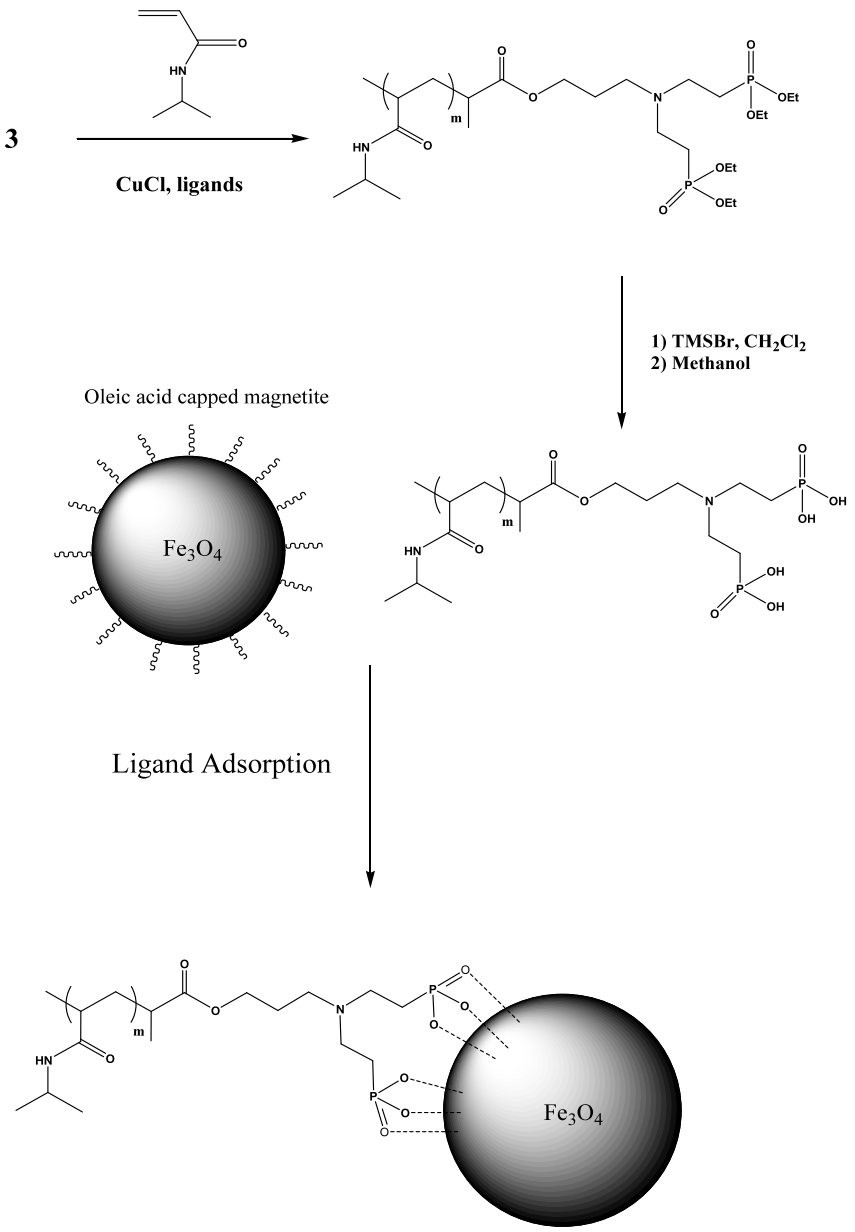

Figure 5.2. Synthesis of ammonium bis(phosphonate) terminated macromolecules via ATRP and adsorption onto magnetite surfaces

5.2 Experimental

5.2.1 Materials

Benzyl alcohol (>98%), diethyl ether, diethyl vinyl phosphonate (97%), hexanes (HPLC grade), iron (III) acetylacetonate ($Fe(acac)_3$), trimethylsilyl bromide (TMSBr,

97%), oleic acid (90%, technical grade), 2-bromoisobutyryl bromide, 2-chloropropionyl chloride, and 3-amino-1-propanol were purchased from Aldrich. N-isopropyl acrylamide (NIPAM) was recrystallized twice from hexane. Tris[2-(dimethylamino)ethylamine] (Me_6TREN) was synthesized and purified according to a previously-reported method.[175] Dichloromethane (anhydrous) and acetone (HPLC grade) were purchased from Fisher Scientific and used as received. Dialysis tubing (25,000 and 3,500 g mol^{-1} MWCO) was obtained from Spectra/Por. Phosphate buffered saline 10X (PBS) was obtained from Mediatech and diluted to appropriate concentrations.

5.2.2 Characterization

^{1}H NMR spectral analyses of compounds were performed using a Varian Unity 400 NMR or a Varian Inova 400 NMR operating at 399.8 MHz.

Size exclusion chromatography (SEC) was performed on a liquid chromato- graph equipped with a Waters 1515 isocratic HPLC pump, Waters Autosampler, Waters 2414 refractive index detector and Viscotek 270 RALLS/viscometric dual detector. The mobile phase was NMP solvent containing 0.05 M LiBr. The column temperature was maintained at 60 ^oC because of the viscous nature of NMP. Both the solvent and the sample solution were filtered before introduction into the SEC system. Molecular weights were determined by universal calibration calibrated with polystyrene standards.

Thermogravimetric analysis (TGA) was used to determine the polymer loading for each complex. TGA measurements were carried out on the PNIPAM-magnetite nanoparticles using a TA Instruments TGA Q500 to determine the fraction of polymer in each complex. Each sample was first held at 110 ºC for 10 min to drive off any excess moisture. The sample (10-15 mg) was then equilibrated at 100 ºC and heated in a

nitrogen atmosphere up to 600 °C at a rate of 10 °C min^{-1}. The mass remaining was recorded throughout the experiment. The mass remaining at 600 °C was taken as the fraction of magnetite in the complex corrected for the char yield of ~10 wt% from PNIPAM. Inductively coupled plasma atomic emission spectroscopy (ICP-AES) was performed on a SPECTRO ARCOS 165 ICP spectrometer (SPECTRO Analytical Instruments, Germany). The particles (10 mg) were dispersed in Millipore DI water (5 mL). The dispersion (1 mL) was mixed with 4 mL of concentrated nitric acid to digest magnetite and release free iron. The mixture was reacted for 5 days at room temperature and diluted with DI water to a concentration of 0.02 mg mL^{-1} prior to measurement.

Dynamic light scattering (DLS) measurements on the magnetite/PNIPAM complexes were performed with a Zetasizer NanoZS particle analyzer (Malvern Instruments Ltd., Malvern, U. K.) equipped with a solid-state He-Ne laser (λ = 633 nm) and 173° backscatter detection. The autocorrelation function of the scattered intensity was fitted using cumulants analysis to extract the average translational diffusion coefficient and the hydrodynamic diameter was determined through the Stokes-Einstein relation. Intensity-averaged diameters were converted to volume- and number-averaged diameters using the Zetasizer Nano 4.2 software. Samples were dispersed in de-ionized water at a concentration of 1 mg mL^{-1}, sonicated in an ultrasonic bath sonicator (VWR 75T, 45 kHz) and passed through a 1.0 μm PTFE filter before measurements.

Transmission electron microscopy was performed on a Philips EM-420 field emission gun TEM operating at an acceleration voltage of 100 kV. Samples were prepared by casting a drop of a dilute aqueous solution of PNIPAM-coated magnetite nanoparticles onto amorphous carbon-coated copper grids. Images were acquired at a

magnification of 96,000X, corresponding to a resolution of 3.88 pixels nm^{-2}. The sizes of over 2000 particles from different regions of the grid were measured using Reindeer Graphics' Fovea Pro 4 plug-in for Adobe Photoshop 7.0®.

The sample magnetization (*M*) as a function of applied field (*H*) (*M*-*H* curve) was measured at 300 K and 5 K using a superconducting quantum interference device (SQuID) magnetometer (MPMS XL, Quantum Design) in the range of ±7 T.

5.2.3 Synthesis

5.2.3.1 Synthesis of magnetite nanoparticles

Magnetite nanoparticles were synthesized using a slightly modified method to that previously reported.[6] $Fe(acac)_3$ (2.14 g, 8.4 mmol) and benzyl alcohol (45 mL, 0.43 mol) were charged to a 250-mL, three-neck, round-bottom flask equipped with a water condenser and nitrogen inlet and placed in a Belmont metal bath with an overhead stirrer with thermostatic (+/- 1 ^oC) control. The solution was held at 110 °C for 1 h under N_2, then the temperature was raised to 205 ^oC and maintained for 40 h. The reaction was cooled to room temperature and the particles were collected by centrifugation (4000 rpm, 30 min). The magnetite nanoparticles were washed 3 times with acetone (100 mL each), then were dispersed in chloroform (20 mL) containing oleic acid (0.3 g). The solvent was removed under vacuum at room temperature, and the oleic acid-stabilized magnetittes were washed 3X with acetone (100 mL each) and dried under vacuum for 24 h at 25 ˚C.

5.2.3.2 Synthesis of an amino bis(phosphonate) initiator for ATRP

3-Amino-1-propanol (**1**, 12.0 g, 0.160 mol), diethylvinylphosphonate (53.0 g, 0.323 mol), and DI water (260 mL) were added into a 500-mL round-bottom flask

equipped with a magnetic stir bar. The solution was placed into an oil bath and stirred at 50 ^{o}C for 24 h. After cooling, the pH was adjusted to ~11 with 5 N NaOH and the aqueous solution was extracted with dichloromethane (5 x 120 mL). The organic layers were combined and dried with sodium sulfate, filtered and dried under vacuum to give a clear liquid product (**2**, 62 g, 95 % yield) and used without further purification. To add a halogen atom for ATRP, **2** (10.0 g, 2.48 x 10^{-2} mol) and triethylamine (4.0 g, 3.97 x 10^{-2} mol) were dissolved in anhydrous dichloromethane (150 mL) in a flame-dried, 250-mL, round-bottom flask equipped with a magnetic stir bar. After cooling in an ice bath, 2-chloropropionyl chloride (5.0 g, 3.95 x 10^{-2} mol) was added slowly via syringe and the reaction mixture was allowed to warm to room temperature and stirred for 24 h. The mixture was washed with 0.1 N NaOH (3 x 30 mL), saturated NaCl solution (2 x 50 mL), and DI water (50 mL). The organic solution was dried with sodium sulfate, filtered and the solvent was evaporated. A clear orange-brown viscous oil (**3**, 12.0 g, 83 % yield) was obtained after drying in vacuo at 40 ^{o}C. An initiator containing a bromoalkane functional group was synthesized by reacting **2** with 2-bromoisobutyryl bromide in a similar procedure.

5.2.3.3 Synthesis of an ammonium bis(phosphonate)-functional PNIPAM via ATRP

Synthesis of ammonium bis(phosphonate)-PNIPAM (**3**) was carried out using the alkyl chloride initiator and CuCl/Me_6TREN as the metal activator and ligand. The initiator (0.32 g, 6.48 x 10^{-4} mol), NIPAM (4.6 g, 4.07 x 10^{-2} mol), CuCl (65 mg, 6.48 x 10^{-4} mol), Me_6TREN (190 uL, 6.48 x 10^{-4} mol), and a DMF:H_2O mixture (v:v 3:1, 8 mL) were added to a 25-mL Schlenk flask. After it was degassed by three freeze-pump-thaw cycles, the flask was kept under a slight pressure of N_2. The reaction mixture was

immersed in an oil bath at 25 ^{o}C for polymerization. After 60 min, the reaction was stopped by diluting with THF (20 mL), and the mixture was passed through an alumina column to remove the copper catalyst. The polymer was purified by precipitation in n-hexane twice, collected by filtration, and dried in a vacuum oven at 30 ^{o}C for 24 h.

To remove the ethyl ester groups from the initiator, bis(phosphonate)-PNIPAM (1.10 g, 1.53 x 10^{-4} mol) was dissolved in anhydrous dichloromethane (30 mL). Trimethylsilyl bromide (0.190 g, 1.22 x 10^{-3} mol) was slowly added dropwise to the mixture under a dry N_2 atmosphere. The solution was allowed to stir at room temperature for 24 h, then the solvent and excess TMSBr were removed under vacuum at room temperature. Anhydrous methanol (5 mL) was added to the resultant polymer and the mixture was stirred for 4 h. Bis(phosphonic acid)-PNIPAM was recovered by precipitation into hexane and dried in vacuo at 40 ^{o}C.

5.2.3.4 Synthesis of polymer-magnetite complexes

A representative method for preparing a targeted composition of 67:33 wt:wt polymer:magnetite complex is provided. Oleic acid-stabilized magnetite nanoparticles (33.0 mg) were dispersed in chloroform (10 mL) and charged to a 50-mL round-bottom flask. An ammonium bis(phosphonate) functional PNIPAM (67.0 mg) was dissolved in DMF (10 mL) and added to the dispersion. The reaction mixture was sonicated in a VWR 75T sonicator for 2 h under N_2, and then stirred at RT for 24 h. The nanoparticles were precipitated in hexanes (300 mL). A permanent magnet was utilized to collect the magnetite nanoparticles and free oleic acid was decanted with the supernatant. The particles were dried under vacuum overnight and dispersed in DI water (20 mL) using sonication for 30-60 s. The complexes were dialyzed against DI water (1 L) for 24 h in a

25,000 g mol^{-1} MWCO dialysis bag to remove free polymer, then freeze-dried to obtain a black-brown solid product.

5.3 Results and Discussion

5.3.1 Synthesis of an ammonium bis(phosphonate) functional ATRP initiator

One of the key features of our design is having ammonium bis(phosphonate) moieties at the end of the polymer without further post-polymerization functionalization. The effort focused on preparing initiators that contained phosphonate zwitterions. Vinyldiethylphosphonate was reacted with an aminoalcohol through a double aza-Michael reaction to afford hydroxy γ-amino(bisphosphonate). However, in common organic solvents, it is known that aza-Michael reactions are sluggish without a use of elevated temperature and a catalyst.[176] Double-fold addition of an amine onto weakly-active Michael acceptors such as vinylphosphonate, therefore, is even more difficult. Recently, organic reactions in water have received much attention due to the enhanced rate of reaction in water.[177, 178] The catalytic activity of water molecules was described by the formation of a chair-like intermediate involving the Michael donor and acceptor.[179] In our case, double addition of an amine onto vinylphosphonates in water was found to be smooth and marked with very high yields of > 95%. The intermediates could be used without purification since no side reactions were observed. Integration of the two resonances in the ^{31}P NMR spectrum was 99:1, indicating that almost all of the crude product was the targeted compound. The hydroxyalkylamino bis(diethylphosphonate) intermediate was reacted with either chloropropionyl chloride or bromoisobutyryl bromide to obtain ATRP initiators. Purification processes of the initiators were simple and required no chromatography. The overall yields of the products exceeded ~70 % after

repetitive washing and extraction followed by drying in vacuo. The initiator structures were confirmed by both ^{1}H and ^{31}P NMR (Figures 5.3-5.6)

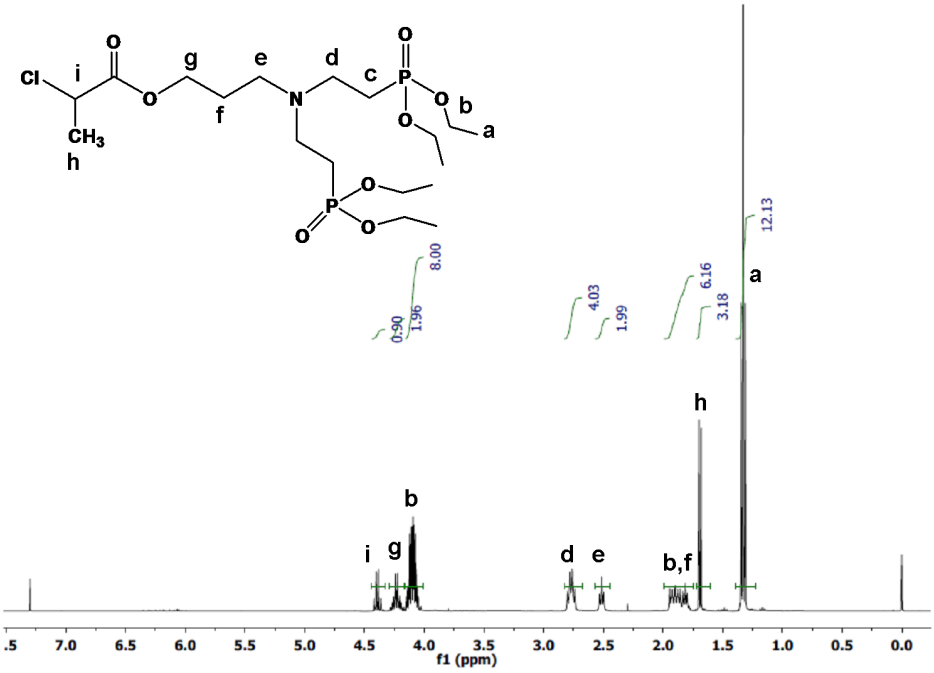

Figure 5.3 ^{1}H NMR spectrum of initiator 3

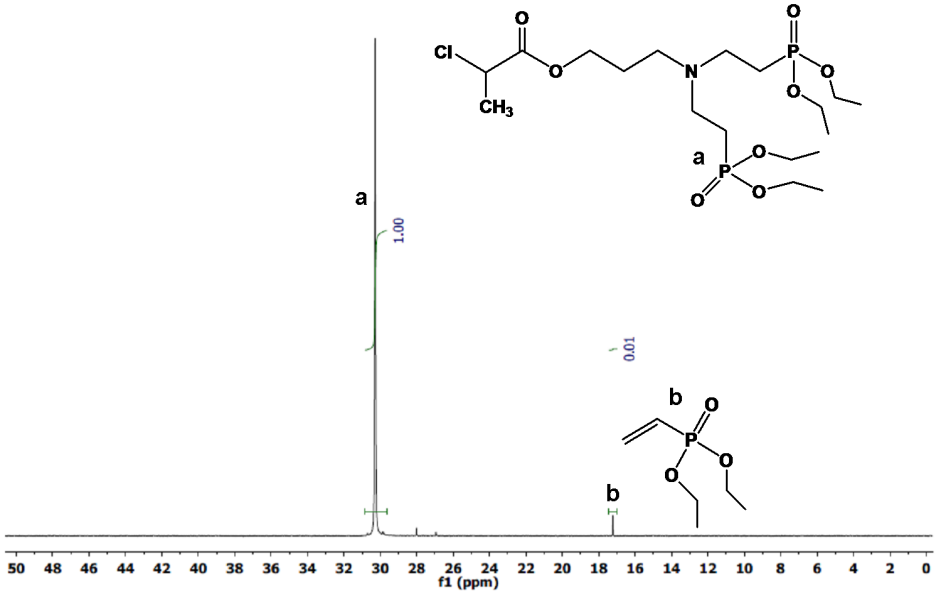

Figure 5.4 ^{31}P NMR spectrum of initiator 3

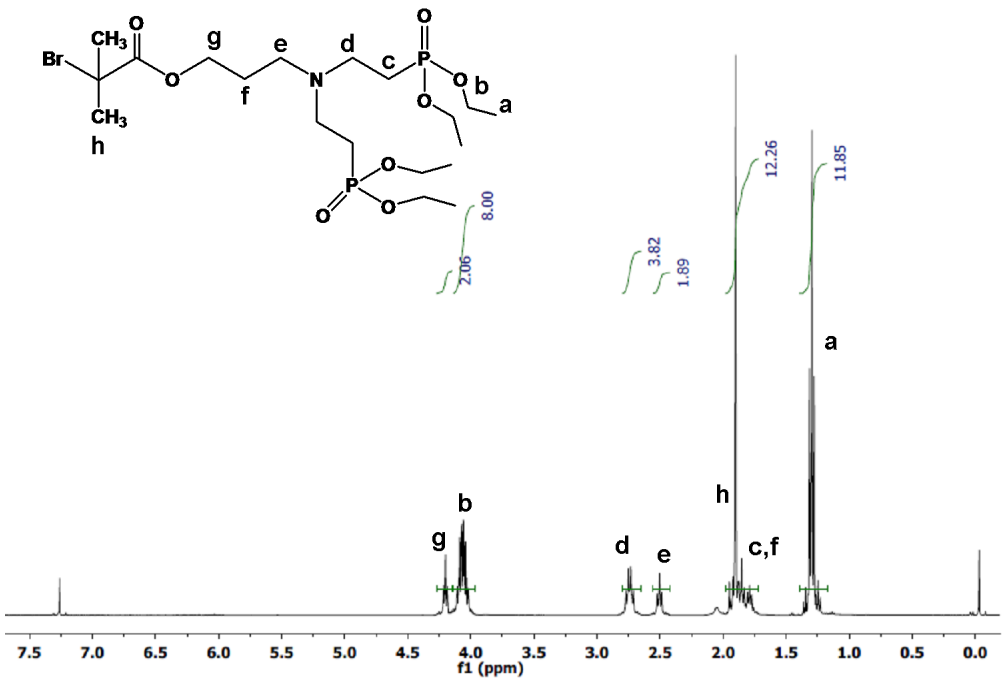

Figure 5.5 ^{1}H NMR spectrum of initiator 4

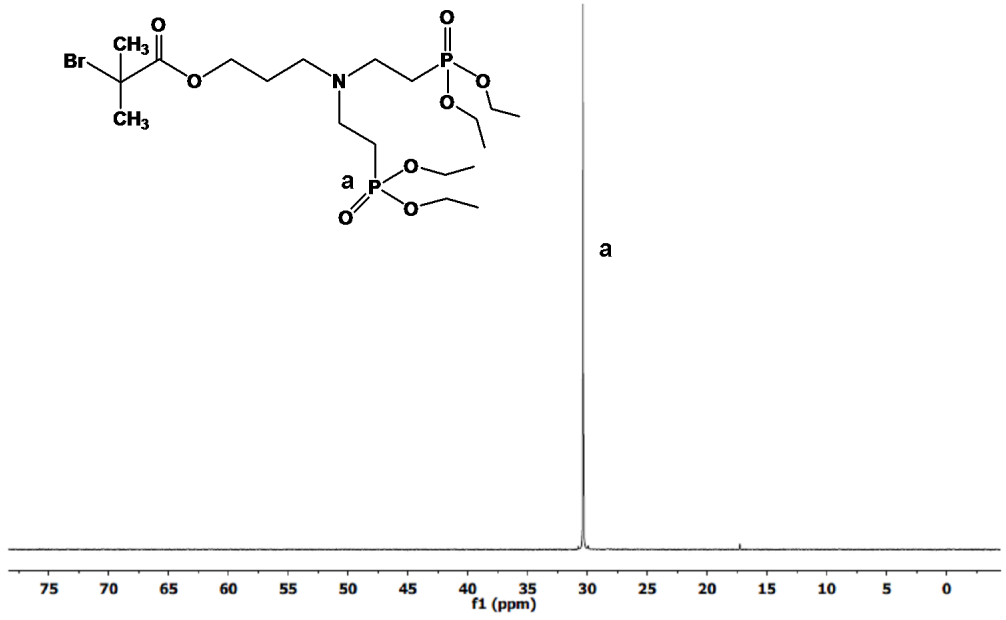

Figure 5.6 ^{31}P NMR spectrum of initiator 4

5.3.2 Synthesis of ammonium bis(phosphonate) functional macromolecules

Polymerization of NIPAM through ATRP is met with challenges which have been attributed to 1) occurrence of slow deactivation in conjunction with fast activation, 2) the loss of halogen endgroups attributed to a cyclization reaction involving nucleophilic displacement of the halogen endgroup by amide nitrogens from monomers, and 3) copper catalyst complexation with amide groups.[180] Several catalyst systems have been employed to circumvent such problems. Most NIPAM polymerizations using linear amine or bipyridine based ligands generally result in low conversions.[181, 182] Masci *et al.* was the first to report the successful use of ATRP for polymerizing NIPAM with good control and high conversion by using Me_6TREN as a ligand and a DMF/water mixture as a solvent.[183] Hydrogen-bonding between the solvent and amide groups of monomers and the polymer chain markedly reduces both their catalyst association and chain-end termination. Similar observations were also reported by Stover *et al.* who reported that alcohol solvents could be employed to polymerize NIPAM with high conversion and narrow dispersions of molecular weight though ATRP.[184]

In the work reported herein, we have investigated bis(phosphonate)-containing chloride and bromide initiators. As expected based on previous reports, the chloride initiator in conjunction with Me_6TREN provided better control. The polydispersity index (PDI) decreased from 1.43 to 1.07 (table 1) when changing from the bromide to chloride initiator in conjunction with cuprous bromide or cuprous chloride respectively. High conversions (>95%) were observed within 60 minutes of reaction under the specified conditions. Molecular weights were slightly higher than targeted based on the ratio of monomer to initiator, and this was attributed to a minor amount of radical-radical

coupling during the process, likely at high conversions. Increasing the reaction time apparently amplified the coupling and resulted in a high molecular weight tail on the SEC chromatograms (Figure 5.7).

Initiator	Time (min)	M_n (NMR) g mol^{-1}	M_n (SEC) g mol^{-1}	PDI
3	60	7900	11000	1.07
3	180	7300	13000	1.17
4	60	7200	12000	1.43

Table 1. Reaction conditions, molecular weights and polydispersities of PNIPAM. DMF:water = 3:1 v:v, T = 25 ^{o}C, $[M]_o/[I]_o/[CuCl]_o/[ligand]_o$ = 60:1:1:1.

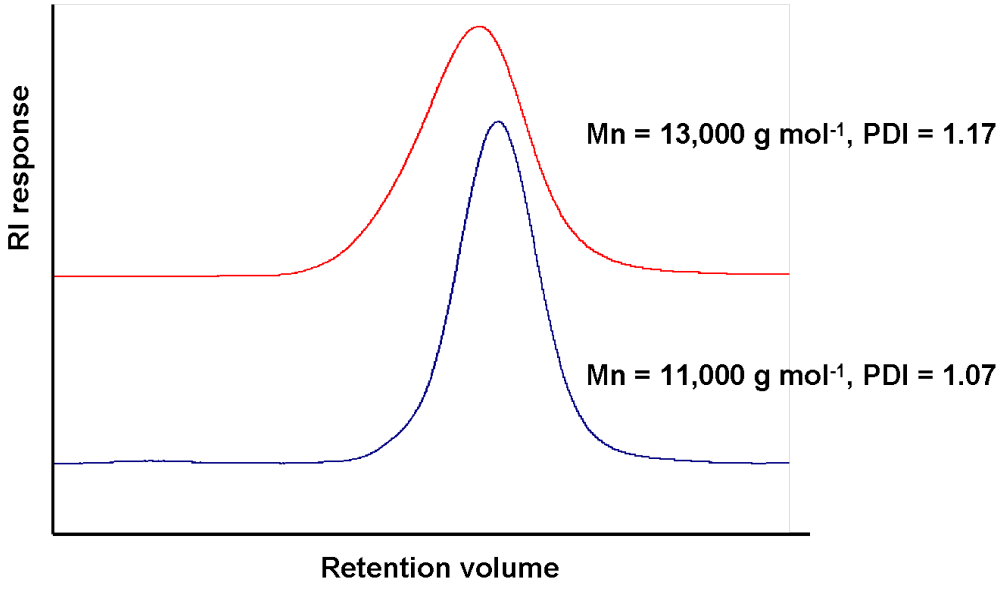

Figure 5.7 SEC traces of PNIPAM reacted for 60 min (bottom) and 180 min (top)

^{1}H and ^{1}P NMR revealed that the aminoalkyl bis(phosphonate) endgroup was retained throughout the course of polymerization. The ethyl ester groups were then removed to afford the corresponding bis(phosphonic acid) prior to immobilization on the surface of magnetite. To prevent non-selective cleavage of the ester linkage between PNIPAM and the aminoalkyl bis(phosphonate) initiator moiety, trimethylsilyl bromide (TMSBr) was used as the silylating agent followed by mild removal of silyl ester groups via methanolysis (Figure 5.8).

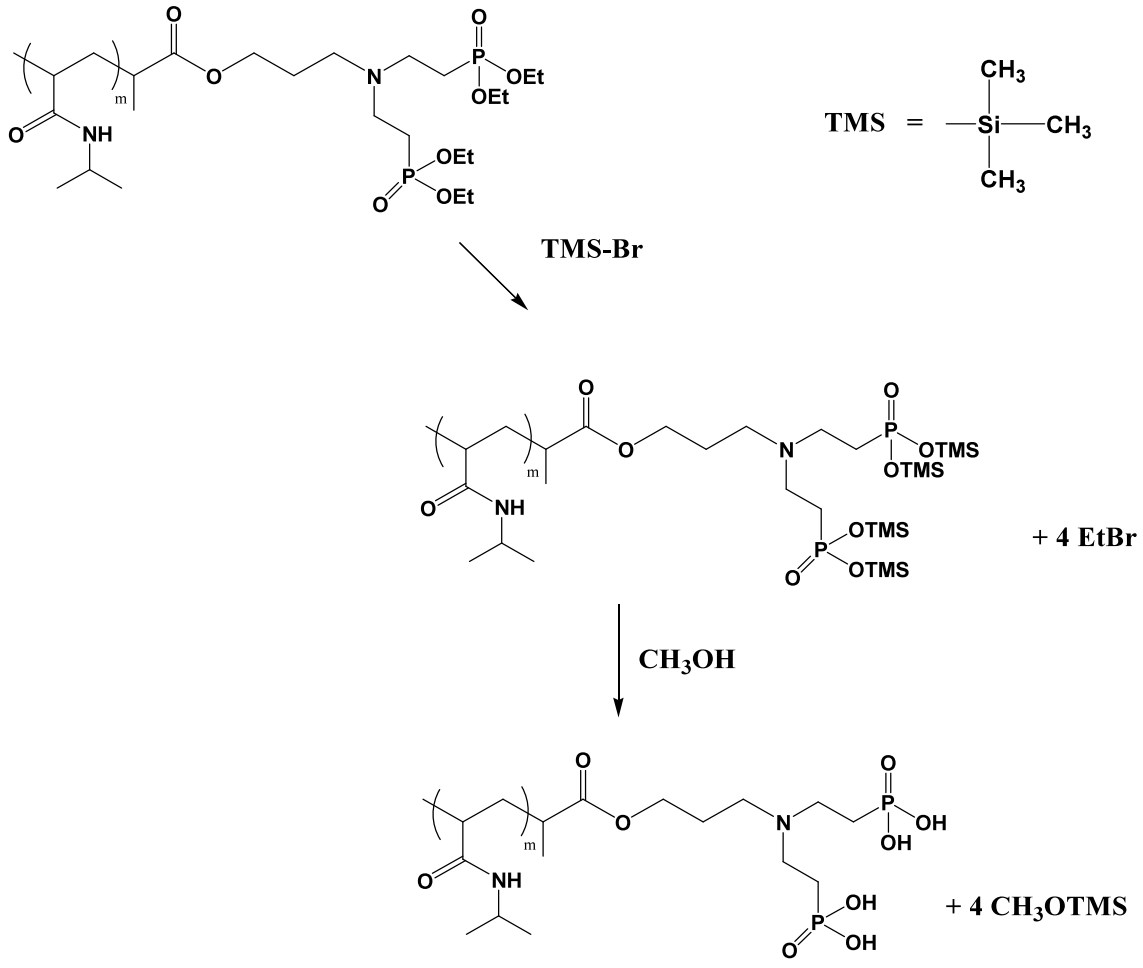

Figure 5.8 Selective deprotection of ethylphosphonate esters

Since an excess of TMSBr was used to ensure quantitative deprotection, the residual TMSBr must be removed prior to methanolysis to avoid any generation of HBr

that might cleave the ester linkage between the bis(phosphonate) initiator and the PNIPAM. It is also important that PNIPAM must be completely dry during this step to prevent side reactions. To ensure this, PNIPAM was dissolved in dichloromethane and dried with sodium sulfate, filtered, precipitated in hexane, and dried under vacuum at 70 ^{o}C for 24 hours prior to the deprotection step. Realizing that the ester bond may be vulnerable to hydrolysis, future efforts will improve upon stability by incorporating a more stable amide linkage.

The complete disappearance of the resonance peaks at chemical shifts of 1.2 and 4.1 ppm indicated that the ethyl ester groups were quantitatively removed. The resonance signal in the ^{31}P NMR spectrum also shifted from approximately 30 to 21 ppm upon removing the ethyl groups (Figure 5.9-5.12)

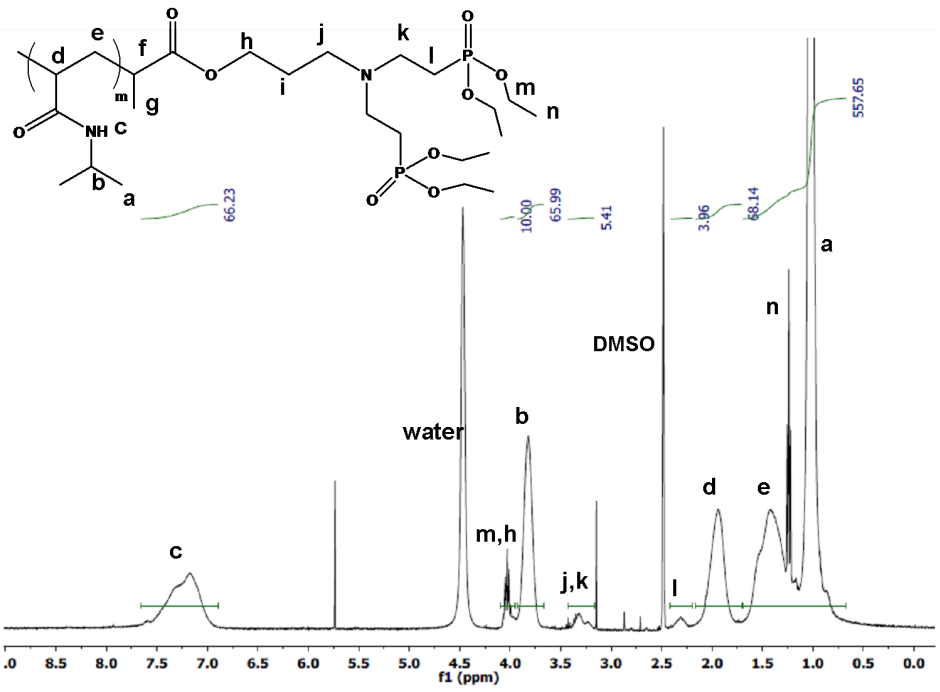

Figure 5.9 ^{1}H NMR spectrum of the bis(diethylphosphonate)-PNIPAM prior removal of the diethyl esters

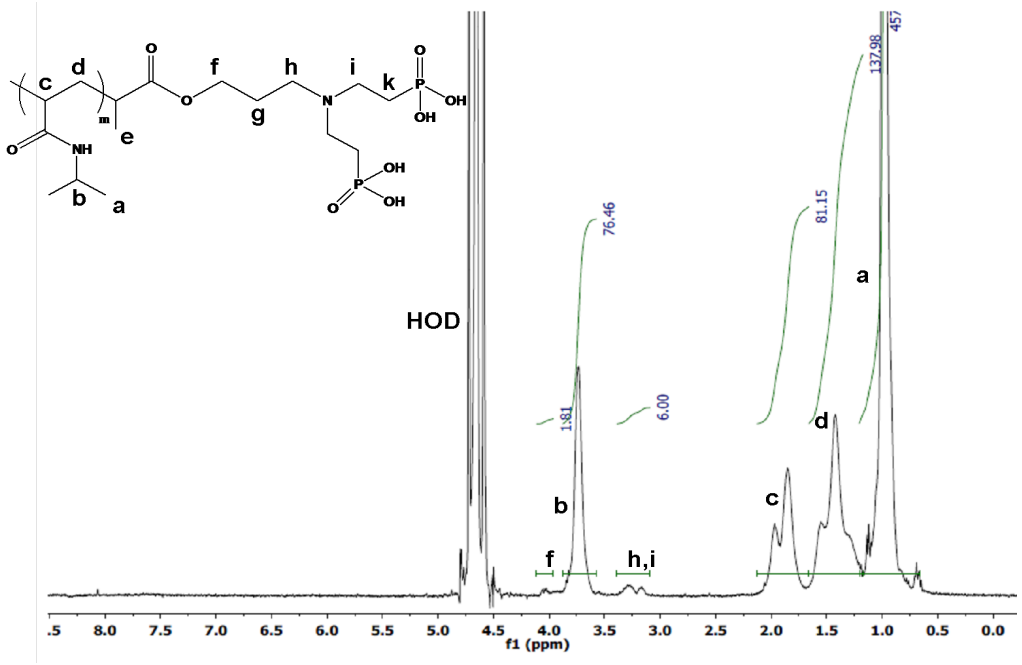

Figure 5.10 ^{1}H NMR spectrum of the bis(phosphonic acid)-PNIPAM after removal of the diethyl esters

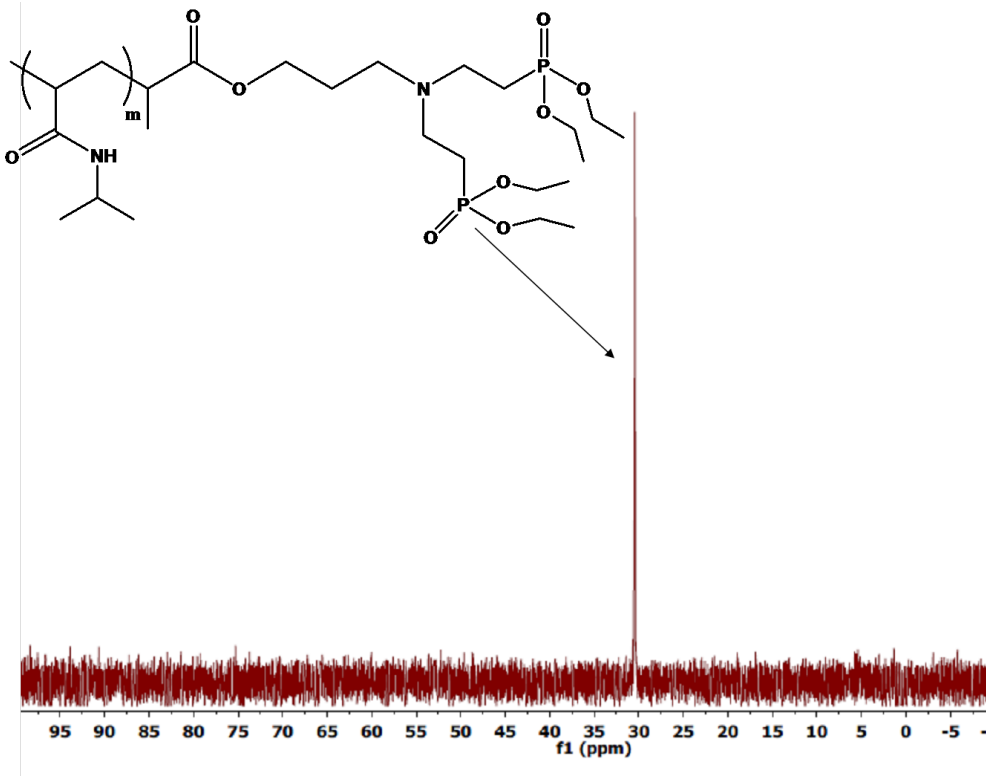

Figure 5.11 ^{31}P NMR spectra of PNIPAM-bis(diethylphosphonate) in d_6-DMSO

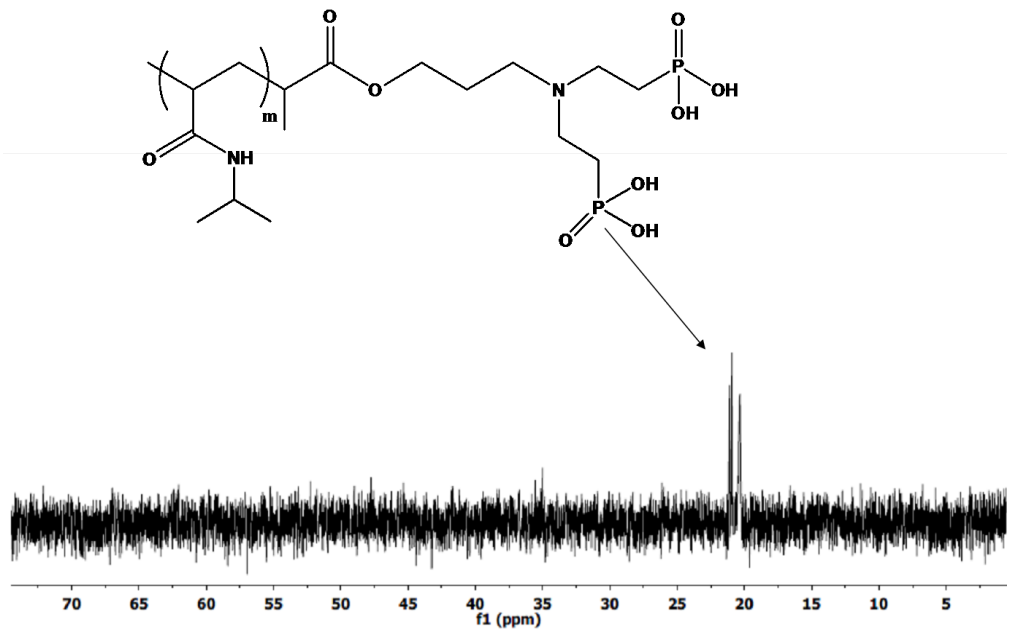

Figure 5.12 ^{31}P NMR spectra of PNIPAM-bis(phosphonic acid) in D_2O

5.3.3 Adsorption of ammonium bis(phosphonate)-functional PNIPAM on magnetite nanoparticles

ATRP has been employed for surface modification of magnetic nanoparticles via a "grafting from" method that propagates polymer chains from nanoparticle surfaces. Most anchor groups on the ligand/initiators have been limited to carboxylates and silanes.[185-188] We have shown that polyethers that are bound to magnetite through one to three carboxylates desorb significantly when the complexes are exposed to phosphate ions in phosphate buffers,[6] so the integrity of the carboxylate-magnetite anchor is a concern for biotechnological applications. Silanol coupling may provide a more stable covalent linkage.[186] Another concern regarding a "grafting from" approach is that several heavy metal ions including copper have been shown to efficiently bind with iron oxide

through formation of inner sphere complexes, and this raises potential contamination and toxicity issues for biomedical applications.[189, 190]

We chose to form the polymer through ATRP first, remove the copper catalyst from a solution of the polymer, then adsorb it onto the magnetite surface through robust phosphonate anchoring moieties. We previously demonstrated that high brush densities can be achieved using homogeneous ligand adsorption.[6, 8] Ligand adsorption was employed to link the bis(phosphonate)-PNIPAM to the magnetite nanoparticles. This process requires that the polymer and nanoparticles are homogeneously dissolved/dispersed in the solvent. While poly(ethylene oxide) with ammonium phosphonate endgroups can be efficiently adsorbed onto magnetite from chloroform,[6] attempts to use chloroform as a solvent for PNIPAM adsorption resulted in less polymer coverage and poor dispersibility of the particles in aqueous media. This was attributed to poor solubility of the PNIPAM-bis(phosphonic acid) in chloroform. Using a mixed solvent of 1:1 DMF and chloroform circumvents this issue. After adsorption, the particles were precipitated into hexane, which is non-solvent for the PNIPAM but a good dispersant for oleic acid-coated magnetite nanoparticles. Any unbound polymer was removed by dialysis against DI water. TGA results (Figure 5.11) indicated that the composition of the PNIPAM-magnetite complex was 65 wt% polymer (corrected with the approximately 10 % char yield of PNIPAM) and this was in close agreement with the targeted 67 wt% polymer composition. ICP-AES results following digestion with nitric acid showed 66.3 wt% polymer. These results were consistent with our previous work showing that high concentrations of phosphonate-functional polymers can be adsorbed onto magnetite. These PNIPAM-magnetite nanoparticles were dispersible in water.

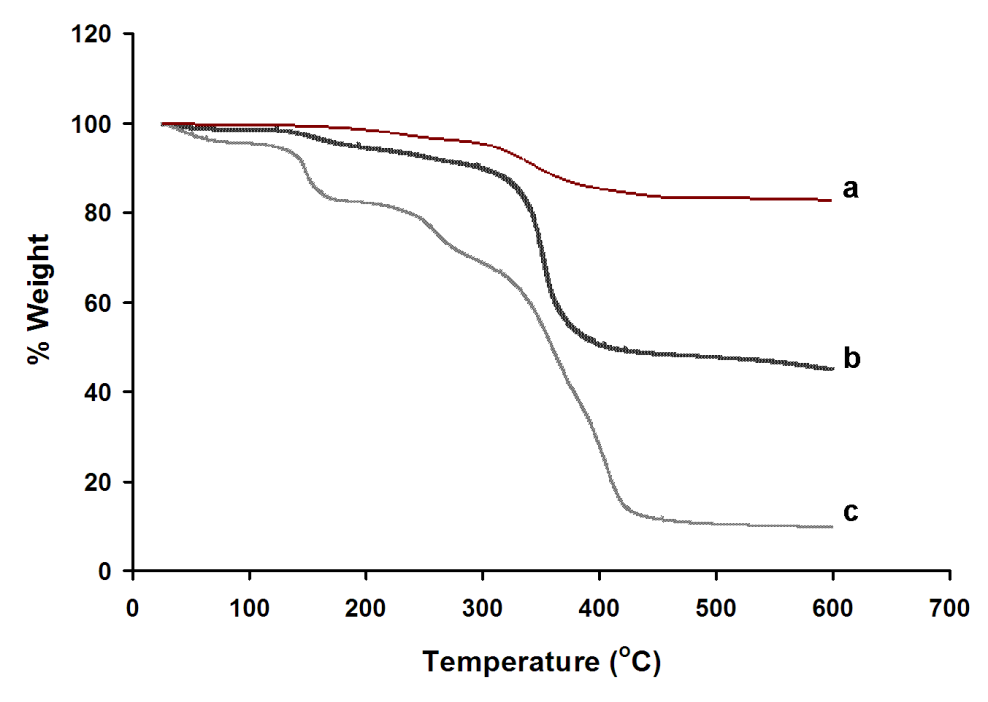

Figure 5.11 TGA of a) oleic acid coated magnetite, b) magnetite-PNIPAM and c) PNIPAM

The magnetic properties of the magnetite nanoparticles were analyzed by SQuID magnetometry. The magnetization (M) versus applied field (H) curves of the magnetite-PNIPAM nanoparticles at 300 K and 5 K are depicted in figure 5.12. The sample was fully superparamagnetic at 300 K with a saturation magnetization (M_S) of 18 emu g^{-1} at an applied field of 70 kOe. This corresponds to an M_S of ~55 emu g^{-1} for the magnetite nanoparticle core. The decrease in saturation magnetization compared to the value of bulk magnetite can be attributed to spin canting caused by reduced coordination and broken exchange at the particle surface and/or broken symmetry associated with crystalline disorder. [191-194]

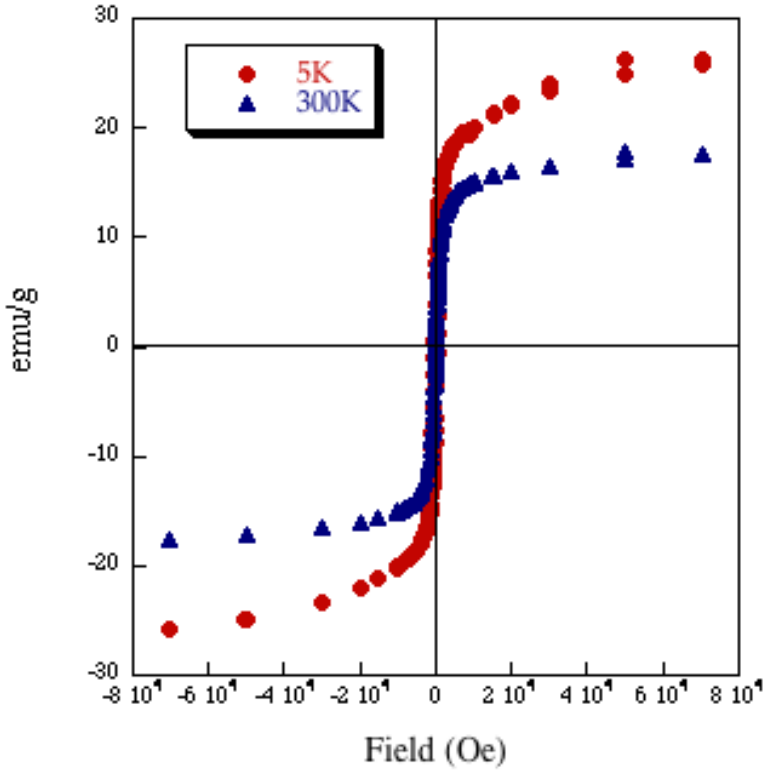

Figure 5.12 Hysteresis loop of magnetite-PNIPAM measured by SQuID

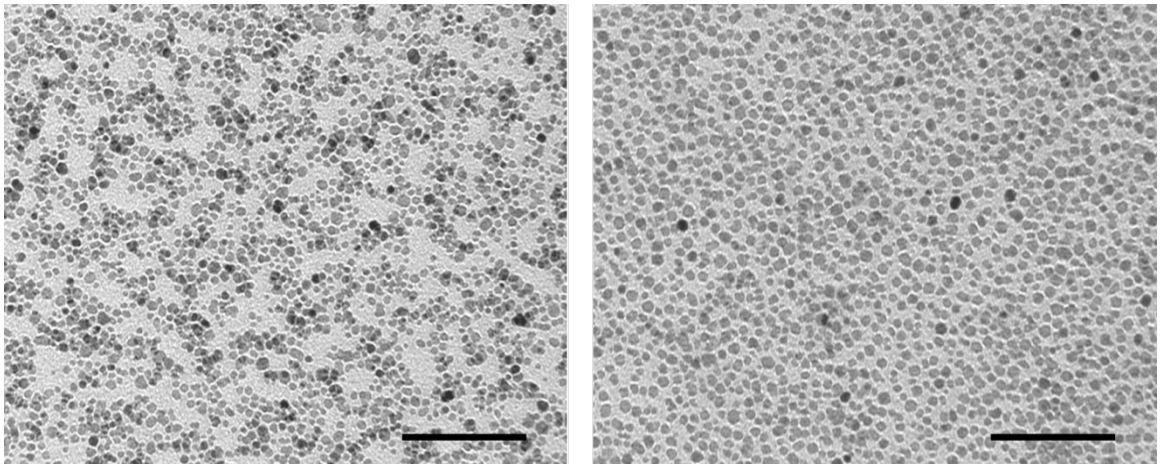

Figure 5.13 TEM images of oleic acid-coated magnetite cast from hexane (left) and PNIPAM-coated magnetite cast from DI water (right). Scale bar = 100 nm

There have been several reports of magnetite nanoparticles coated with PNIPAM. Most of this research utilized conventional solution free radical polymerization in the presence of magnetite. The efforts led to particle and aggregate sizes ranging from approximately 100 to 600 nm in diameter.[195-197] Alternatively, as demonstrated in this work, adsorption of PNIPAM with one bis(phosphonate) functional group precisely positioned at one end onto discrete nanoparticles from a homogeneous dispersion resulted in dispersed particles without significant aggregation (Figure 5.13). The measured sizes of ~1400 particles by TEM were used to describe a log-normal distribution of magnetite cores with a mean diameter of 7.66 ± 0.08 nm and a standard deviation of 0.29 ± 0.01. PNIPAM-coated magnetite nanoparticles could be readily dispersed in aqueous media at room temperature due to the hydrophilic nature of the PNIPAM shell.

The intensity- and number-averaged hydrodynamic diameters of the particles measured by DLS were 38 and 23 nm respectively. The relatively narrow size distribution of the complexes was evident from the low polydispersity indices (< 0.15). The core diameter determined from TEM size analysis and the number-averaged diameter calculated by the Zetasizer software were used to estimate the thickness of the PNIPAM shell to be approximately 8 nm. From DLS, the intensity-average hydrodynamic diameter (D_i) of magnetite coated with PNIPAM (65 wt%, M_n=13000 g mol^{-1}) was 38 nm. To determine if the polymer-magnetite complexes consisted mostly of dispersed primary particles or of aggregates, the average sizes of the polymer-magnetite complex were estimated using a modified density distribution model[198] which predicts the thickness of the polymer brush around the magnetite core using a theory developed originally for star polymers. This modified model was used previously to predict the sizes

of magnetite stabilized with polyethers in water[8] and polydimethylsiloxane in chloroform.[199] For well-defined polymer-magnetite complexes, the model can predict the size to within 7% without any adjustable parameters. To implement this model, the size distribution of the magnetite particles was measured by transmission electron microscopy (Figure 5.13) and fitted with a Weibull probability distribution function. The fitted-mean radius of the magnetite nanoparticles was 4.04 nm. The chain stiffness of the PNIPAM in water at 25 °C is characterized by the statistical segment length, or Kuhn length, of 1.34 nm (given by the product of the characteristic ratio, $C_\infty = 10.6$ and the virtual bond length, $l_o = 0.126$ nm).[200] The polymer-solvent interaction is characterized by the Flory exponent, $\nu = 0.518$ (25 °C in water).[201] Using the above parameters in the density distribution model, the number-average diameter of magnetite coated with PNIPAM (65 wt%, M_n= 13000 g mol^{-1}) was estimated to be 29.4 nm, which corresponds to a brush thickness of ~ 11 nm. The predicted volume- and intensity-average diameters are 31.4 nm and 32.4 nm respectively. Comparison of this last value with D_i measured by DLS indicates that the complex consisted mostly of dispersed particles.

5.3.4 Stability of particles

The stability of the bis(phosphonate) anchor group in binding to the magnetite surface was evaluated in media of different ionic strengths and also in the presence of competitive phosphate ions in PBS. As shown in figure 5.14, the hydrodynamic size of the PNIPAM-coated magnetite nanoparticles remained virtually unchanged in the presence of 0.14 M NaCl with 13 mM phosphate, and this was the case up to 0.5 M NaCl, a 3.5-fold higher ionic strength relative to physiological media and body fluid.

Furthermore, the particles exhibited good colloidal stability in PBS (0.14 M, pH 7.4) without noticeable aggregation (Figure 5.15).

Dispersions of the particles were dialyzed against PBS for 24 hours to measure any polymer desorption that might be caused by displacement by salts or phosphate ions in the medium. The dispersions were subsequently dialyzed against water for an additional 24 hours to remove any desorbed polymer and salts. After freeze-drying, TGA was used to determine the polymer loadings of the particles before and after this process to investigate anchor group stabilities in the presence of phosphate salts in the medium. Any desorption of the polymer from the magnetite surface in PBS should be indicated by a decrease in polymer loading. The amount of polymer after dialysis in PBS was 63 wt%, indicating no significant loss of PNIPAM. Based on this study, it was reasoned that bis(phosphonate) anchor groups would likely have good stability in physiological media, and thus be suitable candidates for biomedical applications.

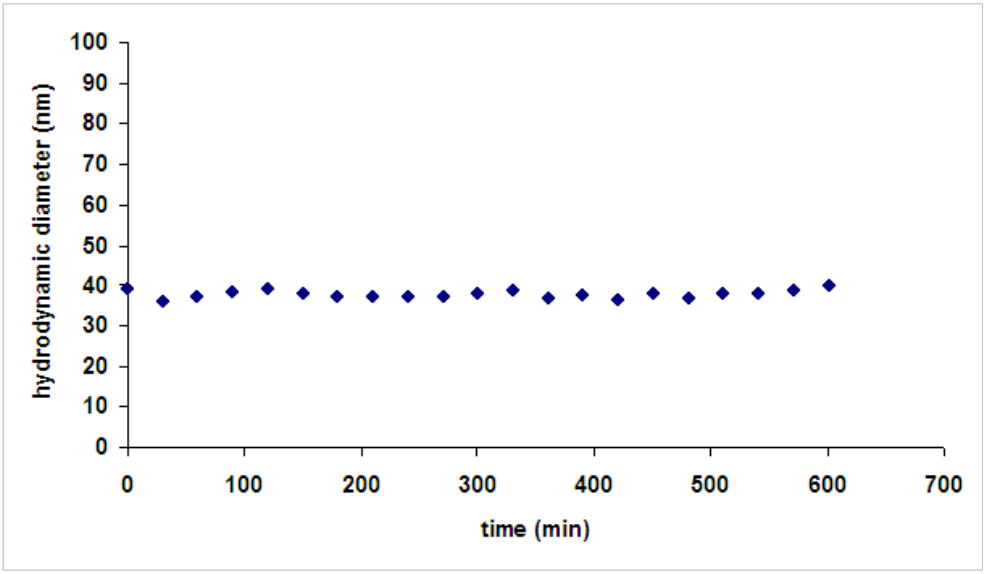

Figure 5.14 Colloidal stability of the nanoparticles in phosphate buffered saline (0.14 M NaCl, pH 7.4, 13 mM phosphate) at 25 ^{o}C.

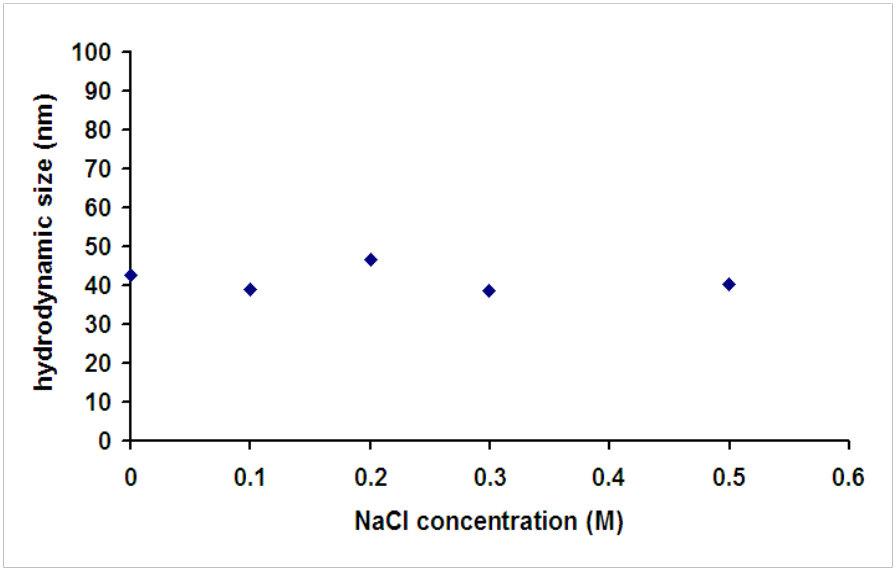

Figure 5.15 Hydrodynamic sizes of magnetite-PNIPAM in NaCl solutions. The particle concentration was kept constant at 1 mg mL^{-1}.

5.3.5 Thermosensitive properties of PNIPAM-magnetite nanoparticles

PNIPAM was chosen as a brush for the magnetite nanoparticles because of its thermoresponsive properties close to body temperature. DLS was used to monitor the temperature-induced change in hydrodynamic size of the PNIPAM-coated magnetite in the range of 20 – 44 ^{o}C. Results shown in figure 5.16 revealed that there is an onset of particle size increase at ~33 ^{o}C, which is in reasonable range of the reported LCST of PNIPAM. This indicates that there is an aggregation of particles since PNIPAM shells dehydrate and become more hydrophobic, thus causing the agglomeration of particles (Figure 5.17). The particle size, however, appeared to be 60 nm at 34 ^{o}C and remain stable at this size even as the temperature was increased up to 44 ^{o}C. This increase in hydrodynamic size and formation of nanoclusters was accompanied by a marked drop in the particle polydispersity indices (PDI) measured by DLS. Evidently, above 33 ^{o}C, the formation of clusters seems to be in a uniform fashion as indicated by very low PDI

values of 0.05-0.02. These results are encouraging and suggest the possibility of engineering controlled magnetic nanoclusters, which may lead to enhanced performance in some biomedical applications.[202, 203] More detailed investigations with respect to the thermally-induced formation of nanoclusters are currently in progress.

PNIPAM-coated magnetite nanoparticles are dispersible in water at room temperature and exhibit good colloidal stability even at high concentrations of ~20 mg mL^{-1}. No sedimentation was observed when a vial containing the dispersion was placed on top of a permanent magnet. By contrast, when heated above the LSCT (Figure 5.17), there was a sharp increase in turbidity and the particles could be collected with the permanent magnet. The dispersibility of the complexes could be fully restored by cooling the dispersions down to room temperature. Therefore, the thermo-responsive behavior of the PNIPAM shell enables reversible flocculation of the nanoparticles by a combination of thermal and magnetic effects.

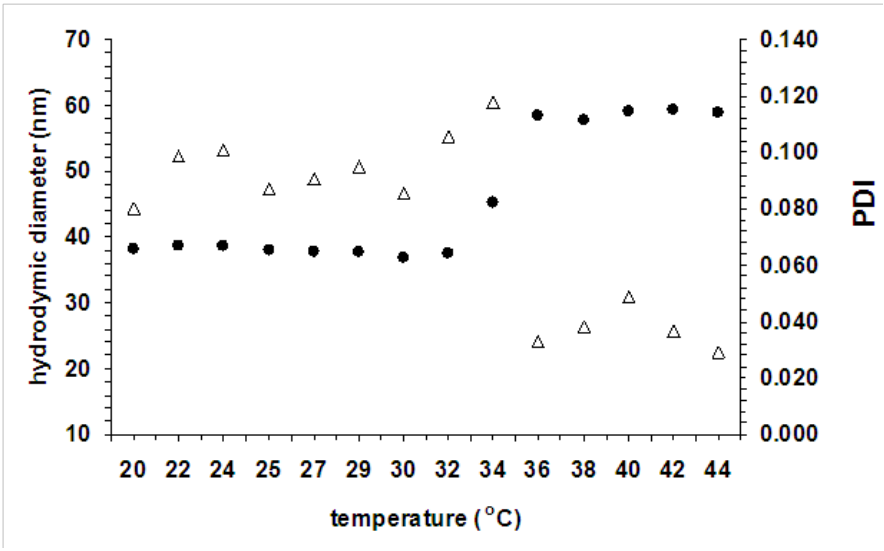

Figure 5.16 DSL measurements of magnetite nanoparticle-PNIPAM at a concentration of 2 mg mL^{-1} in DI water. Hydrodynamic size (black circles) and PDI (open triangles) were

monitored as a function of temperature. The temperature was raised in 2 ^{o}C interval and the sample was equilibrated at each step for 10 minutes before DLS measurement.

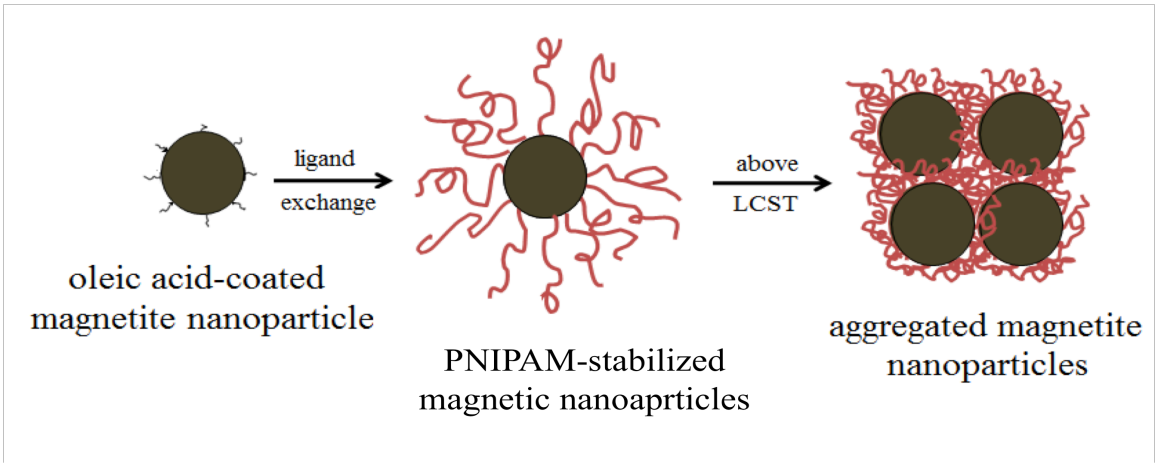

Figure 5.17 Schematic illustration of the LCST-induced aggregation of PNIPAM-stabilized magnetite nanoparticles.

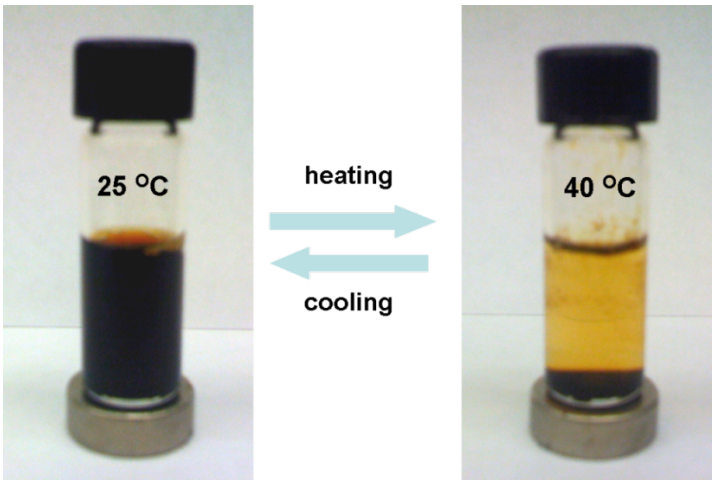

Figure 5.18 Magnetic field-induced reversible flocculation of PNIPAM-magnetite nanoparticles. Concentration of nanoparticles is 20 mg mL^{-1} in DI water.

5.4 Conclusion

We have reported the synthesis and characterization of a new bis(phosphonate)-functional initiator for the polymerization of thermo-responsive PNIPAM through ATRP. In three simple and efficient reaction steps, bis(phosphonate) initiators can be synthesized for the polymerization of NIPAM. After mild deprotection of the phosphonic acid moieties, adsorption of bis(phosphonic acid)-PNIPAM onto magnetite affords well-defined, water-dispersible and thermo-responsive nanoparticles. Combining a thermosensitive polymeric shell with a magnetic core paves the way for multi-stimuli-responsive nanoparticles for biomedical applications. As a continuing effort of our group on investigating nanoparticle-cell interactions and structure-relaxivity relationships of magnetic nanoparticles, we envision that this methodology can be modularly extended and applied to polymerize other monomers to create a library of polymeric shells for magnetic iron oxide nanoparticles.

Chapter 6

Design and synthesis of theranostic core-shell nanostructures for dual delivery of imaging and chemotherapeutic agents

6.1 Synopsis

The term "theranostics" was adopted to define ongoing efforts to develop more specific individualized therapies for various diseases, and to combine diagnostic and therapeutic capabilities into a single agent.[9, 10] The rationale arose from the fact that diseases such as cancers are immensely heterogeneous, and all existing treatments are effective for only limited patient subpopulations and at selective stages of disease development.[204] The concept is that a combination of diagnostic and therapeutic agents could provide therapeutic protocols that are specific to individuals and, therefore, are more likely to offer improved prognoses. The potential impact of combination therapeutic delivery and diagnostic modalities within the same carrier has led to the development of multifunctional nanoparticles.[205-207] Of particular significance to us are magnetic nanoparticles, especially biocompatible nanomagnetite (Fe_3O_4,). Incorporating magnetic nanoparticles into nanocarriers could enable monitoring of biodistribution via magnetic resonance imaging together with treatment.

With an aim to develop nanocarriers with high drug loadings that integrate magnetic nanoparticles for diagnostics into one system, we herein report a facile approach to form magnetic block ionomer complexes (MBICs) based upon assembly of block ionomers with nanomagnetite (Figure 6.1). The magnetite core was first synthesized via reductive decomposition of an iron (III) organometallic precursor, which

allows formation of discrete and uniform particles. Well-defined nonionic-ionic block copolymers of monomethoxy-functional poly(ethylene oxide) (mPEO) and poly(acrylic acid) (mPEO-*b*-PAA) were synthesized through controlled free-radical polymerization (ATRP). The polymer was bound to the surfaces of the magnetic nanoparticles through ligand adsorption of the PAA component, thereby creating a double corona structure comprised of an outer nonionic mPEO shell and an inner ionic layer of PAA.

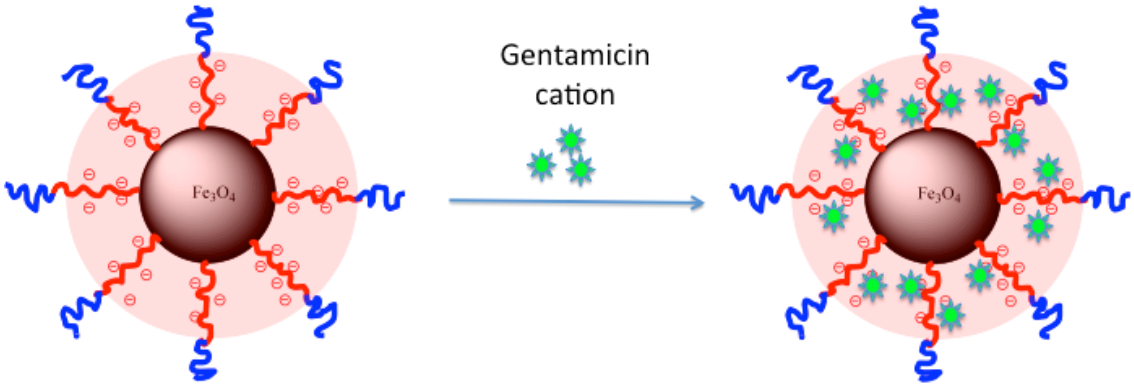

Figure 6.1 Schematic illustration of gentamicin encapsulation into MBICs

The carboxylate-rich segment of the block copolymer functions as a robust anchoring moiety attached to the surface of magnetite owing to the multidentate nature of the polymeric ligand. The portion of carboxylate groups that are not attached to the magnetite provide functionalities and binding sites for drug loading via ionic complexation and chelation as shown in figure 6.1. PEO was chosen as a segment of the block copolymer to improve biocompatibility and aid in dispersion by providing steric repulsion, to avoid interparticle agglomeration.[208, 209] The multi-cationic drug, gentamicin, was used as a model molecule for this encapsulation study. Efficiency of drug loading and in vitro efficacy in reducing the intracellular pathogen *Brucella* were evaluated.

6.2 Experimental

6.2.1 Materials

Benzyl alcohol (>98%), diethyl ether, iron (III) acetylacetonate ($Fe(acac)_3$), oleic acid (90%, technical grade), triethylamine (>99.5%), pentamethyldiethylenetriamine (PMDETA), bromoisobutyryl bromide, and poly(ethylene oxide) monomethylether (mPEO) were purchased from Aldrich and used as received. *tert*-Butyl acrylate (tBA) was distilled from calcium hydride before polymerization. Tetrahydrofuran was dried over sodium using benzophenone as an indicator and was freshly distilled prior to use. Toluene (anhydrous), dichloromethane (HPLC grade), hexane (HPLC grade), and acetone were purchased from Fisher Scientific and used as received. Dialysis tubing was obtained from Spectra/Por. Phosphate buffered saline (PBS) was obtained from Mediatech Inc. (VA, USA). Fetal calf serum (FCS) and DMEM were purchased from Sigma Aldrich.

6.2.2 Characterization

^{1}H NMR spectral analyses of compounds were performed using a Varian Unity 400 NMR or a Varian Inova 400 NMR operating at 399.97 MHz. An Alliance Waters 2690 Separations Module with a Viscotek T60A dual viscosity detector and laser refractometer equipped with a Waters HR 0.5 + HR 2 + HR 3 + HR 4 styragel column set was used for size exclusion chromatography (SEC) analyses. SEC data were collected in chloroform at 30 °C. Data were analyzed utilizing a Universal calibration made with polystyrene standards to obtain absolute molecular weights.

Thermogravimetric analysis (TGA) was used to determine the polymer loading for each complex. TGA measurements were carried out on the mPEO-*b*-PAA-magnetite

nanoparticles using a TA Instruments TGA Q500 to determine the fraction of each complex that was comprised of polymer. Each sample was first held at 110 ºC for 10 min to drive off any excess moisture. The sample (10-15 mg) was then equilibrated at 100 ºC and the temperature was ramped at 10 °C min^{-1} to a maximum of 700 ºC in a nitrogen atmosphere. The mass remaining was recorded throughout the experiment. The mass remaining at 700 °C was taken as the fraction of magnetite in the complexes. The experiments were conducted in triplicate.

DLS measurements were conducted with a Malvern Zetasizer NanoZS particle analyzer (Malvern Instruments Ltd, Malvern, UK) at a wavelength of 633 nm from a 4.0 mW, solid-state He-Ne laser at a scattering angle of 173° and at 25 ± 0.1 ˚C. Intensity, volume and number average diameters were calculated with the Zetasizer Nano 4.2 software utilizing an algorithm, based upon Mie theory, that transforms time-varying intensities to particle diameters.[210] For DLS analysis, the dialyzed complexes were dispersed in DI water at a concentration of 1.0 mg mL^{-1} and filtered through a 1.0 um, Teflon filter directly into a polystyrene cuvette for analysis.

A 7T MPMS SQuID magnetometer (Quantum Design) was used to determine magnetic properties. Hysteresis loops were generated for the magnetite nanoparticles at 300K and 5K. Inductively coupled plasma atomic emission spectroscopy (ICP-AES) were performed on SPECTRO ARCOS 165 ICP spectrometer (SPECTRO Analytical Instrument, Germany) The particles were digested to release free iron by reacting with concentrated nitric acid and diluted to appropriate concentration prior to measurement.

6.2.3 Synthesis of block copolymer

The block copolymer of poly(acrylic acid) and poly(ethylene oxide) was synthesized according to a previous literature procedure.[134] mPEO (6.0 g, 3.0 x 10^{-3} mol) was dissolved in 50 mL of THF in a 100-mL round-bottom flask. Triethylamine (0.840 mL, 6.0 x 10^{-3} mol) was added to the mixture, and then 2-bromoisobutyryl bromide (0.740 mL, 6.0 x 10^{-3} mol) was added dropwise at room temperature. After 48 h, the reaction mixture was filtered and concentrated. The polymer was isolated by precipitation into a large amount of hexane (500 mL) twice and dried under vacuum at 40 °C. mPEO-Br was used as a macroinitiator for polymerization of *t*-butyl acrylate through ATRP.[134, 135] Briefly, mPEO-Br (M_n 2,150 g mol^{-1} , 1.075 g, 5.0 x 10^{-4} mol), *t*-butyl acrylate (9.75 mL, 6.0 x 10^{-2} mol), and 9 mL dry toluene were added into a 50-mL Schlenk flask. After degassing, 72 mg of copper bromide (Cu(I)Br, 5.0 x 10^{-4} mol) and 0.100 mL of pentamethyldiethylenetriamine (PMDETA, 5.0 x 10^{-4} mol) were added quickly under nitrogen. The reaction mixture was deoxygenated with 3 freeze-thaw cycles, and then heated at 80 ^{o}C for 12 h. After the polymerization, the catalyst was removed by filtering the reaction mixture through neutral alumina using dichloromethane as the eluent. The solvent was evaporated and the block copolymer was dried under vacuum at 50 ^{o}C overnight. Removal of t-butyl ester groups was performed by dissolving mPEO-*b*-PtBA (2.0 g, 1.09 x 10^{-2} eq of t-butyl ester groups) in 50 mL of dichloromethane. Trifluoroacetic acid (5 mL, 6.50 x 10^{-2} mol) was added and the reaction mixture was stirred at room temperature for 24 h. the polymer was precipitated into hexane and dried under vacuum. This polymer was redissolved in THF and dialyzed against 4 L of DI water through a cellulose acetate membrane (MWCO 3,500 g mol^{-1}) for 24 h. The

mPEO-*b*-PAA with PEO M_n of 2,000 g mol^{-1} and PAA M_n of 7,200 g mol^{-1} was recovered by freeze-drying.

6.2.4 Synthesis of nanomagnetite

$Fe(acac)_3$ (2.14 g, 8.4 mmol) and benzyl alcohol (45 mL, 0.43 mol) were charged to a 250-mL, three-neck, round-bottom flask equipped with a water condenser and placed in a Belmont metal bath with an overhead stirrer with thermostatic (+/- 1 ^oC) control. The solution was dehydrated at 110 °C for 1 h under a N_2 stream. The temperature was raised to 205 ^oC and maintained for 40 h. The reaction was cooled to room temperature and the particles were collected by centrifugation (4000 rpm, 30 min). The magnetite nanoparticles were washed 3 times with acetone (100 mL each), then were dispersed in chloroform (20 mL) containing oleic acid (0.3 g). The solvent was removed under vacuum at room temperature, and the oleic acid-stabilized magnetite nanoparticles were washed 3 times with acetone (50 mL each) to remove excess oleic acid. The particles were dried under vacuum overnight and stored as a dispersion in chloroform at a concentration of 20 mg mL^{-1} prior to use.

6.2.5 Preparation of core-shell magnetite block ionomer complexes

Homogeneous ligand adsorption from an organic solvent was employed to assemble block ionomers onto nanomagnetite. A representative method for preparing a targeted composition of 66:34 % by weight polymer to magnetite is provided. Oleic acid-stabilized magnetite nanoparticles (50.0 mg) were dispersed in chloroform (10 mL) and charged to a 50-mL round-bottom flask. mPEO-*b*-PAA (100.0 mg) was dissolved in DMF (10 mL) and added to the dispersion. The mixture was sonicated in a VWR 75T sonicator for 4 h under N_2, and then stirred at RT for 24 h. The nanoparticles were

precipitated in hexanes (200 mL). A permanent magnet was utilized to collect the magnetite nanoparticles and free oleic acid was decanted with the supernatant. The particles were dried under vacuum overnight, then dispersed in DI water (20 mL) with adjustment of the pH to ~ 7 with 1 N NaOH and sonicated for 30 min. The particles were dialyzed against DI water (1 L) for 24 h in a 25,000 g mol^{-1} MWCO dialysis bag to remove free polymer. The dispersion was filtered through 0.2 μm Teflon filter to sterile and to remove any aggreagates. a black-brown solid product was obtained after freeze-drying.

6.2.6 Preparation of drug loaded MBICs

mPEO-*b*-PAA coated magnetite (40 mg, 2.18 x 10^{-4} eq COOH) was weighed into a 20-mL glass vial. Gentamicin sulfate solution in 10 mM phosphate buffer pH 7.2 (45 mg gentamicin sulfate, 27 mg gentamicin, 5 mL) was added. The solution was sonicated for 5 min and transferred to a centrifugal filter unit equipped with cellulose acetate membrane (MWCO of 10,000 $gmol^{-1}$). The free drug and salt solution were removed by centrifuging the dispersion at 3750 rpm for 1 h. This allowed the liquid to pass through the membrane into the bottom of the centrifugation unit, and the particles were collected on the membrane. They were removed from the membrane by re-dispersing them in a small amount of DI water (10 mL), then the dispersion was freeze-dried to obtain gentamicin-loaded MBICs.

6.2.7 Quantification of gentamicin content

The amount of encapsulated gentamicin in the MBICs was measured by reacting gentamicin-loaded MBICs with *o*-phthalaldehyde and mercaptoethanol in borate buffer at pH 9.7 fluorescence emission intensity was measured in a fluorimeter (Biotek, USA)

using an excitation wavelength of 340 nm and an emission wavelength of 450 nm.[211] All samples including a series of standard solutions of gentamicin were transferred into 48-well plates and the fluorescence emission was measured. The concentration of gentamicin was calculated from a standard calibration curve.

6.2.8 Drug release studies of gentamicin-loaded MBICs

To determine the release of gentamicin from the nanoplexes in PBS, 10 mg of gentamicin-loaded MBICs (equivalent to 3.1 mg gentamicin) were dispersed in 2 mL of PBS and placed in a 3,500 MWCO dialysis cassette (Fisher Scientific). The cassette was placed in a 250-mL beaker and 150 mL of PBS as the receptor medium was added to the beaker. The beaker was covered with Parafilm and maintained at 37 °C in a temperature-controlled Environ shaker agitated at 50 RPM. Aliquots of 3 mL were taken from the receptor medium and placed in separate scintillation vials after each time point. Each time, 3 mL of fresh PBS was added to the beaker to retain constant volume. The gentamicin in each aliquot was derivatized with *o*-phthalaldehyde and mercaptoethanol as described above and the fluorescence intensity was measured at 450 nm. The amount of free drug (the control) that passed through the dialysis membrane was compared at pH 7.4 at the respective time points using a standardized curve.

6.2.9 *In vitro* efficacy of nanostructures against an intracellular brucellosis model

Brucella melitensis 16M was routinely grown at 37 ºC in tryptic soy broth (TSB) or on tryptic soy agar (TSA, Difco). Efficacies of the MBIC complexes compared to free drug against intracellular *Brucella* were tested in murine J774A.1 macrophages. The cells were seeded at a density of $5x10^6$ cells/well in a 24-well cell culture plate (Corning) 24-36 h prior to infection. At 90% confluency, the cells were infected with *B. melitensis* for

1 h at a multiplicity of infection of 100:1. After phagocytosis, the media was removed and fresh media containing 50 μg mL^{-1} gentamicin was added and the cells were incubated for 45 min to kill the extracellular bacteria. Again, the media was removed and finally the infected cells were incubated with DMEM containing 10% FBS for 24 h to set up the infection model. At 24 h post-infection, the cells were washed twice with DMEM and 50 μL of either free drug or the MBIC complexes containing 50 μg gentamicin, re-suspended in DNAase and RNAase enzyme-free water, was added to the infected cells along with 2 mL DMEM+10% FBS and incubated further for 24 h. The media was removed and the cells were washed twice with PBS. To determine the intracellular bacterial load, the cells were lysed using 250 μL of 0.1% Triton X-100™ and 10-fold serial dilutions of lysates were prepared and spread on TSA plates. Colony forming units (CFUs) were determined after incubating the plates for 48 h at 37 ^{o}C under 5% CO_2.

6.3. Results and Discussion

6.3.1 Synthesis and stability of MBIC nanostructures

In this work, MBICs were prepared using magnetite nanoparticles as a substrate for mPEO-*b*-PAA assembly. Ligand adsorption was employed to link the block ionomer to the magnetite. Carboxylate groups on mPEO-*b*-PAA were used as anchor groups and this resulted in adsorption on the magnetite surfaces. It is crucial that the polymer is soluble and that the magnetite is dispersible in the medium used for adsorption. mPEO-*b*-PAA was insoluble in chloroform. Thus, the block copolymer was first dissolved in DMF and this was mixed with the magnetic particle dispersion in chloroform to form a homogeneous solution/dispersion. After purification, the polymer-magnetite complexes

were recovered in high yields, usually exceeding 95 %.

The magnetic properties of the magnetite nanoparticles were characterized via SQuID analyses. Hysteresis loops revealed that the complexes were superparamagnetic at 300 K with a saturation magnetization of approximately 23 emu g^{-1}. Compositions of the MBICs were assessed by TGA. One example had 63 wt% polymer and 37 wt% magnetite, and this corresponded to a saturation magnetization of ~62 emu g^{-1} magnetite (Figure 6.2).

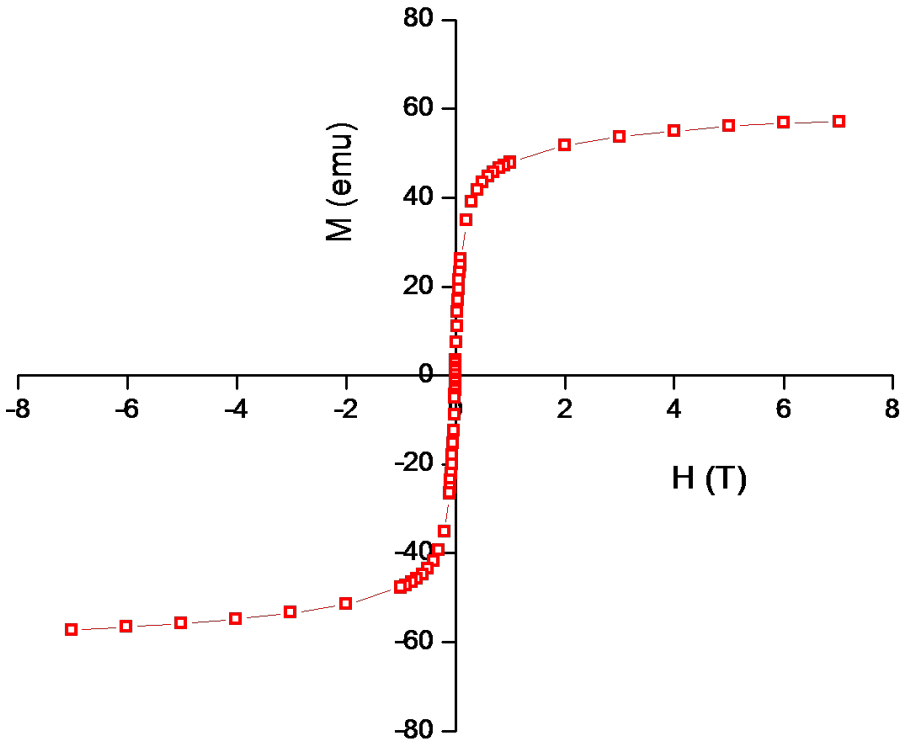

Figure 6.2 Hysteresis loops of MBICs at 300K

The nanoparticles, as expected, are dispersible in water and aqueous buffers. TEM showed that the particles were well-dispersed with relatively uniform sizes (Figure 6.3). However, weak ligands such as carboxylate groups can undergo chemical desorption

from the surfaces of metals and metal oxides in aqueous environments with high ionic strength through competitive binding from ligand-rich molecules such as proteins and phosphate ions.[6] To demonstrate that these nanostructures are potential suitable candidates for drug delivery vehicles, their stability in physiological conditions and various ionic strengths were evaluated. As shown in figure 6.4, dispersions of the MBICs remained stable in PBS containing 0.14 M NaCl for up to 10 days. Furthermore, their stability in the presence of serum was demonstrated in PBS containing fetal bovine serum (FBS). The particles were easily dispersed in buffer containing various concentrations of serum without any visible aggregation, and the dispersions remained transparent for a period of several weeks (Figure 6.5).

To confirm this observation, DLS was used to evaluate any nano- or micro-scale agglomeration (Figure 6.6). The intensity averaged hydrodynamic sizes of globular proteins in FBS as measured by DLS were ~10 nm in diameter. The sizes of these MBICs on the other hand were ~35 nm. When the particles were dispersed in FBS solution, DLS revealed two distinct peaks of nanoparticulate species that were likely attributable to the corresponding globular proteins and the MBICs. Upon continuous monitoring without any agitation at 37 ^{o}C, no apparent increase of size or aggregation was observed by DLS. This indicates that the particles were stable against serum, even at the high level of serum, that were comparable to physiological conditions in the blood stream.

Although we have shown previously that carboxylate groups are considered to be weak anchor groups for magnetite[6, 8], the polymeric nature of the PAA component in the block ionomer likely enhances binding through cooperative adsorption. The results

clearly suggest that these MBICs should be sufficiently stable in physiological conditions, and therefore suitable for use as a drug carrier.

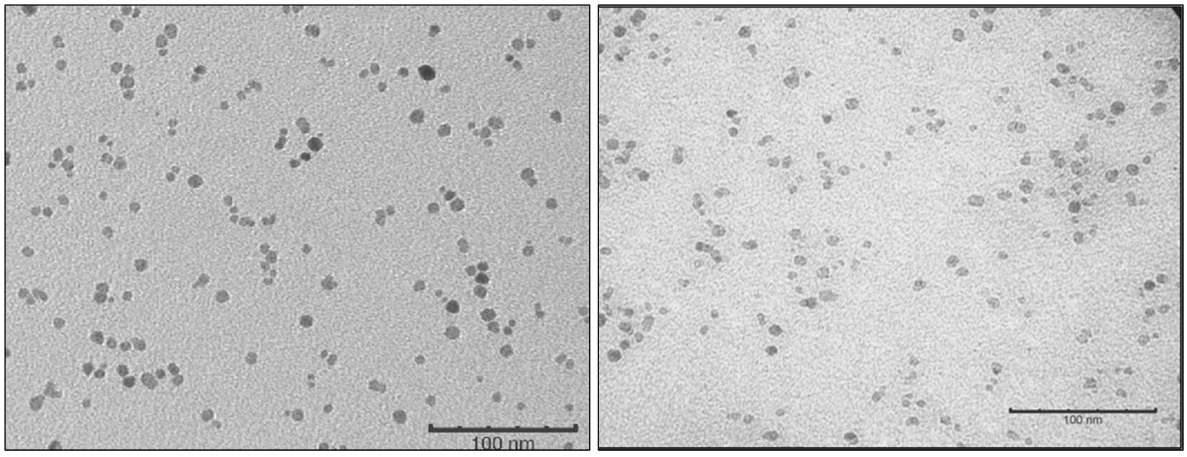

Figure 6.3 TEM images of oleic acid-coated magnetite cast from hexane (left) and MBICs cast from deionized water (right). Scale bar = 100 nm.

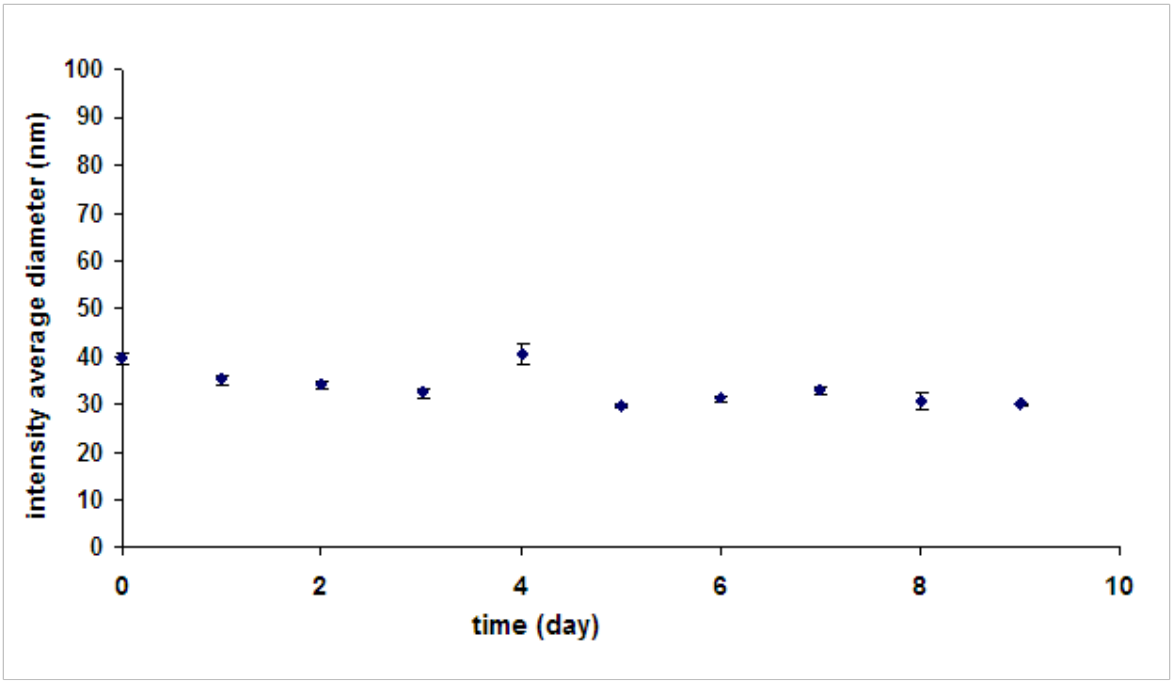

Figure 6.4 Stability of MBICs in PBS (0.14 M NaCl, pH 7.2). The measurements were made on a sample that was stored at room temperature in a cuvette without agitation.

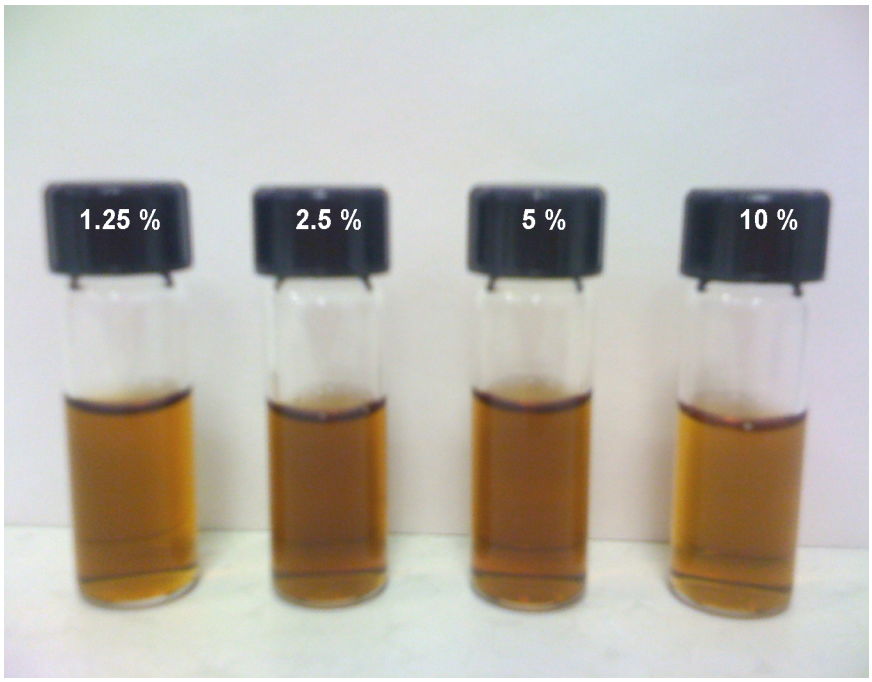

Figure 6.5 Dispersions of MBICs in PBS containing various concentrations (% wt/wt) of serum showing good stability against serum

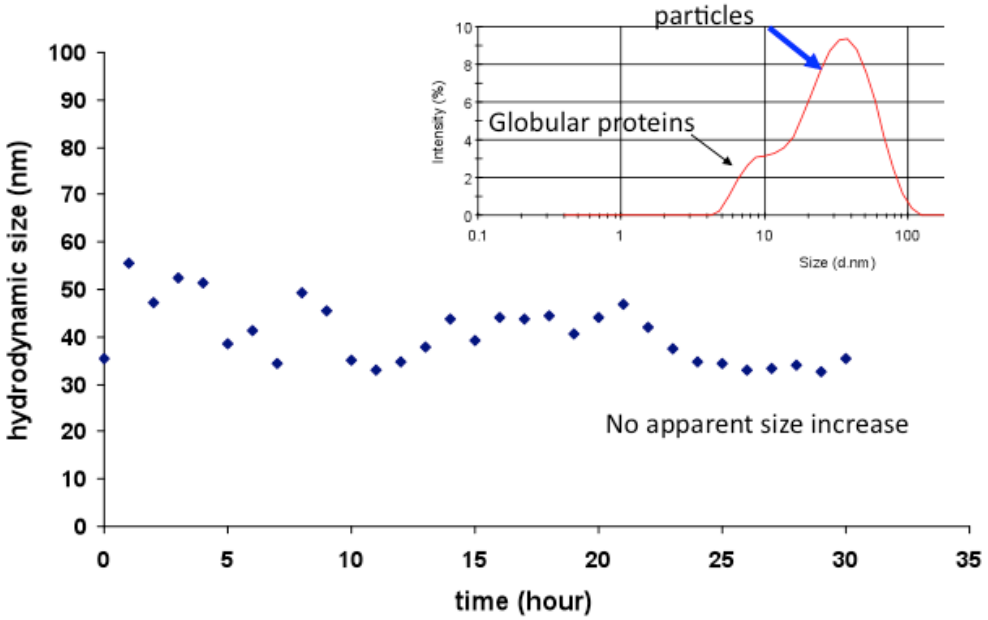

Figure 6.6 Intensity-averaged sizes of MBICs over time in PBS containing 10 % FBS at 37 ^{o}C

6.3.2 Preparation and characterization of gentamicin loaded nanostructures

Micellization of amphiphilic block copolymers where magnetic nanoparticles and drug molecules are co-encapsulated in the hydrophobic domains of micelles have been widely employed.[212, 213] However, the success of such approaches is limited to a very low drug loading capacity as a consequence of a lack of strong carrier-drug interaction and slow kinetics of encapsulation. This makes them only suitable for hydrophobic drugs that have poor solubilities in water. For examples, Gao and co-workers have described the preparation of micelles comprised of PEO-*b*-poly(D,L-lactide) encapsulating doxorubicin and a cluster of magnetic nanoparticles by hydrophobic interactions, with a doxorubicin loading of 2.7%.[212] Similarly, the loading capacity of multifunctional doxorubicin- and magnetic nanoparticle-loaded micelles of poly(ethylene oxide)-*b*-poly(lactide-*co*-glycolide) was only 3.5%.[214]

Herein, we utilized a loading protocol where the model drug gentamicin was entrapped by simply mixing the drug solution with the MBIC particles. The ionic attraction of complementary charges was utilized to load gentamicin into the anionic shell of the MBICs. After removing any free drug by centrifugation of the dispersion through a membrane, the amount of gentamicin in the complexes was analyzed through derivatization of the aminoglycoside primary amines with *o*-phthalaldehyde in the presence of mercaptoethanol. However, the attempt to measure absorbance at the wavelength of 340 nm, which is normally utilized for assaying the intensity of the derivative[7], was hampered by interference from the magnetite.

Thus, a fluorimetric assay was used instead of relying on UV-Vis absorption of the gentamicin-pthalaldehyde derivative. The derivatives were excited at 340 nm and the

fluorescence intensities were measured at 450 nm. This method provides better sensitivity and lower concentration detection limits for the gentamicin. While the lowest concentration of gentamicin that could be detected by UV-vis spectroscopy of the phthalaldehyde-mercaptoethanol derivative was ~4 ug mL^{-1}, the fluorimetric technique could detect down to ~1 ug mL^{-1}. More importantly, the fluorimetric assay is without any interference from the magnetite. The purification process showed that 78% of the initial charged concentration of gentamicin was encapsulated into the MBICs at the charge ratio of 1:1 cation to anion. The marked high gentamicin content of ca. 31 weight % was achieved. This is advantageous from the clinical point of view since a high payload can reduce the total required dosage of pharmaceutical formulations for treatment. Furthermore, the drug loading procedure was rather simple relative to approaches that are used for other nanoparticle-drug delivery systems including liposomes, nanoparticles and microspheres, which generally involve several steps.[44, 48, 57]

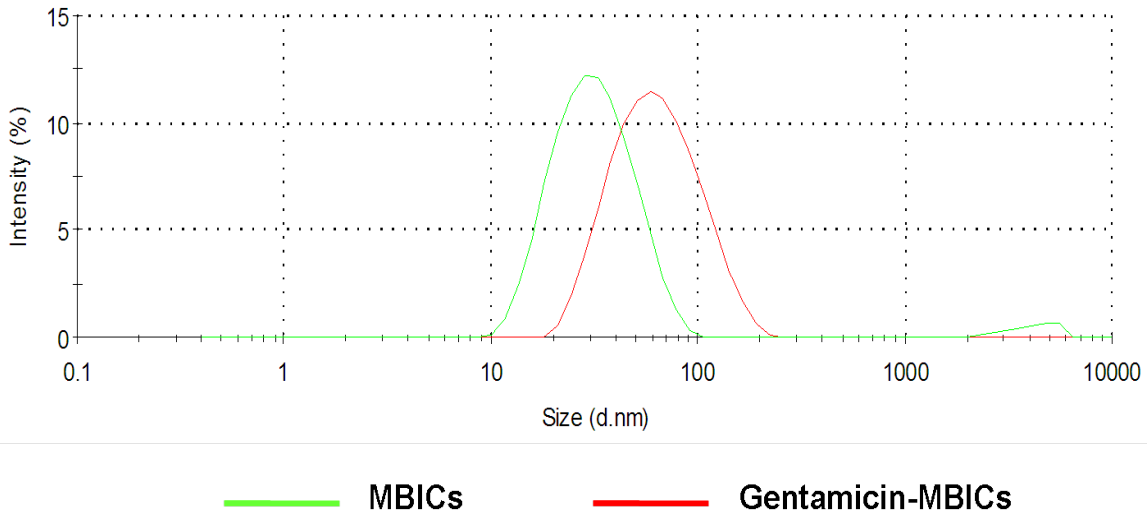

Figure 6.7 Intensity-averaged hydrodynamic sizes of MBICs and gentamicin-loaded MBICs in phosphate buffer (pH 7.2)

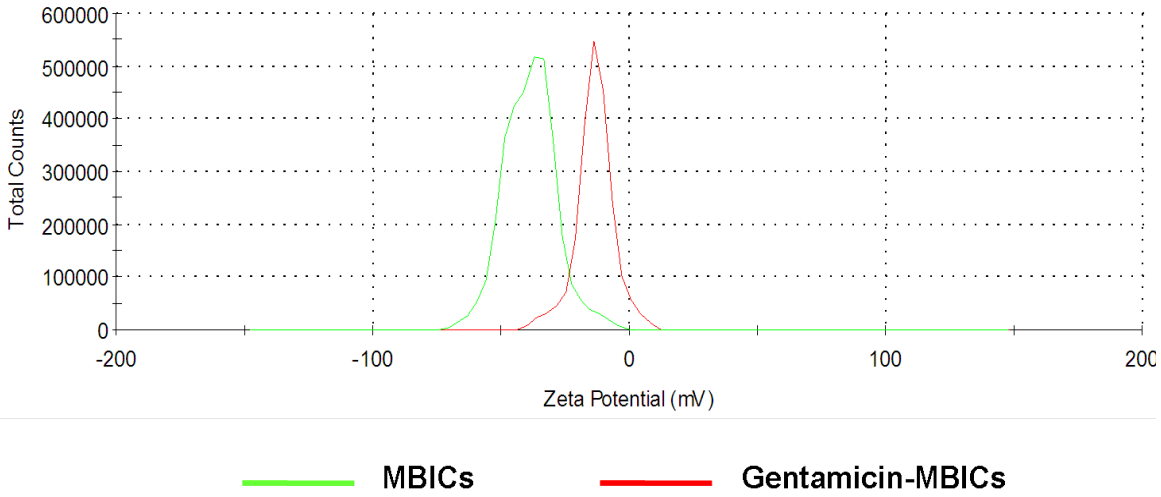

Figure 6.8 Zeta potential measurements of surface change of MBICs and gentamicin-loaded MBICs in phosphate buffer at pH 7.2

Particles	Intensity average size (nm)	PDI	Zetapotential (mV)	Gentamicin loading (% wt)
MBICs	34 +/- 1	0.200	-38.6 +/- 10.1	-
Gentamicin-MIBICs	72 +/- 4	0.176	-13.4 +/- 7.4	31 +/- 7

Table 6.1 physicochemical characterization of MBICs and gentamicin-loaded MBICs

The physicochemical properties of MBICs were significantly altered upon gentamicin encapsulation (Figures 6.7-6.8 and Table 6.1). The hydrodynamic sizes of the particles increased from 34 to 72 nm in diameter, suggesting that the particles formed small clusters due to gentamicin acting as a bridging agent between particles.

Polydispersity indices for the MBICs of less than 0.180 indicated relatively uniform size distributions of particles. Moreover, the zeta potential of the gentamicin-containing MBICs dramatically decreased from ~ -40 to ~ -10 mV, indicating that the cationic gentamicin effectively neutralized negative charges on the MBICs. These results are clearly commensurate with gentamicin being successfully loaded into the MBICs.

6.3.3 Drug release study

Release studies of gentamicin from the magnetic nanoparticles were performed at pH 7.4. Either free gentamicin or gentamicin-loaded MBICs were dispersed in PBS and placed in the dialysis cassette. The cassettes were fully submersed in a beaker containing a 75-fold volume of receptor medium to ensure sink conditions. The release of gentamicin into the receptor medium was measured at respective time points. As expected, the free drug fully diffused through the membrane into the receptor medium within 5 hours. Evidently, the MBICs can distinctly slow down release of the gentamicin. A near zero-order release of gentamicin that reaches ~35 wt% of the initial gentamicin within 10 hours was observed. There was an additional release of 8% of the gentamicin by 24-hours. This second phase of the release behavior appears to be slower than the initial 10 hours. As drug molecules were released, the ratio between negative charge and positive charge continued to increase. This may contribute to the slower release rate that was observed in the later time point.

In our previous studies on block ionomer complexes without magnetite cores, we reported a significant burst release of gentamicin (chapter 3). As observed in figure 6.9, no burst release of gentamicin from MBICs was observed. This is not too surprising that

such different release behaviors were observed from complexes with magnetite cores. The solid inorganic core of iron oxide particles serves as a multifunctional substrate for block ionomers to stably adsorb, and it thus acts as a pseudo-crosslinking site in the complexes, thus enhancing stability. It is important to note that the corresponding complexes between mPEO-*b*-PAA and gentamicin (without magnetite nanoparticles) instantaneously dissociate in saline buffer. When the very same copolymer was adsorbed onto the magnetite nanoparticles, subsequent complexation with gentamicin resulted in stable complexes that could withstand media with physiological ionic strength.

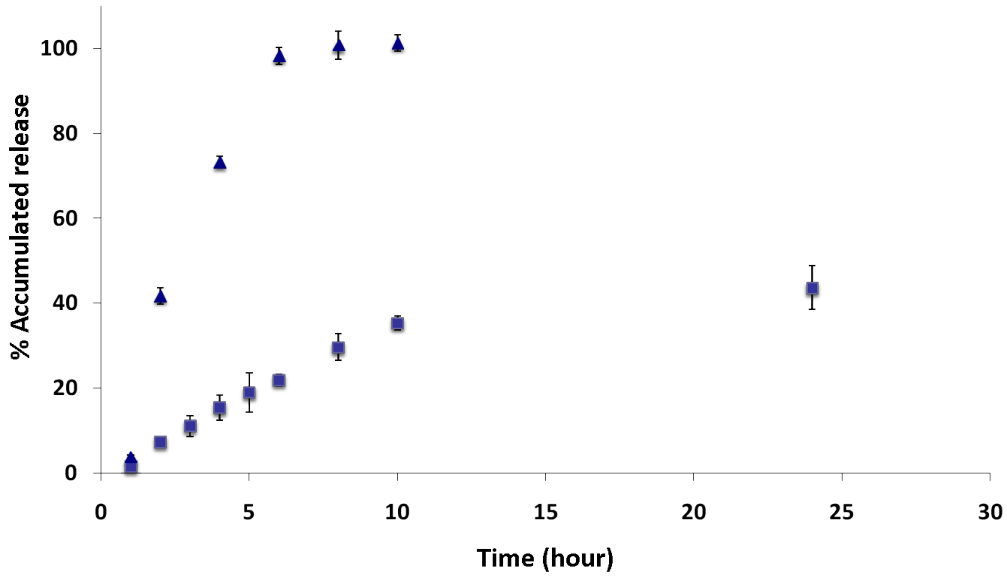

Figure 6.9 Release profile of gentamicin from MBICs (squares) compared to free gentamicin (triangles) in phosphate buffered saline, pH 7.4 at 37 ^{o}C.

The advantage of slower release and higher stability may play a vital role when testing the efficacies of the complexes in animal models where delivery vehicles must avoid disintegration before reaching target sites and cells. Based on these results, the

gentamicin-loaded MBICs with superior stability should be suitable for *in vivo* investigations.

6.3.4 *In vitro* efficacy against intracellular brucellosis

Efficacy of the gentamicin-loaded MBICs to reduce intracellular *Brucella* was studied in J774A.1 murine cells and compared to free drug. The cells were infected with *Brucella*, and any extracellular *Brucella* were eliminated with free gentamicin and discarded, then the macrophages infected with only the intracellular *Brucella* were incubated with either MBICs, free gentamicin, or gentamicin-loaded MBICs for 24 hours. A reduction of 2.10 log CFUs, corresponding to >99% killing of the intracellular bacteria, was achieved with gentamicin-loaded MBICs relative to the control without any treatment (Figure 6.10). This reduction was significantly higher than the reduction by free drug (0.45 logs). Thus, it is hypothesized that the MBICs can efficiently carry gentamicin into the J774.1A cells and release the drug within the cells, resulting in higher antibacterial activities.

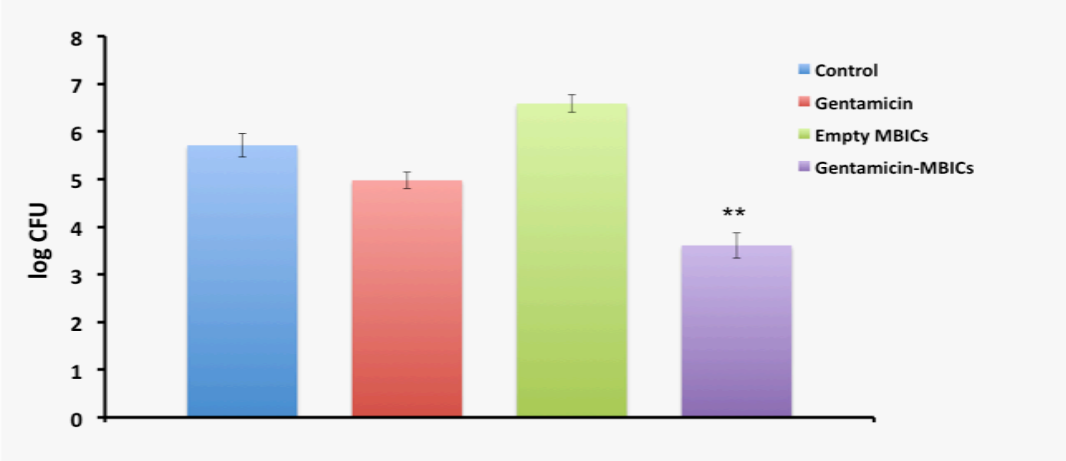

Figure 6.10 *In vitro* killing of intracellular *Brucella* in J774.1A murine macrophages: the bacterial colony forming unit (CFU) is expressed on a log scale. The results were averages of three replicates

6.5 Conclusions

Overall we have demonstrated that nanomagnetite can be efficiently complexed with mPEO-*b*-PAA block copolymers through binding of a portion of the anionic segment of the copolymer with the metal oxide surfaces. The remainder of the carboxylates can then be utilized to bind with high concentrations of gentamicin which has multiple cationic sites. The resultant polymer-magnetite-drug nanoparticles have excellent colloidal stability in physiological media and conditions, and the dispersions are stable against high levels of serum. This makes such materials good candidates for delivering the highly polar cationic drugs such as gentamicin into phagocytic cells where many Gram-negative as well as Gram-positive bacteria live and replicate. Owing to the magnetic iron oxide core, we envision that such hybrid nanocarriers could enable simultaneous diagnosis and treatment. Further research will include an investigation of biodistribution through magnetic resonance imaging and investigations of efficacies of the drug-loaded MBICs to eradicate intracellular bacterial infections in animals

Chapter 7

Conclusions

Core-shell polyelectrolyte nanostructures containing nonionic-anionic polyether-acrylate block copolymers and cationic drugs were formed and stabilized in aqueous media through ionic and hydrophobic interactions. Amphiphilic shells comprised of poly(ethylene oxide-*b*-propylene oxide-*b*-ethylene oxide), as opposed to only the hydrophilic poly(ethylene oxide), resulted in enhanced stability in physiological media. These nanostructures were demonstrated to efficiently deliver gentamicin into phagocytic immune cells and significantly improve efficacies of killing intracellular pathogens that reside within the cells. The complexes can be fabricated in either a batch or continuous engineering process. In the latter method, solutions of polymeric carriers and antibiotics were mixed by introducing the components at prescribed rates so that the composition in residence in the mixer was always constant.

Polymeric shells for magnetic iron oxide nanoparticles were designed and synthesized via ATRP. Bis(phosphonate)-functional ATRP initiators were utilized to initiate polymerization of N-isopropylacrylamide to afford PNIPAM that contained two ethyl phosphonates at one terminus. Upon selective and mild deprotection, the bis(phosphonic acid)-PNIPAM could be readily adsorbed onto iron oxide nanoparticles yielding nanostructures with magnetic cores and thermosensitive shells. These core-shell nanostructures exhibit interesting thermoresponsive behavior that undergo cluster formation upon heating above the LCST of PNIPAM of ~33 ^{o}C. The applicability of this

methodology, utilizing the ATRP initiator moiety as the anchor, could be modularly extended to create a library of polymeric shells for magnetic iron oxide nanoparticles.

The combined design and synthesis of (co)polymers with knowledge of their adsorption on metal oxide nanoparticles has opened the door of opportunity to develop hybrid core-shell nanostructures that could serve as versatile carriers for drug delivery, monitoring of biodistribution, and with potential for diagnostic imaging. The molecular toolbox was developed based on the block copolymers and magnetic nanoparticles. In this approach, the block copolymer and magnetite were synthesized separately and were later bound together by ligand adsorption techniques. The block copolymers were designed to stably adsorb on the magnetite surface and also to encapsulate the target drug. We have shown that cationic gentamicin was successfully loaded into mPEO-*b*-PAA coated magnetite complexes. These complexes are stable in aqueous physiological solutions with with high ionic strength. Furthermore, the complexes appeared to enhance intracellular antimicrobial activities of gentamicin. These results warrant further investigations of in vivo efficacies, and biodistribution via magnetic resonance imaging.

Bibliography

1. Cammasa, S.; Suzukia, K.; Sonea, C.; Sakuraia, Y.; Kataoka, K.; Okano, T., *Journal of Controlled Release* **1997,** *48* (2-3), 157-164.
2. Haag, R., *Angew Chem Int Ed Engl* **2004,** *43* (3), 278-82.
3. Soppimath, K. S.; Tan, D. C. W.; Yang, Y. Y., *Advanced Materials* **2005,** *17* (3), 318-323.
4. Mefford, O. T.; Vadala, M. L.; Goff, J. D.; Carroll, M. R.; Mejia-Ariza, R.; Caba, B. L.; Pierre, T. G.; Woodward, R. C.; Davis, R. M.; Riffle, J. S., *Langmuir* **2008,** *24* (9), 5060-9.
5. Ranjan, A.; Pothayee, N.; Seleem, M. N.; Sriranganathan, N.; Kasimanickam, R.; Makris, M.; Riffle, J. S., *Antimicrob Agents Chemother* **2009,** *53* (9), 3985-8.
6. Goff, J. D.; Huffstetler, P. P.; Miles, W. C.; Pothayee, N.; Reinholz, C. M.; Ball, S.; Davis, R. M.; Riffle, J. S., *Chemistry of Materials* **2009,** *21* (20), 4784-4795.
7. Ranjan, A.; Pothayee, N.; Vadala, T. P.; Seleem, M. N.; Restis, E.; Sriranganathan, N.; Riffle, J. S.; Kasimanickam, R., *Antimicrob Agents Chemother* **2010,** *54* (8), 3524-6.
8. Miles, W. C.; Goff, J. D.; Huffstetler, P. P.; Reinholz, C. M.; Pothayee, N.; Caba, B. L.; Boyd, J. S.; Davis, R. M.; Riffle, J. S., *Langmuir* **2009,** *25* (2), 803-13.
9. Xie, J.; Lee, S.; Chen, X., *Adv Drug Deliv Rev* **2010**.
10. Mackay, J. A.; Li, Z., *Adv Drug Deliv Rev* **2010**.
11. Matsumura, Y.; Maeda, H., *Cancer Res* **1986,** *46*, 6387-6392.
12. Shi, J.; Votruba, A. R.; Farokhzad, O. C.; Langer, R., *Nano Lett 10* (9), 3223-30.
13. Shuai, X.; Ai, H.; Nasongkla, N.; Kim, S.; Gao, J., *J Control Release* **2004,** *98* (3), 415-26.
14. Rowan, S. J., *Nat Mater* **2009,** *8* (2), 89-91.
15. Du, J. Z.; Tang, L. Y.; Song, W. J.; Shi, Y.; Wang, J., *Biomacromolecules* **2009,** *10* (8), 2169-74.
16. Gao, Z.; N., N. L. A.; Singhal, A.; Torchilin, V. P., *Nano Lett* **2002,** *2*, 797-782.
17. Huh, K. M.; Lee, S. C.; Cho, Y. W.; Lee, J.; Jeong, J. H.; Park, K., *J Control Release* **2005,** *101* (1-3), 59-68.
18. Bronich, T. K.; Kabanov, A. V.; Kabanov, V. A.; Yu, K.; Eisenberg, A., *Macromolecules* **1997,** *30* (12), 3519-3525.
19. Bronich, T. K.; Nehls, A.; Eisenberg, A.; Kabanov, V. A.; Kabanov, A. V., *Colloids and Surfaces B-Biointerfaces* **1999,** *16* (1-4), 243-251.
20. Bronich, T. K.; Popov, A. M.; Eisenberg, A.; Kabanov, V. A.; Kabanov, A. V., *Langmuir* **2000,** *16* (2), 481-489.
21. Kabanov, A. V.; Bronich, T. K.; Kabanov, V. A.; Yu, K.; Eisenberg, A., *Macromolecules* **1996,** *29* (21), 6797-6802.
22. Harada, A.; Kataoka, K., *Macromolecules* **1995,** *28* (15), 5294-5299.
23. K. Kataoka, H. T., A. Harda, K. Yasugi, T. Matsumoto, S. Katayose, **1996,** *29* (26), 8556-8557
24. Bromberg, L., *Journal of Controlled Release* **2008,** *128* (2), 99-112.

25. Oh, K. T.; Bronich, T. K.; Bromberg, L.; Hatton, T. A.; Kabanov, A. V., *Journal of Controlled Release* **2006,** *115* (1), 9-17.
26. Lee, J. H.; Lee, K.; Moon, S. H.; Lee, Y.; Park, T. G.; Cheon, J., *Angew Chem Int Ed Engl* **2009,** *48* (23), 4174-9.
27. Kaprelyants, A. S.; Gottschal, J. C.; Kell, D. B., *FEMS Microbiol Rev* **1993,** *10* (3-4), 271-85.
28. Gilbert, P.; Collier, P. J.; Brown, M. R., *Antimicrob Agents Chemother* **1990,** *34* (10), 1865-8.
29. Costerton J.W.; Cheng K.J; Geesey G.G.; Ladd T.I.; Nickel J.C.; Dasgupta M; *Annu Rev Microbiol* **1987,** *41*, 435-464
30. Monack, D. M.; Bouley, D. M.; Falkow, S., *J Exp Med* **2004,** *199* (2), 231-41.
31. Seleem, M. N.; Boyle, S. M.; Sriranganathan, N., *Vet Microbiol* **2008,** *129* (1-2), 1-14.
32. Steinberg, B. E.; Grinstein, S., *J Clin Invest* **2008,** *118* (6), 2002-11.
33. Briones, E.; Colino, C. I.; Lanao, J. M., *J Control Release* **2008,** *125* (3), 210-27.
34. Finlay, B. B.; Cossart, P., *Science* **1997,** *276* (5313), 718-25.
35. Silva, J. G.; Carvalho, I., *Curr Med Chem* **2007,** *14* (10), 1101-19.
36. Schatz, A.; Waksan, S. A., *Proc. Soc. Exp. Biol. Med.* **1944,** *57*, 244-248.
37. Mingeot-Leclercq, M. P.; Glupczynski, Y.; Tulkens, P. M., *Antimicrob Agents Chemother* **1999,** *43* (4), 727-37.
38. Thomas, G., *Medicinal Chemistry: An Introduction*. Wiley: Chichester, 2000; p 392-395.
39. Gamazo, C.; Lecaroz, M. C.; Prior, S.; Vitas, A. I.; Campanero, M. A.; Irache, J. M.; Blanco-Prieto, M. J., *Curr Drug Deliv* **2006,** *3* (4), 359-65.
40. Lecaroz, C.; Gamazo, C.; Blanco-Prieto, M. J., *J Nanosci Nanotechnol* **2006,** *6* (9-10), 3296-302.
41. Lesniak, W.; Pecoraro, V. L.; Schacht, J., *Chem. Res. Toxical.* **2005,** *18*, 357-364.
42. Takumida, M.; Anniko, M., *Acta Oto-Laryngol.* **2001,** *121*, 346-350.
43. Samad, A.; Sultana, Y.; Aqil, M., *Curr Drug Deliv* **2007,** *4* (4), 297-305.
44. Fountain, M. W.; Weiss, S. J.; Fountain, A. G.; Shen, A.; Lenk, R. P., *J. Infect. Dis.* **1985,** *152* (3), 529-35.
45. Dees, C.; Fountain, M. W.; Taylor, J. R.; Schultz, R. D., *Vet Immunol Immunopathol* **1985,** *8* (1-2), 171-82.
46. Kesavalu, L.; Goldstein, J. A.; Debs, R. J.; Duzgunes, N.; Gangadharam, P. R., *Tubercle* **1990,** *71* (3), 215-7.
47. Vitas, A. I.; Diaz, R.; Gamazo, C., *Antimicrob Agents Chemother* **1996,** *40* (1), 146-51.
48. Ruijgrok, E. J.; Vulto, A. G.; Van Etten, E. W. M., *J. Liposome Res* **1999,** ***9*** (2), 291-300.
49. Abraham, A. M.; Walubo, A., *Int J Antimicrob Agents* **2005,** *25* (5), 392-7.
50. Barrow, E. L.; Winchester, G. A.; Staas, J. K.; Quenelle, D. C.; Barrow, W. W., *Antimicrob Agents Chemother* **1998,** *42* (10), 2682-9.
51. Dutt, M.; Khuller, G. K., *Antimicrob Agents Chemother* **2001,** *45* (1), 363-6.
52. Puisieux, F.; Barrat, G.; Couarraze, G., *Polymeric micro- and nanoparticles as drug carriers.* . Marcel Dekker: New York, Basle, Hong Kong., **1994**.

53. Quenelle, D. C.; Winchester, G. A.; Staas, J. K.; Barrow, E. L.; Barrow, W. W., *Antimicrob Agents Chemother* **2001,** *45* (6), 1637-44.
54. Virto, M. R.; Elorza, B.; Torrado, S.; Elorza Mde, L.; Frutos, G., *Biomaterials* **2007,** *28* (5), 877-85.
55. Prior, S.; Gamazo, C.; Irache, J. M.; Merkle, H. P.; Gander, B., *Int J Pharm* **2000,** *196* (1), 115-25.
56. Lecaroz, M. C.; Blanco-Prieto, M. J.; Campanero, M. A.; Salman, H.; Gamazo, C., *Antimicrob Agents Chemother* **2007,** *51* (4), 1185-90.
57. Prior, S.; Gander, B.; Irache, J. M.; Gamazo, C., *J Antimicrob Chemother* **2005,** *55* (6), 1032-6.
58. Jani, P. U.; Florence, A. T.; McCarthy, D. E., *Int. J. Pharm.* **1992,** *84*, 245-252. .
59. Rauschmann, M. A.; Wichelhaus, T. A.; Stirnal, V.; Dingeldein, E.; Zichner, L.; Schnettler, R.; Alt, V., *Biomaterials* **2005,** *26* (15), 2677-84.
60. Meseguer-Olmo, L.; Ros-Nicolas, M. J.; Clavel-Sainz, M.; Vicente-Ortega, V.; Alcaraz-Banos, M.; Lax-Perez, A.; Arcos, D.; Ragel, C. V.; Vallet-Regi, M., *J Biomed Mater Res* **2002,** *61* (3), 458-65.
61. Ueno, Y.; Futagawa, H.; Takagi, Y.; Ueno, A.; Mizushima, Y., *J Control Release* **2005,** *103* (1), 93-8.
62. Vallet-Regi, M.; Ramila, A.; del Real, R. P.; Perez-Pariente, J., *Chem Mater* **2001,** *13*, 308-311.
63. Tourne-Peteilh, C.; Lerner, D. A.; Charnay, C.; Nicole, L.; Begu, S.; Devoisselle, J. M., *Chemphyschem* **2003,** *4* (3), 281-6.
64. Doadrio, A. L.; Sousa, E. M.; Doadrio, J. C.; Perez Pariente, J.; Izquierdo-Barba, I.; Vallet-Regi, M., *J Control Release* **2004,** *97* (1), 125-32.
65. Xue, J. M.; Shi, M., *J Control Release* **2004,** *98* (2), 209-17.
66. Xue, J. M.; Tan, C. H.; Lukito, D., *J Biomed Mater Res Part B: Appl Biomater.* **2005,** *78B*, 417-422.
67. Rejman, J.; Oberle, V.; Zuhorn, I. S.; Hoekstra, D., *Biochem J* **2004,** *377* (Pt 1), 159-69.
68. Champion, J. A.; Walker, A.; Mitragotri, S., *Pharm Res* **2008,** *25* (8), 1815-21.
69. Vallet-Reg, M.; Balas, F.; Arcos, D., *Angew. Chem. Int. Ed.* **2007,** *46*, 7548 - 7558.
70. Slowing, II; Vivero-Escoto, J. L.; Wu, C. W.; Lin, V. S., *Adv Drug Deliv Rev* **2008,** *60* (11), 1278-88.
71. Jiang, C. Y.; Tsukruk, V. V., *Adv. Mater.* **2006,** *18*, 829-840.
72. Yow, H. N.; Routh, A. F., *Soft Matter* **2006,** *2*, 940-949.
73. Ma, Y.; Dong, W. F.; Hempenius, M. A.; Mohwald, H.; Vancso, G. J., *Nat Mater* **2006,** *5* (9), 724-9.
74. Hammond, P. T., *Adv. Mater.* **2004***, 16*, 1271-1293
75. Wang, T.; Lacik, I.; Brissova, M.; Anilkumar, A. V.; Prokop, A.; Hunkeler, D.; Green, R.; Shahrokhi, K.; Powers, A. C., *Nat Biotechnol* **1997,** *15* (4), 358-62.
76. Bertrand, P.; Jonas, A.; Laschewsky, A.; Legras, R., *Macromol. Rapid Commun.* **2000,** *21*, 319-348.
77. Rungsardthong, U.; Deshpande, M.; Bailey, L.; Vamvakaki, M.; Armes, S. P.; Garnett, M. C.; Stolnik, S., *J Control Release* **2001,** *73* (2-3), 359-80.

78. Changez, M.; Burugapalli, K.; Koul, V.; Choudhary, V., *Biomaterials* **2003,** *24* (4), 527-36.
79. Chuang, H. F.; Smith, R. C.; Hammond, P. T., *Biomacromolecules* **2008,** *9* (6), 1660-8.
80. Fonseca, M. J.; Cabanes, A.; Alsina, M. A.; Reig, F., *International Journal of Pharmaceutics.* **1996,** *1333*, 265-268.
81. Nurkeeva, Z. S.; Khutoryanskiy, V. V.; Mun, G. A.; Sherbakova, M. V.; Ivaschenko, A. T.; Aitkhozhina, N. A.; , *Europ. J. Pharm. & Biopharm.* **2004,** *57* (2), 245-249
82. Donath, E.; Sukhorukov, G. B.; Caruso, F.; Davis, S. A.; Möhwald, H., *Angew. Chem. Int. Ed.* **1998,** *37*, 2201-2205
83. Khopade, A. J.; Caruso, F., *Nano Lett.* **2002,** *2*, 415-418.
84. Schuler, C.; Caruso, F., *Biomacromolecules* **2001,** *2* (3), 921-6.
85. Caruso, F.; Trau, D.; Mo¨hwald, H.; Renneberg, R., *Langmuir* **2000,** *16*, 1485-1488
86. Tiourina, O. P.; Sukhorukov, G. B., *Int J Pharm* **2002,** *242* (1-2), 155-61.
87. Balabushevich, N. G.; Tiourina, O. P.; Volodkin, D. V.; Larionova, N. I.; Sukhorukov, G. B., *Biomacromolecules* **2003,** *4* (5), 1191-7.
88. Dai, Z. F.; Voigt, A.; Leporatti, S.; Donath, E.; Dähne, L.; Möhwald, H., *Adv. Mater.* **2001,** *13*, 1339-1342.
89. Khopade, A. J.; Arulsudar, N.; Khopade, S. A.; Hartmann, J., *Biomacromolecules* **2005,** *6* (1), 229-34.
90. Bronich, T. N., H.; Eisenberg, A.; Kabanov, A., *Journal of the American Chemical Society* **2000,** *122*, 8339-8343.
91. Jung, C. J., P., *Magnetic Resonance Imaging* **1995,** *13* (5), 661-674.
92. Mefford, O. T.; Carroll, M. R. J.; Vadala, M. L.; Goff, J. D.; Mejia-Ariza, R.; Saunders, M.; Woodward, R. C.; Pierre, T. G. S.; Davis, R. M.; Riffle, J. S., *Chemistry of Materials* **2008,** *20* (6), 2184-2191.
93. Mefford, O. T.; Vadala, M. L.; Goff, J. D.; Carroll, M. R. J.; Mejia-Ariza, R.; Caba, B. L.; Pierre, T. G. S.; Woodward, R. C.; Davis, R. M.; Riffle, J. S., *Langmuir* **2008,** *24* (9), 5060-5069.
94. Thunemann, A. S., D.; Kaufner, L.; Pison, U.; Mohwald, H., *Langmuir* **2006,** *22* (2351-2357).
95. Wilson, K. S.; Goff, J. D.; Riffle, J. S.; Harris, L. A.; St Pierre, T. G., *Polymers for Advanced Technologies* **2005,** *16* (2-3), 200-211.
96. Martinez-Mera, I.; Espinosa, M. E.; Perez-Hermandez, R.; Arenas-Alatorre, J., *Mater. Lett.* **2007,** *61*, 4447-4451.
97. Morrsison, S. A.; Cahill, C. L.; Carpenter, E.; Calvin, S.; Harris, V. G., *J. Nanosci. Nanotechnol.* **2005,** *5*, 1323.
98. Jolivert, J. P.; Chaneac, C.; Tronc, E., *Chem. Commun.* **2004,** *5*, 481.
99. Calero-DdelC, V.; Rinaldi, C., *J. Magn. Magn. Mater.* **2007,** *314*, 60-67.
100. Sun, S.; Zeng, H.; Robinson, D. B.; Raoux, S.; Rice, P. M.; Wang, S. X.; Li, G., *J Am Chem Soc* **2004,** *126* (1), 273-9.
101. Pinna, N.; Grancharov, S.; Beato, P.; Bonville, P.; Antonietti, M.; Niederberger, M., *Chem. Mater.* **2005,** *17*, 3044-3049.
102. Zhang, Y.; Kohler, N.; Zhang, M., *Biomaterials* **2002,** *23* (7), 1553-61.

103. Jarrett, B. R.; Frendo, M.; Vogan, J.; Louie, A. Y., *Nanotechnology* **2007,** *18* (3), 035603.
104. Chastellain, M.; Petri, A.; Hofmann, H., *J Colloid Interface Sci* **2004,** *278* (2), 353-60.
105. Molday, R. S.; Mackenzie, D. J., *J. Immunol. Methods* **1982,** *52*, 353.
106. Cabuil, V., *Curr. Opin. Colloid Interface Sci.* **2000,** *5*, 44.
107. Buatista, M. C.; Bomati-Miguel, O.; Morales, M. P.; Serna, C. J.; Veintermillas-Verdauer, S. J., *J. Magn. Magn. Mater.* **2005,** *293*, 20.
108. Fournier, C.; Leonard, M.; Le Coq-Lenard, I.; Delacherie, E., *Langmair* **1995,** *11*, 2344.
109. Kroll, E.; Winnik, F. M.; Ziolo, R. F., *Chem. Mater.* **1996,** *8*, 1594.
110. Nishio, Y.; Yamada, A.; Ezaki, K.; Miyashita, Y.; Furukawa, H.; Horie, K., *Polymer* **2004,** *45*, 7129.
111. Ma, H. L.; Qi, X. R.; Maitani, Y.; Nagai, T., *Int. J. Pharmaceut.* **2006**.
112. Jia, Z.; Yujun, W.; Yangcheng, L.; Jingyu, M.; Guangsheng, L., *Reac. Funct. Polym.* **2006,** *66*, 1552.
113. KIm, E. H.; Lee, H. S.; Kwak, B. K.; Kim, B. K., *J. Magn. Magn. Mater.* **2005,** *293*, 328.
114. Lee, H. S.; KIm, E. H.; Shao, H.; Kwak, B. K., *J. Magn. Magn. Mater.* **2005,** *293*, 102.
115. Paul, K. G.; Frigo, T. B.; Groman, J. Y.; Groman, E. V., *Bioconjug Chem* **2004,** *15* (2), 394-401.
116. Moghimi, S. M.; Hunter, A. C.; Murray, J. C., *Pharmacol Rev* **2001,** *53* (2), 283-318.
117. Harris, L. A.; Goff, J. D.; Carmichael, A. Y.; Riffle, J. S.; Harburn, J. J.; St Pierre, T. G.; Saunders, M., *Chemistry of Materials* **2003,** *15*, 1367-1377.
118. De las Heras, C.; Pennadam, S.; Alexander, C., *Chemical Society Reviews* **2005,** *34*, 276-285.
119. Shamim, N.; Hong, L.; Hidajat, K.; Uddin, M. S., *Colloids Surf B Biointerfaces* **2007,** *55* (1), 51-8.
120. Eeckman, F.; Moes, A. J.; Amighi, K., *Int J Pharm* **2004,** *273* (1-2), 109-19.
121. Dallas, P.; Georgakilas, V.; Niarchos, D.; Komninou, P.; Kehagias, T.; Petridis, D., *Nanotechnology* **2006,** *17*, 2046-2053.
122. Wang, J. S.; Matyjaszewski, K., *Macromolecules* **1995,** *28*, 7901.
123. Patten, T. E.; Xia, J.; Abernathy, T.; Matyjaszewski, K., *Science* **1996,** *272* (5263), 866-8.
124. Matyjaszewski, K., *Macromolecules* **1998,** *31* (15), 4710-7.
125. Matyjaszewski, K., *Macromolecular Symposia* **2000,** *161*, 1-9.
126. Matyjaszewski, K.; Paik, H. J.; Zhou, P.; Diamanti, S. J., *Macromolecules* **2001,** *34* (15), 5125-5131.
127. Matyjaszewski, K.; Hong, S. C.; Teodorescu, M.; Miller, P. J.; Coca, S.; Paik, H. J., *Abstracts of Papers of the American Chemical Society* **2001,** *221*, U380-U380.
128. Matyjaszewski, K.; Xia, J., *Chem Rev* **2001,** *101* (9), 2921-90.
129. Matyjaszewski, K., *Abstracts of Papers of the American Chemical Society* **2001,** *221*, U297-U297.
130. Golas, P. L.; Matyjaszewski, K., *Chem Soc Rev* **2010,** *39* (4), 1338-54.

131. Matyjaszewski, K., *Abstracts of Papers of the American Chemical Society* **2001,** *221*, U389-U389.
132. Bencherif, S. A.; Gao, H.; Srinivasan, A.; Siegwart, D. J.; Hollinger, J. O.; Washburn, N. R.; Matyjaszewski, K., *Biomacromolecules* **2009**.
133. Matyjaszewski, K.; Ziegler, M. J.; Arehart, S. V.; Greszta, D.; Pakula, T., *J. Phys. Org.* **2000,** *13*, 775-786.
134. Hou, S. J.; Chaikof, E. L.; Taton, D.; Gnanou, Y., *Macromolecules* **2003,** *36*, 3874-3881.
135. Y. Tian; L. Bromberg; S. N. Lin; T. A., H.; Tam, K. C., *J.Control. Release* **2007,** *121*, 137-145.
136. Perumal, O. P.; Inapagolla, R.; Kannan, S.; Kannan, R. M., *Biomaterials* **2008,** *29* (24-25), 3469-76.
137. McClelland, M.; Sanderson, K. E.; Spieth, J.; Clifton, S. W.; Latreille, P.; Courtney, L.; Porwollik, S.; Ali, J.; Dante, M.; Du, F.; Hou, S.; Layman, D.; Leonard, S.; Nguyen, C.; Scott, K.; Holmes, A.; Grewal, N.; Mulvaney, E.; Ryan, E.; Sun, H.; Florea, L.; Miller, W.; Stoneking, T.; Nhan, M.; Waterston, R.; Wilson, R. K., *Nature* **2001,** *413* (6858), 852-6.
138. Smith, A. L.; Daum, R. S.; Siber, G. R.; Scheifele, D. W.; Syriopoulou, V. P., *Antimicrob Agents Chemother* **1988,** *32* (7), 1034-9.
139. Zhang, X.; Wyss, U. P.; Pichora, D.; Goosen, M. F., *J Pharm Pharmacol* **1994,** *46* (9), 718-24.
140. Xia, S.; Dun, X. P.; Hu, P. S.; Kjaer, S.; Zheng, K.; Qian, Y.; Solen, C.; Xu, T.; Fredholm, B.; Hokfelt, T.; Xu, Z. Q., *Proc Natl Acad Sci U S A* **2008,** *105* (14), 5609-13.
141. Lutwyche, P.; Cordeiro, C.; Wiseman, D. J.; St-Louis, M.; Uh, M.; Hope, M. J.; Webb, M. S.; Finlay, B. B., *Antimicrob Agents Chemother* **1998,** *42* (10), 2511-20.
142. Nagai, J.; Takano, M., *Drug Metab Pharmacokinet* **2004,** *19* (3), 159-70.
143. Sano, G.; Takada, Y.; Goto, S.; Maruyama, K.; Shindo, Y.; Oka, K.; Matsui, H.; Matsuo, K., *J Bacteriol* **2007,** *189* (22), 8224-32.
144. Gindy, M. E.; Panagiotopoulos, A. Z.; Prud'homme, R. K., *Langmuir* **2008,** *24* (1), 83-90.
145. Johnson, B. K.; Prud'homme, R. K., Flash NanoPrecipitation of organic actives and block copolymers using a confined impinging jet mixer. In *Australian Colloid and Interface Symposium*, CSIRO Publishing: Sydney, Australia, 2003; pp 1021-1024.
146. Johnson, B. K.; Prud'homme, R. K., *Physical Review Letters* **2003,** *91* (11).
147. Johnson, B. K.; Prud'homme, R. K., *AIChE Journal* **2003,** *49* (9), 2264-2282.
148. Liu, Y.; Cheng, C. Y.; Prud'homme, R. K.; Fox, R. O., *Chem Eng Sci* **2008,** *63* (11), 2829-2842.
149. Ranjan, A.; Pothayee, N.; Seleem, M.; Jain, N.; Sriranganathan, N.; Riffle, J. S.; Kasimanickam, R., *Journal of Nanoparticle Research* **2010,** *12* (3), 905-914.
150. Ranjan, A.; Pothayee, N.; Seleem, M. N.; R. D. Tyler, J.; Brenseke, B.; Sriranganathan, N.; Riffle, J. S., *International Journal of Nanomedicine* **2009,** *4* 289-297.

151. Ranjan, A.; Pothayee, N.; Seleem, M. N.; Sriranganathan, N.; Kasimanickam, R.; Makris, M.; Riffle, J. S., *Antimicrobial Agents and Chemotherapy* **2009,** *53* (9), 3985-3988.
152. Ranjan, A.; Pothayee, N.; Vadala, T. P.; Seleem, M. N.; Restis, E.; Sriranganathan, N.; Riffle, J. S.; Kasimanickam, R., *Antimicrobial Agents and Chemotherapy* **2010,** *54* (8), 3524-3526.
153. Seleem, M. N.; Jain, N.; Pothayee, N.; Ranjan, A.; Riffle, J. S.; Sriranganathan, N., *Fems Microbiology Letters* **2009,** *294* (1), 24-31.
154. Kaale, E.; Govaerts, C.; Hoogmartens, J.; Van Schepdael, A., *Rapid Communications in Mass Spectrometry* **2005,** *19* (20), 2918-2922.
155. Nakamura, Y.; Okubo, M.; Matsumoto, T., *Kobunshi Ronbunshu* **1982,** *39* (2), 71-77.
156. Simons, S. S.; Johnson, D. F., *Analytical Biochemistry* **1977,** *82* (1), 250-254.
157. Simons, S. S.; Johnson, D. F., *Analytical Biochemistry* **1978,** *90* (2), 705-725.
158. Stobaugh, J. F.; Repta, A. J.; Sternson, L. A.; Garren, K. W., *Analytical Biochemistry* **1983,** *135* (2), 495-504.
159. Harris, L. A.; Goff, J. D.; Carmichael, A. Y.; Riffle, J. S.; Harburn, J. J.; St. Pierre, T. G.; Saunders, M., *Chemistry of Materials* **2003,** *15* (6), 1367-1377.
160. Vadala, M. L.; Thompson, M. S.; Ashworth, M. A.; Lin, Y.; Vadala, T. P.; Ragheb, R.; Riffle, J. S., *Biomacromolecules* **2008,** *9* (3), 1035-1043.
161. Huffstetler, P. P.; Miles, W. C.; Goff, J. D., et al. , *Polymer Preprints* **2008,** *49* (2), 1103-1104.
162. Xu, C.; Xu, K.; Gu, H.; Zheng, R.; Liu, H.; Zhang, X.; Guo, Z.; Xu, B., *J Am Chem Soc* **2004,** *126* (32), 9938-9.
163. Xie, J.; Xu, C.; Xu, Z.; Hou, Y.; Young, K. L.; Wang, S.; Pourmond, N.; Sun, S., *Chem Mater* **2006,** *18* (23), 5401-5403.
164. Shultz, M. D.; Reveles, J. U.; Khanna, S. N.; Carpenter, E. E., *J Am Chem Soc* **2007,** *129* (9), 2482-7.
165. Traina, C. A.; Schwartz, J., *Langmuir* **2007,** *23* (18), 9158-61.
166. T. J. Daou, J. M. G. c., G. Pourroy, S. Buathong, A. Derory, C. Ulhaq-Bouillet, B. Donnio, D. Guillon, S. Begin-Colin, *Chemistry of Materials* **2008,** *20* (18), 5869-5875.
167. Sahay, G.; Batrakova, E. V.; Kabanov, A. V., *Bioconjug Chem* **2008,** *19* (10), 2023-9.
168. Batrakova, E. V.; Li, S.; Brynskikh, A. M.; Sharma, A. K.; Li, Y.; Boska, M.; Gong, N.; Mosley, R. L.; Alakhov, V. Y.; Gendelman, H. E.; Kabanov, A. V., *J Control Release* **2010,** *143* (3), 290-301.
169. Yavuz, M. S.; Cheng, Y.; Chen, J.; Cobley, C. M.; Zhang, Q.; Rycenga, M.; Xie, J.; Kim, C.; Song, K. H.; Schwartz, A. G.; Wang, L. V.; Xia, Y., *Nat Mater* **2009,** *8* (12), 935-9.
170. Matyjaszewski, K., *Abstracts of Papers of the American Chemical Society* **2001,** *221*, U326-U326.
171. Lele, B. S.; Murata, H.; Matyjaszewski, K.; Russell, A. J., *Biomacromolecules* **2005,** *6* (6), 3380-7.
172. Gao, H.; Matyjaszewski, K., *J Am Chem Soc* **2007,** *129* (20), 6633-9.

173. Wei, H.; Cheng, S. X.; Zhang, X. Z.; Zhuo, R. X., *Progress in Polymer Science* **2009,** *34*, 893-910.
174. Wu, C.; Wang, X., *Phys Rev Lett* **1998,** *80*, 4029-4094.
175. Xia, J.; Gaynor, S. G.; Matyjaszewski, K., *Macromolecules* **1998,** *31* (17), 5958–5959.
176. Bartoli, G.; Bosco, M.; Marcantoni, E.; Petrini, M.; Sambri, L.; Torregiani, E., *J. Org. Chem.* **2001,** *66*, 9052-9055.
177. Azizi, N.; Saidi, M. R., *Org Lett* **2005,** *7* (17), 3649-51.
178. Khatik, G. L.; Kumar, R.; Chakraborti, A. K., *Org Lett* **2006,** *8* (11), 2433-6.
179. Ranu, B. C.; S., B., *Tetrahedron Letters* **2007,** *48*, 141-143.
180. Rademacher, J. T.; Baum, M.; Pallack, M. E.; Brittain, W. J., *macromolecules* **2000,** *22* (2), 284-288.
181. Teodorescu, M.; Matyjaszewski, K., *Macromolecules* **1999,** *32*, 4826-4831.
182. Rademacher, J. T.; Baum, M.; Pallack, M. E.; Brittain, W. J.; Simonsick, W. J., *Macromolecules* **2000,** *33*, 284-288.
183. Masci, G.; Giacomelli, L.; Crescenzi, V., *Macromolecular Rapid Communications* **2004,** *25* (4), 559–564.
184. Xie, Y.; Yin, X.; Burke, N. A. D.; Stöve, H. D. H., *Macromolecules* **2005,** *38* (14), 5937-5943.
185. Vestal, C. R.; Zhang, Z. J., *J Am Chem Soc* **2002,** *124* (48), 14312-3.
186. Hu, F.; Neoh, K. G.; Cen, L.; Kang, E. T., *Biomacromolecules* **2006,** *7* (3), 809-16.
187. Fan, Q. L.; Neoh, K. G.; Kang, E. T.; Shuter, B.; Wang, S. C., *Biomaterials* **2007,** *28* (36), 5426-36.
188. Marutani, E.; Yamamoto, S.; Ninjbadgar, T.; Tsujii, Y.; Fukuda, T.; Takano, M., *Polymer* **2004,** *45*, 2231-2235.
189. Puttamraju, P.; SenGupta, A. K., *Ind. Eng. Chem. Res.* **2006,** *45* (22), 7737-7742.
190. Ebner, A. D.; Ritter, J. A.; Navrati, J. D., *Ind. Eng. Chem. Res.* **2001,** *40* (7), 1615-1623.
191. Kodama, R. H.; Berkowitz, A. E.; McNiff, E. J.; Foner, S., *Physical Review Letters* **1996,** *77* (2), 384-397.
192. Morup, S., *Journal of Magnetism and Magnetic Materials* **2003,** *266 (1-2)* (1-2), 110-118.
193. Li, D.; Teoh, W. Y.; Woodward, R. C.; Cashion, J. D.; Selomulya, C.; Amal, R., *Journal of Physical Chemistry C* **2009,** *11328*, 12040-12047.
194. Morales, M. P.; Veintemillas-Verdaguer, S.; Montero, M. I.; Serna, C. J.; Roig, A.; Casas, L.; Martinez, B.; Sandiumenge, F., *Chemistry of Materials* **1999,** *11* (11), 3058-3064.
195. Rubio-Retama, J.; Zafeiropoulos, N. E.; Serafinelli, C.; Rojas-Reyna, R.; Voit, B.; Cabarcos, E. L.; Stamm, M., *Langmuir* **2007,** *23* (20), 10280-5.
196. Regmi, R.; Bhattarai, S. R.; Sudakar, C.; Wani, A. S.; Cunningham, R.; Vaishnava, P. P.; Naik, R.; Oupicky, D.; Lawes, G., *Journal of Material Chemistry* **2010,** *23*, 6158–6163.
197. Herrera, A. P.; Rodríguez, M.; Torres-Lugo, M.; Rinaldi, C., *Journal of Material Chemistry* **2008,** *18*, 855 - 858.

198. Vagberg, L. J. M.; Cogan, K. A.; Gast, A. P., *Macromolecules* **1991,** *24* (7), 1670-1677.
199. Miles, W. C.; Goff, J. D.; Huffstetler, P. P.; Mefford, O. T.; Riffle, J. S.; Davis, R. M., *Polymer* **2010,** *51* (2), 482-491.
200. Fang, Z.; Zhen, T.; Sato, T., *Science in China (B)* **1999,** *42* (3), 290-297.
201. Hirotsu, S., *J. Chem. Phys.* **1991,** *94*, 3949.
202. Carroll, M. R.; Woodward, R. C.; House, M. J.; Teoh, W. Y.; Amal, R.; Hanley, T. L.; St Pierre, T. G., *Nanotechnology 21* (3), 035103.
203. Lin, J. J.; Chen, J. S.; Huang, S. J.; Ko, J. H.; Wang, Y. M.; Chen, T. L.; Wang, L. F., *Biomaterials* **2009,** *30* (28), 5114-24.
204. Janib, S. M.; Moses, A. S.; Mackay, J. A., *Adv Drug Deliv Rev* **2010**.
205. McCarthy, J. R., *Nanomedicine (Lond)* **2009,** *4* (7), 693-5.
206. Comes Franchini, M.; Baldi, G.; Bonacchi, D.; Gentili, D.; Giudetti, G.; Lascialfari, A.; Corti, M.; Marmorato, P.; Ponti, J.; Micotti, E.; Guerrini, U.; Sironi, L.; Gelosa, P.; Ravagli, C.; Ricci, A., *Small* **2010,** *6* (3), 366-70.
207. Bhojani, M. S.; Van Dort, M.; Rehemtulla, A.; Ross, B. D., *Mol Pharm* **2010**.
208. Otsuka, H.; Nagasaki, Y.; Kataoka, K., *Adv Drug Deliv Rev* **2003,** *55* (3), 403-19.
209. Kakizawa, Y.; Kataoka, K., *Adv Drug Deliv Rev* **2002,** *54* (2), 203-22.
210. *Zetasizer Nano Series User Manual*. Malvern Instruments, Ltd.: Worcestershire, 2005.
211. Lecaroz, C.; Campanero, M. A.; Gamazo, C.; Blanco-Prieto, M. J., *J Antimicrob Chemother* **2006,** *58* (3), 557-63.
212. Nasongkla, N.; Bey, E.; Ren, J.; Ai, H.; Khemtong, C.; Guthi, J. S.; Chin, S. F.; Sherry, A. D.; Boothman, D. A.; Gao, J., *Nano Lett* **2006,** *6* (11), 2427-30.
213. Taton, T. A.; Kim, B.-S. K., *Langmair* **2006,** *23* (4), 2198-2202.
214. Wan, S.; Zheng, Y.; Liu, Y.; Yan, H.; Liu, K., *J. Mater. Chem.* **2005,** *15*, 3424-3430.